AD-757 085

STIMULATED AMPLIFICATION OF VLF AND ULF WAVES IN THE MAGNETOSPHERE BY LOCALIZED INJECTIONS OF PLASMA CLOUDS AND PARTICLE BEAMS

Harold B. Liemohn, et al

Washington University

DISCLAIMER NOTICE

THIS DOCUMENT IS THE BEST
QUALITY AVAILABLE.

COPY FURNISHED CONTAINED
A SIGNIFICANT NUMBER OF
PAGES WHICH DO NOT
REPRODUCE LEGIBLY.

STIMULATED AMPLIFICATION OF VLF AND ULF WAVES IN THE MAGNETOSPHERE BY LOCALIZED INJECTIONS OF PLASMA CLOUDS AND PARTICLE BEAMS

by

Harold B. Liemohn

Geophysics Program
University of Washington
Seattle, Washington 98195

and

Aeronomy Program, Space Sciences Section*
Battelle Memorial Institute
Pacific Northwest Laboratories
Richland, Washington   99352

December 1972

*Permanent address

DOCUMENT CONTROL DATA - R & D

Security classification of title, body of abstract and indexing annotation must be entered when the overall report is classified)

1 ORIGINATING ACTIVITY (Corporate author)	2a. REPORT SECURITY CLASSIFICATION
University of Washington	Unclassified
	2b GROUP

3 REPORT TITLE

Stimulated Amplification of VLF and ULF Waves in the Magnetosphere by Localized Injections of Plasma Clouds and Particle Beams

4 DESCRIPTIVE NOTES (Type of report and inclusive dates)

Final Report

5 AUTHOR(S) (First name, middle initial, last name)

Harold B. Liemohn

6 REPORT DATE	7a. TOTAL NO. OF PAGES	7b. NO OF REFS
December, 1972	134 135	49
8a CONTRACT OR GRANT NO	9a. ORIGINATOR'S REPORT NUMBER(S)	
N00014-67-A-0103-0027		
b. PROJECT NO	None	
c.	9b. OTHER REPORT NO(S) (Any other numbers that may be assigned this report)	
d		

10 DISTRIBUTION STATEMENT

Distribution of this document is unlimited.

11 SUPPLEMENTARY NOTES	12 SPONSORING MILITARY ACTIVITY
	Contract from ONR
	Funding from ARPA

13 ABSTRACT

The cyclotron resonance interaction between ULF-VLF waves and trapped particles may be strongly enhanced in the magnetosphere by the injection of either cold plasma or energetic particle beams. A variety of natural conditions and injections are investigated numerically using the linear theory. Both satellite and rocket injection of cold plasma provide significant enhancements of amplification. Conventional hot electron beams may also amplify narrow frequency bands, if the beam geometry can be effectively altered at injection. Heavy ion beams appear to offer attractive propagation conditions as well as stimulate amplification.

KEY WORDS	LINK A		LINK B		LINK C	
	ROLE	WT	ROLE	WT	ROLE	WT
Ultra-Low Frequency						
Very-Low-Frequency						
Wave Amplification						
Magnetospheric Physics						
Plasma Injection Experiments						
Cyclotron-Resonance Interaction						
Whistler-Mode Propagation						
Radio Noise Enhancements						
Space Physics Applications						

DD FORM 1 NOV 65 1473 (BACK)

ib

STIMULATED AMPLIFICATION OF VLF AND ULF WAVES
IN THE MAGNETOSPHERE   BY LOCALIZED INJECTIONS
OF PLASMA CLOUDS   AND PARTICLE BEAMS

by

Harold B. Liemohn

Geophysics Program
University of Washington
Seattle, Washington 98195

and

Aeronomy Program, Space Sciences Section*
Battelle Memorial Institute
Pacific Northwest Laboratories
Richland, Washington   99352

December 1972

*Permanent address

1 C

ARPA Order No. 1479/2141

Program Code 1E20

Contract No. N00014-67-A-0103-0027,
NR 012-712

Principal Investigators:

Dr. H. B. Liemohn
Battelle-Northwest
Richland, Washington 99352
509/942-7136

Prof. G. K. Parks
University of Washington
Seattle, Washington 98195
206/543-0953

Name of Contractor:

University of Washington

Short Title of Work:

Stimulated Amplification of VLF and ULF

Effective Date of Contract:

From March 1, 1972 to December 31, 1972

Amount of Contract: $47,966

STIMULATED AMPLIFICATION OF VLF AND ULF WAVES
IN THE MAGNETOSPHERE BY LOCALIZED INJECTIONS
OF PLASMA CLOUDS AND PARTICLE BEAMS

TABLE OF CONTENTS

STIMULATED AMPLIFICATION OF VLF AND ULF WAVES IN THE MAGNETOSPHERE BY LOCALIZED INJECTIONS OF PLASMA CLOUDS AND PARTICLE BEAMS

by

Harold B. Liemohn

SUMMARY

The geomagnetic cavity surrounding the earth, called the magneto-
sphere, contains an enormous amount of energy in the form of electro-
magnetic waves, trapped energetic particles, and the static magnetic
field. The waves and particles are in a state of dynamic equilibrium
as they interact with each other through various plasma instabilities.
Our understanding of this equilibrium state has progressed to the point
where it may be possible to stimulate wave amplification at ULF ($\sim$0.1-10 Hz)
and VLF ($\sim$1-100 kHz) by disturbing the equilibrium through catalytic
injections of plasma clouds or particle beams. Such a prospect has great
significance. First, it offers a direct test of the fundamental physical
processes that are believed to control the state of the magnetosphere.
Second, controlled injections might be used to stimulate artificial
amplification of VLF or ULF emissions on command and allow them to be used
as a wide-area communication system.

One of the dominant plasma instabilities in the magnetosphere is the
cyclotron-resonance interaction between energetic particles and electro-
magnetic waves. The condition for the interaction to occur is that the
motion of the particle Doppler shifts the wave frequency to its local
cyclotron frequency. The net exchange of energy between a band of waves
and a group of particles depends upon the shape of the phase-space dis-
tribution of the particles and the local frequency parameters of the plasma
medium. The interaction is undoubtedly responsible for significant wave

amplification and particle precipitation in certain circumstances and appears to be the process responsible for maintenance of an equilibrium configuration of waves and particles in the magnetosphere.

These qualities make this interaction a logical first choice for investigation as a means of stimulating artifical amplification of VLF and ULF waves in the magnetosphere. The interaction is sensitive to both the background magnetoplasma parameters and the hot energetic particle distribution. Modification of the interaction can be achieved by the introduction of localized clouds of plasma that reduce the phase velocity of the waves and cause enhanced amplification by lowering the resonance velocity. Alternatively, direct injection of hot energetic particle beams can also appreciably alter the local amplification characteristics of the beam. These two methods of modifying the cyclotron-resonance interaction are explored in this document for a variety of cases.

Many different methods for injecting plasma clouds or particle beams have been modelled quantitatively to assess their relative merits as a means of inducing strong wave amplification. The injection of a dense jet of barium that travels upward along the geomagnetic field toward the equatorial region produces significant amounts of enhanced VLF amplification when the jet is within 30° of the geomagnetic equator some thirty minutes after injection. Injection of a geosynchronous lithium cloud stimulates amplification of both VLF and ULF waves, but the latter are limited to frequencies below the equatorial lithium gyrofrequency (~ 0.2 Hz). The extent of the lithium amplification effect depends critically on the the natural conditions in the magnetosphere, particularly the intensity of the proton ring current. Amplifications of many tens of decibels appear to be feasible with injections of only 1-2 kgm of material.

vi

Beam injections were included in the study because they offer the opportunity for prompt localized interactions with the waves that can produce readily identifiable signatures of the amplified signal. Electron beams amplify VLF whereas proton beams amplify ULF signals. Unfortunately, the beam diameter from a conventional particle gun on board a satellite or rocket is too small for effective amplification. An adequate interaction of the beam with a wave front requires a cross section comparable to several wave lengths. Nevertheless, if such a broad beam is achievable in the near future, appreciable amounts of amplification are possible and their natural frequency signature is quite distinct. Furthermore, modulation of such beams offers the opportunity to transmit information instead of merely enhancing background noise.

Injection of low-energy beams of heavy ions appears to be practical for stimulation of VLF amplification. For example, a beam of 43 eV cesium ions has a gyroradius that is comparable to a VLF wave front. When such a beam travels up a field line it drags along a neutralizing low-energy electron beam which changes the local propagation conditions. The amplification of VLF by such a beam appears to be on the order of tens of decibels at frequencies near the local electron gyrofrequency. Again the characteristic frequency signature is present and beam modulation can further enhance the detectability of induced amplification.

Several conclusions can be drawn from the study. Amplifications of 40-60 decibels are indicated for several cases of interest. Such

enhancements of VLF or ULF noise levels are easily detectable with ground or satellite receivers located along the injection field lines. One of the most promising cases is lithium injection at geosynchronous altitude where broad regions at the surface of the earth would be illuminated by ULF noise in the band 0.4 - 0.5 Hz. At VLF the low-energy cesium-electron beam works well as an amplifier and also provides a fluxtube waveguide for the electromagnetic energy. Although the electron and proton beams appear to generate amplification, the interaction region is severely limited with present particle gun technology and the total energy transferred to the waves is quite small. Plasma injections into the more dense inner magnetosphere are relatively ineffective due to the local propagation characteristics.

The study is based on the linear theory for the cyclotron-resonance interaction. Since some of the linearity assumptions are not valid in the injection region, the quantitative results are open to question. Nevertheless, the linear results are believed to provide a reasonable basis for selecting injection methods that appear to be effective for stimulating amplification. As might be anticipated, the application of the nonlinear theory is much more involved and requires extensive computer time. Nevertheless, a thorough nonlinear study of promising cases is recommended.

LIST OF FIGURES

LIST OF FIGURES

xi

ACKNOWLEDGMENTS

STIMULATED AMPLIFICATION OF VLF AND ULF WAVES IN THE MAGNETOSPHERE BY LOCALIZED INJECTIONS OF PLASMA CLOUDS AND PARTICLE BEAMS

INTRODUCTION

There is an ongoing military and civilian requirement to improve the reliability of global radio communications. Long distance transmission of information is interrupted frequently by the diurnal excursions of ionospheric propagation conditions and occasionally by strong geomagnetic disturbances that cause exceptionally intense ionization. To some extent these vagaries are overcome at VLF (3-30 kHz) where the long wavelengths are less affected by changing conditions in the ionosphere. At lower frequencies, notably ELF (3-3000 Hz) and ULF (below 3 Hz), the signals readily propagate on a global scale with relatively negligible attenuation. At these latter frequencies, of course, the information band width is severely limited. Furthermore, efficient generation of such signals is exceedingly difficult due to the extremely long free-space wavelengths.

Since VLF, ELF, and ULF noise bands occur naturally in the magnetosphere surrounding earth, it is appropriate to inquire about ways of exciting this energy on command. The electromagnetic waves are apparently guided by the geomagnetic field to ionospheric alitudes where they subsequently illuminate wide surface areas around the base of the field line. In the magnetosphere, VLF and ULF noise is believed to be caused by the cyclotron-resonance interation with energetic (1-100 keV) electrons and protons. In fact, the dynamic equilibrium state between waves and

energetic particles in the magnetosphere is believed to be controlled
by this dominant interaction (Kennel and Petschek, 1966). Furthermore,
observed amplification of VLF and ULF whistlers is explained by this inter-
action (e.g., Cornwall, 1966; and Liemohn, 1967). The amount of energy
exchange that may occur depends critically on such parameters as the
local ambient plasma density, the local geomagnetic field strength, and
the shape of the energetic particle distribution. Thus, it is appropriate
to explore ways of altering some of these parameters which might catalytically
enhance the amplification process. Such experiments would be valuable as
a quantitative test of the cyclotron-resonance interaction theory and subse-
quently provide a basis for an operational communications system.

The physics of the cyclotron-resonance interaction is really
simple to understand, although its mathematical description in magneto-
spheric applications is relatively complicated. In essence, it is a simple
resonance trapping of selected charged particles in the electromagnetic
potential of the wave. Although all particles are perturbed by the circu-
larly polarized wave fields, there is a select group of particles with
velocities that Doppler shift the propagation frequency to the vicinity of
their local gyrofrequency. The electromagnetic forces slow down some of these
particles and speed up others to bring them closer to the resonance fre-
quency and a net exchange of energy occurs between each monochromatic wave
and the relevant particles. If more particles give up energy than gain, the
wave is amplified and otherwise, attenuated. The amount of energy ex-
change depends on the shape of the particle distribution in the vicinity

of the resonance velocity band. The local parameters of the medium which prescribe the phase velocity of the wave also influence the extent of the interaction by establishing minimum resonance energies for the particles.

In order to estimate its effect in the magnetosphere, the interaction must be evaluated for a wide range of propagation frequencies, field-line paths, and particle distributions. Several cases that are typical of magnetospheric conditions have been investigated (e.g., Cocke and Cornwall, 1967; Liemohn, 1967 and Ho and Liemohn, 1972) for a wide range of conditions. It was concluded that the magnetosphere behaves like a convective traveling-wave amplifier at both VLF and ULF, and that observable amounts of VLF and ULF amplification occurred over a wide range of frequencies but varied appreciably with geomagnetic activity. A considerable body of indirect evidence has been gathered in support of the cyclotron-resonance amplification theory (Cocke and Cornwall, 1967; Liemohn, 1969; Cornwall et al., 1971; Thorne and Kennel, 1971; Rosenberg et al., 1971). Unfortunately, there have been no direct experimental observations to verify the quantitative aspects of the cyclotron-resonance theory.

Thus the possibility of a controlled experiment to enhance VLF or ULF amplification by a known amount has a two-fold purpose. First, it can be used to test the quantitative conclusions that have been drawn from the theoretical analyses. Second, successful artificial simulation of wave amplification in the magnetosphere is an essential step toward its ulilization in communication systems.

There are essentially two known methods for artificial stimulation of

the cyclotron-resonance interaction in the magnetosphere. The first
method involves injection of dense plasma clouds of low-energy electrons
or ions (Brice, 1970; and Cornwall & Schulz, 1971) into regions of the
magnetosphere where the ambient plasma density is low but energetic
particles abound. Selective placement of these clouds reduces the phase
velocity of the VLF or ULF waves and thereby reduces the minimum particle
energy necessary for resonance. Generally there are many more hot particles
at the reduced resonance energy so that appreciable amplification enhance-
ments are anticipated. Since the plasma clouds do not enter directly into
the amplification, their injection is viewed as a catalytic process whereby
the increased wave energy is derived from the natural energetic particle
population.

The second method of artificially stimulating the amplification
involves direct injection of hot plasma beams by rocket or satellite
particle guns. Beam densities comparable to the ambient natural particle
densities along the flux tube are apparently achievable with current
technology (Hendrickson et al., 1970; Hess et al., 1971; and Cartwright
& Kellogg, 1971). In this case the particle beam merely adds a known
distortion in the energetic particle distribution along the field line,
and the enhanced wave amplification is derived entirely from the energy
of the injected beam. This method of stimulation is severely limited by
the low energy-conversion efficiency and the relatively small beam diameter.
Beams are attractive, however, because they do not rely significantly on
the ambient conditions in the magnetosphere, and their injections can be
modulated to transmit information.

In this document selected cases of plasma cloud and beam injections are analyzed quantitatively using the linear theory for the cyclotron-resonance interaction. The linear theory has several advantages for an initial investigation but it suffers certain inadequacies that necessitate non linear investigations to corroborate the results. The principle advantage of the linear expressions is that their computer evaluation along magnetospheric propagation paths is relatively inexpensive. Furthermore, the computer program was generated some years ago (Liemohn, 1967). Computer programs for the complete non linear solutions have been prepared (Ossakow et al., 1972; Cuperman and Salu, 1972; Denavit, private communication), but they currently require about 100 times more computer time for each uniform element of the magnetospheric path. Thus, the linear theory provides a useful means of exploring a variety of parameter regimes to optimize promising injection schemes before they are subjected to a detailed non linear investigation.

The next section of the paper summarizes the linear theory for the cyclotron-resonance interaction and introduces relevant propagation properties of the magnetosphere. Specific injection schemes for stimulating amplification of VLF and ULF are treated separately in the following two sections. The final section summarizes the important results of the study and draws specific conclusions about future research.

CYCLOTRON-RESONANCE THEORY

The fundamental linear theory for the cyclotron-resonance inter-
action and its application to VLF and ULF propagation in the magneto-
sphere is summarized in this section. Only the key equations are presented
here; for a complete derivation of the theoretical expressions, the reader
is referred to the early literature (e.g., Scarf, 1962; Kennel and Petschek,
1966). The solutions of the dispersion equation for circularly polarized
VLF and ULF waves lead naturally to a discussion of the propagation
characteristics in the magnetosphere. Some subtle aspects of the matha-
matical solutions are described in order to alert the reader to the
limitations of the theoretical expressions. Finally, models of the
plasma medium encountered in the magnetosphere during disturbed
and quiescent conditions are described. These models provide a quanti-
tative basis for estimating the effectiveness of various methods of
stimulating the interaction.

Dispersion Equation. In order to allow tractible mathematical
expressions, several assumptions are built into the theoretical description-
tion presented here. First, it is assumed that the wavelengths are suf-
ficiently small that the propagation can be described in a localized
region where the magnetoplasma has a uniform static field $\underline{B}$ and a
homogeneous particle density N. Second, the analysis is restricted to
the special case where the propagation vector $\underline{k}$ is parallel to $\underline{B}$ so that
the waves are necessarily circularly polarized.   When $\underline{k}$ is not parallel
to $\underline{B}$, Landau damping is introduced by the presence of a longitudinal
electric field component (Kennel and Thorne, 1967; and Kennel and Wong,

1967). Third, the transfer of energy between the waves and particles is assumed to be sufficiently small and localized that non-linear effects can be ignored. Implications of these specific assumptions will be discussed below.

Circularly polarized monochromatic waves are described by the Fourier component form exp $(ikz-i\omega t)$ where ω is the propagation frequency of interest. For the foregoing conditions, the dispersion equation for the wave characteristics in the cyclotron-resonance interaction may be derived from the coupled Vlasov and Maxwell equations (e.g. Montgomery and Tidman, 1964)

$$\frac{c^2 k^2}{\omega^2} = 1 + \sum_{i,e} \frac{\pi \omega_p^2}{k\omega} \int_0^\infty dv_\perp \int_{-\infty}^{+\infty} \frac{dv_{\parallel} I}{v_{\parallel} - v_c} \tag{1}$$

where

$$I(v_\perp, v_{\parallel}) = -v_\perp^2 \frac{\partial F}{\partial v_\perp} + \frac{k}{\omega} v_\perp^2 \left(v_{\parallel} \frac{\partial F}{\partial v_\perp} - v_\perp \frac{\partial F}{\partial v_{\parallel}} \right) \tag{2}$$

and

$$v_c = (\omega \pm \omega_c)/k \tag{3}$$

$F^{i,e}(v_\perp, v_{\parallel})$ are the phase-space distributions of the charged particles with velocity components perpendicular and parallel to $\underline{B}$. The quantities $\omega_p^{i,e} = (4\pi N^{i,e} e^2/m^{i,e})^{1/2}$ and $\omega_c^{i,e} = (\pm e) B/m^{i,e} c$ are the plasma and cyclotron frequencies of the medium. The particle labels for the ions (i) and electrons (e) are generally suppressed throughout the remainder of the paper to simplify notation.

The resonance speed v_c is the particle velocity component necessary to Doppler shift the wave frequency to the local cyclotron frequency. Only those particles with $v_{\parallel}$ near v_c participate in the energy exchange. The plus and minus signs in v_c refer to right-hand and left-hand

circularly polarized modes, respectively. Clearly, there are four
possible combinations of interactions between waves and particles. By
convention the right-hand electron VLF and the left-hand ion ULF reson-
ance which require the wave and resonance particles to rotate in the same
sense and travel in opposite directions are termed normal interactions.
The right-hand ion and left-hand electron resonances, which require the
particles to overtake the wave, thus reversing their apparent sense of
rotations as required for resonance, are called anomalous. In the analyses
presented subsequently, only the normal interactions are considered be-
cause they occur at much lower energies (0.1-100 keV) than the anomalous
interactions (above 1 meV). At anomalous interaction energies, there simply
are an insufficient number of particles to warrant investigation. Thus,
there is only one plasma component that contributes to the summations in
equation (1), depending on the mode of interest.

The dispersion equation (1) determines the propagation characteristics
$k(\omega)$ or $\omega(k)$ for the electromagnetic wave. In general it has several
solution trajectories in the complex hyperspace $(\omega_r + i\omega_i, k_r + ik_i)$,
depending on the form of F. The space-time conditions in a given
problem determine the appropriate locus of acceptable solutions. For an
initial-value problem, k must be real and ω is allowed to be complex,
whereas a boundary-value problem requires real ω and complex k. Instab-
ilities inherent in the system are prescribed by characteristic roots
of equation (1) that have ω_i greater than 0 or k_i less than 0 corresponding
to wave amplitude growth in the representation used here (with ω_r, k_r
greater than 0). When such roots are present, they normally dominate the
solution. In some applications, however, these roots may be suppressed by

imposed space-time conditions on the system.

In many cases of physical interest such as those presented here, the local boundary conditions remain unspecified, and the dispersion equation alone is the only information available about the nature of the wave-particle system. When instabilities occur in this circumstance, it is important to ascertain whether an unstable system is inherently a non-convective runaway oscillator described by $\omega_i > 0$ and k real, or a convective traveling-wave amplifier described by ω real and $k_i < 0$. The answer is found in a sophisticated mathematical criterion for hot plasma instabilities (Derfler, 1967 and 1970). The criterion has been applied to several cases of interest in the magnetosphere (Ho and Liemohn, 1972) and it has been concluded that instabilities in the magnetosphere are generally convective. The specific cases presented below have not been investigated on the basis of the instability criterion, but they generally fall into the class of interactions which are deemed to be convective.

Before deriving solutions of equation (1) for complex k and real ω, it is necessary to define the form of the distribution function F. Experimental observations of particles in the magnetosphere reveal that F can be divided into a very low energy cold plasma part F_{COLD} for particles below 10 eV, and a hot plasma part F_{HOT} which describes all the energetic particles above 10 eV. The sum of these two distributions is normalized to unity so that the total plasma density N is explicitly included in ω_p.

In order to solve the integral dispersion equation, it is necessary to make an additional assumption that the amplitude changes slowly with wavelength, which can be expressed in the form $|k_i| \ll k_r$. Such a condition

usually applies in the quiescent magnetosphere, but may be violated during artificial stimulation of the interaction by plasma injections. When the condition applies, the imaginary part of v_c is very small and equation (1) may be expanded in a Taylor series in the complex $v_{||}$ plane (Jackson, 1960). By equating real and imaginary parts, the propagation characteristics to lowest order in k_i / k_r are given by

$$\frac{c^2 k_r^2}{\omega^2} = 1 - \sum_{i,e} \frac{\omega_p^2}{\omega (\omega \pm \omega_c)} \tag{4}$$

$$\frac{c k_i}{\omega} = \frac{\pi^2}{2 c^2 k_r^2} \sum_{i,e} \omega_p^2 \int_0^\infty dv_\perp \, I_{HOT} (v_\perp, v_c) \tag{5}$$

In the latter expression only F_{HOT} is substituted in equation (2) to obtain I_{HOT}, and v_c is the real part of equation (3). Expressions (4) and (5) describe the local phase velocity (refractive index n) and amplitude exponent for VLF or ULF waves in the magnetosphere.

In some applications where wave growth is extremely rapid, $|k_i| \gtrsim k_r$ and a proper description requires the nonlinear theory (Cuperman, 1972; Bud'ko, et al., 1972). If $|k_i| >> k_r$, then the propagation characteristics may be described by asymptotic expansions (e.g., Jackson, 1960) of the integral. It is important to emphasize that these analyses are not the same as quasi-linear theory (Kennel and Petschek, 1966; Gendrin, 1968) where repeated interaction with the same particles distorts F_{HOT}. Such distortion is only important for extended interaction regions, where

the longitudinal drift in one bounce period, $4 v/\omega_c^{i,e}$, small compared to the characteristic wavelength, $2\pi/k_r$ (evaluated at $0.5 \omega_c^{i,e}$). For magnetospheric conditions of interest here, these quantities are comparable for 10 keV electrons and protons (3 km and 150 km, respectively). However, in the applications only narrow meridian wedges several wavelengths across are stimulated by injection. Thus quasi-linear theory is not applicable near the edge of the injection region where the particles enter, but may be significant where they exit.

Physical Interpretation. Certain physical attributes of the characteristics deserve further elaboration. First, they can be expressed in much simpler form where their physical interpretation is more transparent. Second, the effects of introducing a plasma cloud or a stream of hot particles are readily evident from the analytical form of the expressions. Finally, the effect of off-axis propagation ($\underline{k}$ not parallel to $\underline{B}$) is examined qualitatively to assess its effect on stimulated amplification and the energy budget of the magnetosphere.

The expression for the phase velocity in equation (4) can be simplified considerably for frequencies just below the electron gyrofrequency (VLF) and the ion gyrofrequency (ULF). By neglecting terms of order m_e/m_i the index of refraction has the two forms

$$n^2 = c^2 k_r^2/\omega^2 = 1 + \frac{(\omega_p^e)^2}{\omega(|\omega_c^e|-\omega)} \qquad \text{for } \omega \lesssim |\omega_c^e| \qquad (6)$$

$$= 1 + \frac{(\omega_p^i)^2}{\omega_c^i(\omega_c^i-\omega)} \qquad \text{for } \omega < \omega_c^i \qquad (7)$$

These are well-known expressions for VLF and ULF whistler-mode propagation which display the characteristic frequency dispersion that is observed experimentally in the magnetosphere.

Regimes of wave growth ($k_i < 0$) and decay ($k_i > 0$) for anisotropic distributions can be formally derived from equation (5). For this purpose it is necessary to introduce the concept of a particle pitch angle α between the velocity and the magnetic field,

$$\alpha = \tan^{-1}(-v_\perp / v_\parallel) \tag{8}$$

Then equation 5 can be expressed in the form

$$\frac{ck_i}{\omega} = \sum_{i,e} \frac{\pi^2 \omega_p^2}{c^2 k_r^2} \left[1 + (1 \pm \frac{\omega_c}{\omega}) a \right] b \tag{9}$$

where $a = \frac{1}{2b} \int_0^\infty dv_\perp \, v_\perp \left[\tan \alpha \, \frac{\partial F_{HOT}}{\partial \alpha} \right]_{v_\parallel = v_c}$ (10)

$$b = \int_0^\infty dv_\perp \, v_\perp \, F_{HOT}(v_\perp, v_c) \tag{11}$$

For an isotropic distribution, $a = 0$ so that its summation term in equation (9) is always positive and the wave is attenuated by that term. The special class of anisotropies $F_{HOT} \propto \sin^m \alpha$ gives a particularly simple result. In this case, $a = m/2$ and the normal interaction terms yield amplification when $\omega / |\omega_c| < m/(m + 2)$. This latter anisotropic behavior is characteristic of natural distributions in the magnetosphere at VLF and ULF.

The physics of the interaction may be explained in terms of particle trapping in the apparent potential well of the wave fields. Although all the particles in the plasma are subjected to the electromagnetic wave fields, only those particles with $v_{\parallel}$ sufficiently close to v_c actually participate in the exchange of energy. The forces tend to drive $v_{\parallel}$ toward v_c but because the circularly polarized wave has a helical electromagnetic potential well, the $\underline{v} \times \underline{B}$ forces also change the perpendicular particle velocity $v_{\perp}$. The velocity vector of each particle is shifted slightly to bring the particle into phase with the potential well and this process leads to a net exchange of particle kinetic energy and electromagnetic energy. As noted above, the net exchange depends rather critically on the shape of the phase-space distribution, particularly the pitch angle distribution. The question of whether more particles lose or gain energy is prescribed by the derivatives in the integrands of equations (5) or (10) which are evaluated at $v_{\parallel} = v_c$. In other words, the slope of the distribution function is a measure of the number of particles that are giving up energy compared to those that are gaining it, as they shift their velocity to follow the helical potential well. The distortion of F_{HOT} by this process is ignored in the linear theory for reasons which were discussed at the end of the preceding sub-section.

Possible ways to enhance VLF or ULF wave amplification in the magnetosphere are now readily identifiable in the foregoing theoretical equations. The expression for the amplitude exponent k_i depends on a variety of parameters and distributions, which might be modified

locally to enhance the cyclotron-resonance interaction. The most obvious
means of stimulating the interaction is to change the hot plasma dis-
tribution F_{HOT}. Amplification is achieved by dumping a large amount of
energetic particles near the equator so that $\sin^m \alpha$ pitch angle dis-
tributions are formed. This type of injection is feasible by nuclear
bursts. The early tests which were detonated in the upper atmosphere
created pitch angle distributions of the form $\cos^m \alpha$ that strongly absorb
VLF and ULF energy. In fact, the only signals detected from these tests
were apparently the initial electromagnetic pulse generated by the local
current system at the source. A second method for causing substantial
amplification is particle beam injection. Such a beam would be additive
to the hot plasma distribution F_{HOT}. Its contribution would only occur
when the parallel component of the beam velocity is near v_c so that the
beam can participate in the resonance interaction. In the following
sections electron beams are investigated as a source of VLF amplification
and proton beams are considered at ULF.

Another relatively simple procedure for stimulating amplification
is to enhance the background plasma density in a local region where
natural amplification is occurring (Brice, 1970; Cornwall and Schulz,
1971). Such an enhancement alters the index of refraction (see equations
6 and 7) for the modes, reducing the phase velocities appreciably. Since
the resonance speed v_c in equation (3) is proportional to $N^{-1/2}$, this
increase in density allows lower energy particles to participate in the
resonance interaction. If the hot plasma distribution has more particles
at these lower energies, the resonance interaction is sharply stimulated,

and considerable amplification is anticipated from catalytic injections of cold plasma. Several specific cases of plasma injections are modeled in the following sections to illustrate these possibilities.

These foregoing theoretical expressions are strictly valid only for propagation vectors $\underline{k}$ parallel to the local magnetic field. But their applicability to propagation conditions in the magnetosphere is expected to extend far beyond this narrow subclass of propagation conditions. Since waves that are not parallel to the local field are subject to conventional Landau damping (Kennel, 1966), only those signals with wave normals near the local magnetic field actually survive propagation through the magnetosphere. Consequently, those VLF and ULF whistler signals that are detected by ground stations and satellites are likely to be contained in the class of propagation vectors included in the foregoing theoretical description. In this sense the theory of circularly polarized waves is quite useful. On the other hand, it must be recalled that the wave normals change their direction as they traverse the magnetosphere (Kitamura and Jacobs, 1967) so that much of the wave energy actually is ultimately lost through the Landau process. An estimate of the fraction of energy that is gained from particle amplification in one region of the magnetosphere and lost by this attenuation elsewhere has not been calculated. Undoubtedly, this energy transfer process plays an important role in the redistribution of energy throughout the magnetosphere during periods of strong disturbance. It must also play a significant role in the quasi-steady-state conditions that describe the dynamic equilibrium between waves and particles during geomagnetically quiet periods. This difficult problem needs further study.

Magnetospheric Models. The magnetosphere consists of a neutral (hydrogen) plasma imbedded in the geomagnetic field. The field is approximately a dipole subject to minor internal distortions and a major boundary distortion due to the solar wind. The cold hydrogen plasma is distributed throughout this geomagnetic cavity but it has a distinctive spatial distribution and is subject to considerable fluctuations with geomagnetic activity. In addition there is a hot plasma component of considerably lower density that consists of energetic (1-100 keV) electrons and protons that follow trapped orbits along the geomagnetic field lines.

Above the ionosphere the medium is assumed to be slowly varying electromagnetically in the sense that the wave length Λ satisfies the condition

$$|\nabla \Lambda| = 2\pi c |\nabla n| / n^2 \omega \ll 1 \qquad (12)$$

for all frequencies of interest. On this basis, the propagation characteristics of a uniform medium that are given in the preceding section are generally applicable locally in the magnetosphere. The theory of VLF and ULF whistler propagation through the magnetosphere is based on the condition (12). At VLF the whistler wave packet propagates along the flux tube field line from one hemisphere to the other in the right-hand mode of circular polarization (e.g., Helliwell, 1965). Similarly, the ULF waves propagate between hemispheres in the left-hand mode (Jacobs and Watanabe, 1964). Much of the whistler guidance along the flux tubes is attributed to field-aligned columns of enhanced ionization (Smith et al.,

1960; Smith, 1961). The time delay between successive hops of a whistler signal between hemispheres and its characteristic frequency dispersion are described very accurately by path integrals of the electromagnetic group velocity for a locally uniform medium.

Similarly, the amplitude exponent k_i for a uniform homogeneous medium is assumed to describe the wave growth or decay along the propagation path. The net path amplification or absorption of power in a wave that propagates through the slowly varying magnetosphere is given by

$$A \text{ (decibels)} = -10 \log_{10}\left[\exp\int_{path} 2 k_i (\omega,s) \, ds\right] \qquad (13)$$

where the path is along a dipole field line segment from the interaction region to the receivers on the ground, and k_i is defined by the integral in equation 5. Evaluation of the double integral contained in expression (12) for a variety of injection models is the primary objective of this research.

Without significant loss of quantitative accuracy the geomagnetic field may be approximated by a pure dipole in this application. Thus the signal path is defined by the equation for a field line

$$R = L \cos^2 \lambda \qquad (14)$$

where R is the radial distance in earth radii, L is the geomagnetic equatorial intercept in earth radii and λ is geomagnetic latitude. The electron-cyclotron frequency along this path has the form

$$\omega_c^e = \omega_{co}^e (1 + 3 \sin^2\lambda)^{1/2} / \cos^6\lambda \qquad (15)$$

where ω_{co}^e is its equatorial value ($-5.5 \times 10^6 L^{-3}$ radians/sec).
At L=4 this corresponds to an electron gyrofrequency of 13.7 kHz and a
proton gyrofrequency of 7.5 Hz.

The thermal background plasma is relatively slowly varying along a
given field line but is subject to a large discontinuity across the plasma-
pause in the vicinity of L = 3-5 (Carpenter 1966, Carpenter et al.,
1969). Inside the plasmapause the thermal plasma is in hydrostatic equil-
ibrium whereas outside the density varies approximately as the geomagnetic
field. For the analyses presented here, the plasma frequency is modeled
by the following expressions,

$$\omega_p^e = \omega_{po}^e \exp (3/R - 3/L) \qquad \text{in plasmasphere} \qquad (14)$$

$$= \omega_{po}^e (L/R)^3 \qquad \text{in plasmatrough} \qquad (15)$$

where ω_{pc}^e is its equatorial value ($5.65 \times 10^4 N_0^{1/2}$ radians/sec)
and the hydrostatic model has a temperature of 1250° K. For modeling
purposes, the equatorial density is assumed to be $N_0 = 232$ particles/cm^3
in the plasmasphere which gives an electron plasma frequency of 137 kHz.
In the plasmatrough $N_0 = 1$ particle/cm^3 which corresponds to a frequency
of 9 kHz.

In order to separate the distribution function into a cold com-
ponent and a hot component, the frequency band of interest must be
somewhat below the local gyrofrequency for the resonant particles. In
practice this requires $\omega \leq 0.9 |\omega_c^e|$ for resonance energies above 10 eV.
For the applications presented here, this arbitrary energy limit establishes

the division between F_{COLD} and F_{HOT}. At these energies the mean free path of the hot plasma particles are so long that they follow conventional first-order trapped orbits in the magnetosphere. The cold plasma, however, behaves like a Maxwellian gas similar to its diffusive source, the ionosphere.

According to Liouville's theorem, the hot plasma distribution, F_{HOT}, is prescribed everywhere in terms of its equatorial distribution Since trapped-particle data is generally in the form of separate pitch-angle and energy distributions, the models for F_{HOT} are assumed to have the form

$$F_{HOT} = G(v) \, H(\alpha) \qquad (16)$$

Along the flux tube G is obviously invariant because particle energy is conserved in the geomagnetic field, but H is not constant. Using the Liouville theorem and the conservation of magnetic moment, it is easily proved that

$$H(\alpha) = H_0 \left(\sin^{-1} \left[(B_0/B)^{1/2} \sin \alpha \right] \right) \qquad (17)$$

where H_0 is the equatorial distribution.

F_{HOT} is normalized to the experimental data in the following manner. The pitch-angle distribution is arbitrarily normalized to unity,

$$4\pi \int_0^{\pi/2} H_0 \, (\alpha) \, \sin \alpha \, d \, \alpha = 1 \qquad (18)$$

and the speed distribution is based on experimental differential density spectra, dN/dE, which are related as follows:

$$dN/N_o \ dE = G \ v^2 \ dv/dE \tag{19}$$

The experimental data for energy and pitch angle distributions of interest in this application are introduced in the following sections of the document.

A computer program for evaluation of the cyclotron-resonance interaction has been prepared based on the foregoing theoretical expressions. A complete listing of the program and its sub-routines is included in an Appendix. The program is designed to handle both electron interactions with VLF and proton interactions with ULF separately. The output of the program includes listings of the amplification exponent k_i as a function of geomagnetic latitude along the propagation path and the net path amplification A for a range of frequencies. In general, these two quantities completely specify the quantitative characteristics of the interaction.

A variety of quantitative models for stimulation of wave amplification are treated in the following sections.

VLF AMPLIFICATION

The artificial stimulation of VLF amplification in the magnetosphere is relatively easy to achieve because of the variety of injection materials and conditions that are available. However, the energetic electron distribution that is responsible for amplification changes its shape (Frank, 1967, 1968) depending upon the state of disturbance in the magnetosphere. Thus, it is important to choose the proper time for injection of plasma clouds that can induce amplification via the cyclotron-resonance interaction. Several cases of interest are modelled quantitatively in the following subsections.

Before discussing specific cases it is necessary to introduce the models for the energetic electron pitch angle and energy distributions. The pitch angle distributions, H_0, are assumed to be of the form $\sim \sin^m \alpha$ which are typical of experimental observations in the magnetosphere (O'Brien, 1963). In practice the model distributions are distorted at small pitch angles in order to introduce an atmospheric loss-cone cutoff at an equatorial pitch angle of 10°. Some cases of interest are illustrated in Figure 1 where the isotropic distribution corresponds to $m = 0$ and the two anisotropic cases, $m = 1$ and $m = 2$, are typical of the energetic electrons in the magnetosphere.

As indicated in the preceding theoretical discussion, the energy distribution may be subdivided into a cold and a hot component. The cold background plasma is relatively more dense and is assumed to have a Maxwellian energy distribution with a mean energy on the order of 0.1 eV.
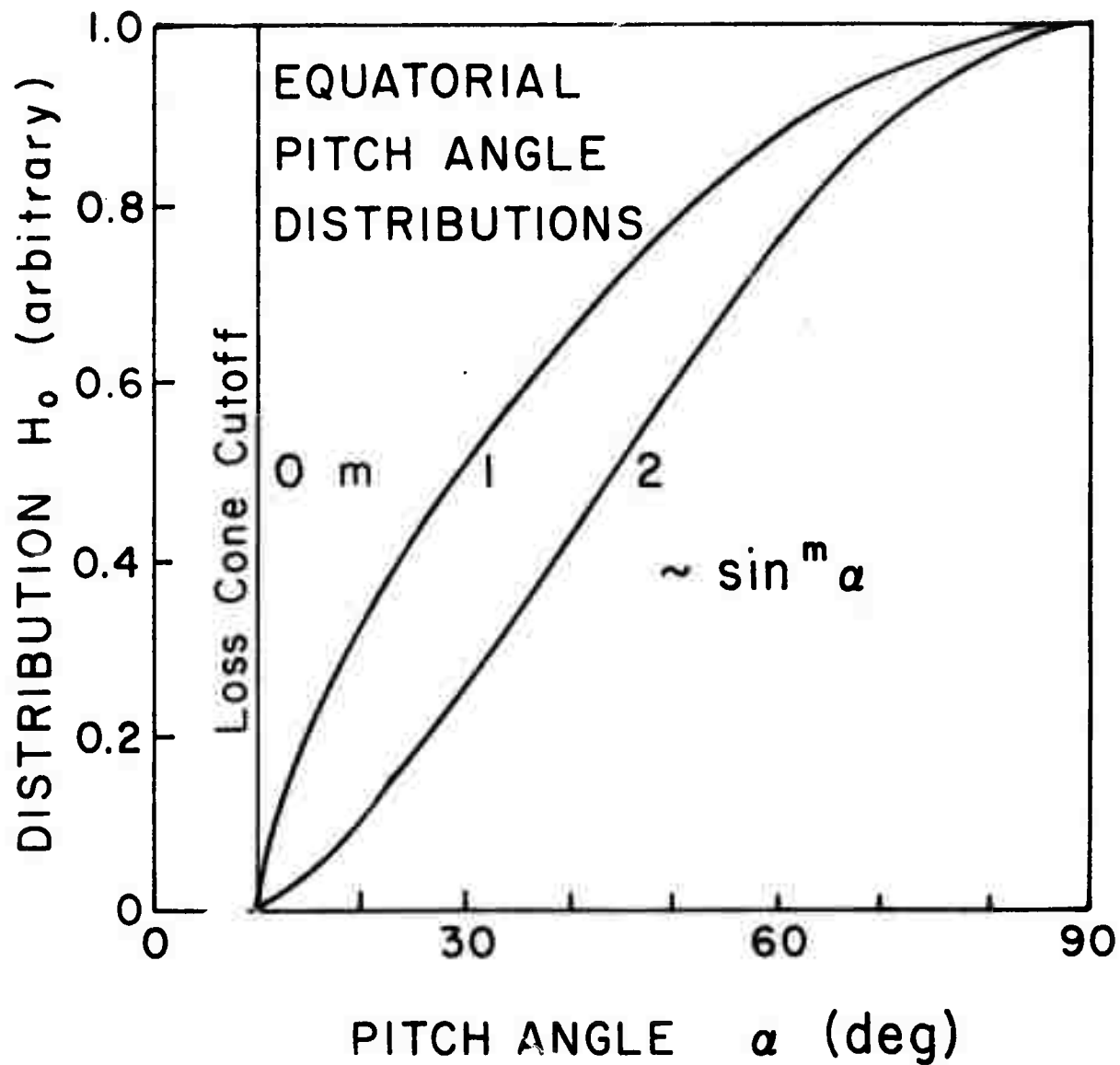
Fig. 1 Pitch Angle distribution models H_0 at the geomagnetic equator.
These anisotropic models including a loss cone cutoff are used
for both electrons and protons in the magnetosphere.
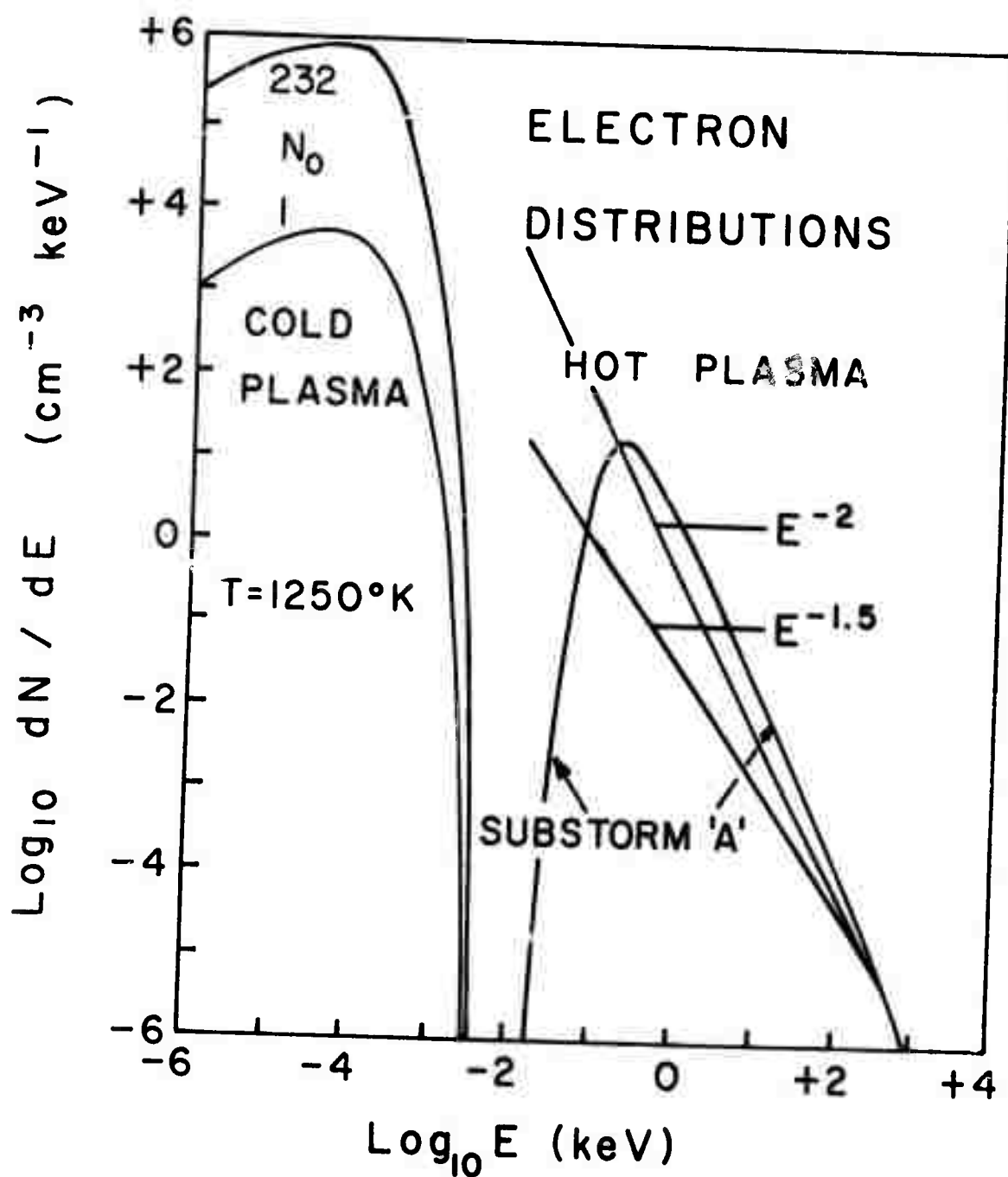
Fig. 2 Typical electron energy distributions in the magnetosphere.
Both the cold background plasma and the hot energetic
particles are illustrated to show their relative magnitudes
and locations on the energy scale. Some of the calculations
are performed for energy distributions of the form E^{-n} that
are typical of many observations. The substorm distribution
'A' was measured on the ATS-5 satellite at geosynchronous
orbit (DeForest and McIlwain, 1971).

It controls the propagation characteristics of VLF waves but transfers
negligible energy to the waves. The hot electrons in the energy range
from 0.1 to 100 keV are responsible for the resonance energy exchange
at VLF in the magnetosphere. Typical electron distributions which are
used here are illustrated in Figure 2. The substorm distribution "A"
is based on satellite observations (DeForest and McIlwain, 1971) located
at $L = 6.6$ in a geosynchronous orbit. The distributions E^{-n} where $n = 1$ or 2
are fairly good approximations to conditions throughout the region inside
the geosynchronous orbit, including the transition across the plasmapause.

Natural Density Enhancements. During disturbed conditions in the
magnetosphere the location of the plasmapause can shift appreciably in its
L-shell location causing local density variations of 1-2 orders of magnitude.
Such changes can cause major modifications in the energy exchange between
VLF waves and energetic electrons which results in a major revision of the
dynamic equilibrium state of the magnetosphere (Brice and Lucas, 1971).

The specific case chosen for analysis is assumed to occur inside the
plasmasphere where the plasma density is assumed to increase by a relatively
small amount. However, the increase in amplification may account for the
VLF emission and whistler activity that is observed in the plasmasphere.
The cold plasma is modeled by the hydrostatic equilibrium described by
equation (14). A propagation path along $L = 4$ is assumed for illustration
with an ambient plasma density of $N_0 = 232$ cm^{-3} and an inhancement to
$N_0 = 733$ cm^{-3}.

The hot electron distribution is assumed to have the form $E^{-1.5} \sin \alpha$ corresponding to the models given in Figures 1 and 2. The change in the amplification exponent due the density enhancement is illustrated in Figure 3 for two frequencies of interest. Although the change in the amplification exponent appears relatively small, the net path amplification is increased by about 5 db (decibels) as shown in Figure 4.

These figures illustrate some important features of the amplification exponent and the net path amplification at VLF. First, the exponent, k_i, varies rapidly with geomagnetic latitude and depends strongly on the local plasma and cyclotron frequency parameters as well as the propagation frequency. Its value at the geomagnetic equator is not a good indicator of its overall average throughout the region of interaction. The amplification actually peaks sharply some 10° to 20° from the geomagnetic equator. At the higher frequencies the signal is sharply attenuated near the geomagnetic equator due to the interaction with lower energy particles which can enter the resonance band. The interaction decreases sharply at some 30° to 40° from the geomagnetic equator because the Doppler shift becomes too large for even very energetic particles to contribute appreciably to the amplification.

The shape of the net path amplification depicted in Figure 4 is typical of the natural growth that can be expected at VLF. The location of the frequency at which maximum amplification occurs and the location of the upper cutoff where amplification ceases depends primarily on the shape of the pitch angle distribution, i.e., exponent m. The relationship
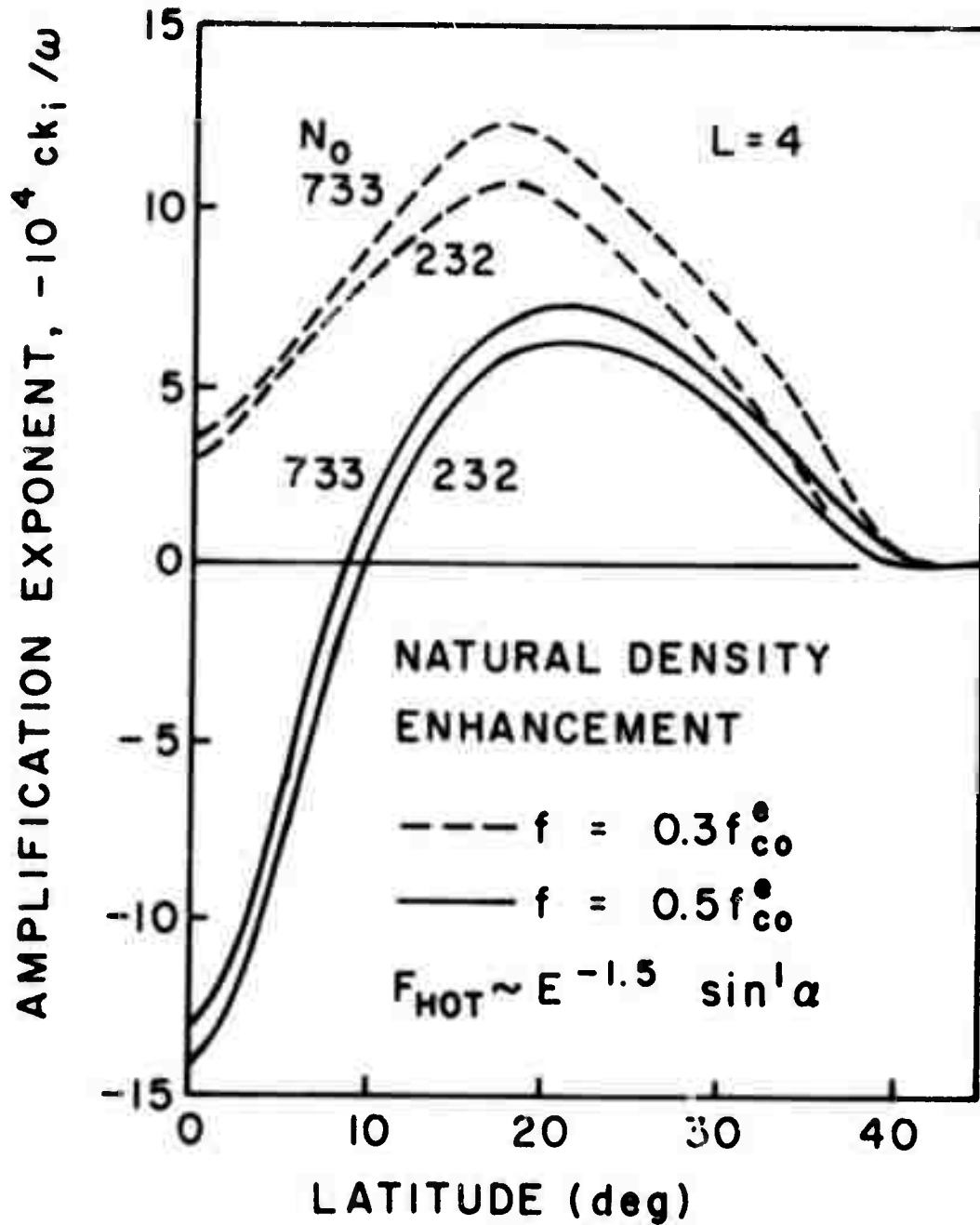
Fig. 3 Increased amplification exponent for VLF waves due to a natural
enhancement in the cold plasma density. The propagation at
L = 4 is assumed to be inside the plasmasphere where the cold
plasma is in hydrostatic equilibrium. For this case, the hot
plasma is assumed to have an energy and pitch angle distribution
of the form $E^{-1.5}$ sin α (see Figures 1 and 2).
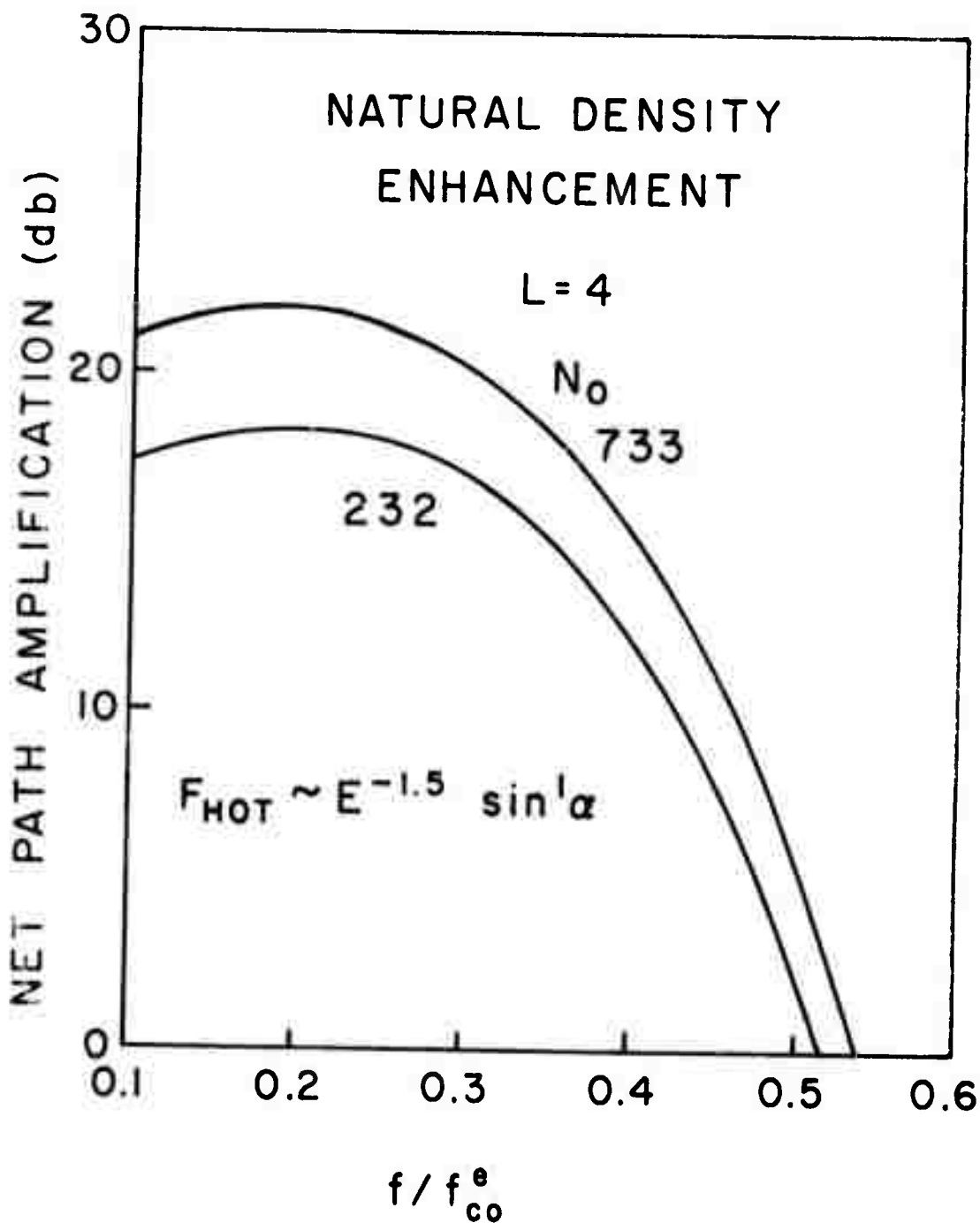
Fig. 4 Increased net path amplification of VLF waves due to a natural
enhancement in the cold plasma density. The propagation path
at L = 4 is assumed to be inside the plasmasphere where the
cold plasma is in hydrostatic equilibrium. For this case,
the hot plasma is assumed to have an energy and pitch angle
distribution of the form E-1.5 sin α (see Figures 1 and 2).

between the upper cutoff frequency and this anisotropy index m was
discussed following equation (9) above. The cutoff location is shifted
somewhat in the inhomogeneous magnetosphere where the effect is smeared
out by the variable parameters of the background medium. The magnitude
of the amplification in general depends on the density of the energetic
particles available to exchange energy with the wave at the resonance
velocity. The shape of the curve for amplification depends on the
shape of the energy distribution, that is, the value of n. As n increases
the bandwidth of amplification tends to increase with it. Of course
all of these characteristic variations depend on both m and n in a
complicated way which is difficult to separate. More complete discussions
of these dependencies on the shape of the distribution function can be
found in the earlier literature (e.g., Liemohn, 1967).

Barium Jet in the Plasmatrough. The technology for rocket injection
of barium has progressed to the point where jets can be propelled along
the geomagnetic field lines by shaped charges located in the nose cone of
the rocket payload.[1] Weight limitations on the launch vehicle limits the
amount of barium to approximately one kgm which corresponds to 5×10^{24}
barium atoms. Energy from the shaped charge as well as the sunlight
rapidly ionizes this barium so that the ions and electrons are trapped
along the geomagnetic field. Apparently plasma instabilities occur in the

[1] Shaped charge injections of barium were carried out in a series of
experiments from Alaska and Hawaii in March and October, 1972, by
Dr. Milton Peek of the Los Alamos Scientific Laboratories. The jet
of neutral barium was quickly ionized and followed the geomagnetic
field line to the opposite hemisphere from its injection region. The
purpose of these experiments was to map the geomagnetic field by
following the optical emission from the cloud of barium ions.

charged cloud and cause striations that reduce the effective density of the beam. Nevertheless tests have shown that an appreciable fraction of the injected barium does progress up the field line toward the other hemisphere.

The leading edge of the barium jet travels at about 14 km/sec and the trailing edge at 9 km/sec. Thus, at the geomagnetic equator along the field line at L = 4, the equatorial enhancement is approximately 15,000 km long and about 15 km in diameter. This corresponds to a volume of approximately 3×10^{21} cm^3. From the intensity of the optical emission, the equatorial density is approximately 2-3 barium ions/cm^3. Approximately 40-50 minutes is required for the jet to reach the geomagnetic equator along L = 4.

On the basis of the foregoing parameters and experimental evidence, a model of the barium injection has been constructed to evaluate its effect on the cyclotron resonance interaction. Some 15 minutes after the release along L = 4 the primary jet is bounded between 30° and 38° from the geomagnetic equator and has a density of approximately 30 ions/cm^3. At 30 minutes, the jet is bounded by 8° and 25° from the geomagnetic equator, and the density has reduced to 5 ions/cm^3. The reduction in density is due to the increased diameter of the jet as well as its elongation. In order for these enhancements to be significant relative to the natural plasma background, the injection must occur during a mild geomagnetic substorm when the plasmapause is inside L = 4. The ambient natural density in the plasmatrough is assumed to be 1 electron/cm^3 and vary radially as as R^{-3}. These properties of the barium shaped-charge injection model are illustrated in Figure 5.

BARIUM SHAPED –
CHARGE INJECTION
L = 4.0 TRAJECTORY

15 min
N_i = 30 cm^{-3}

30 min
N_i = 5 cm^{-3}
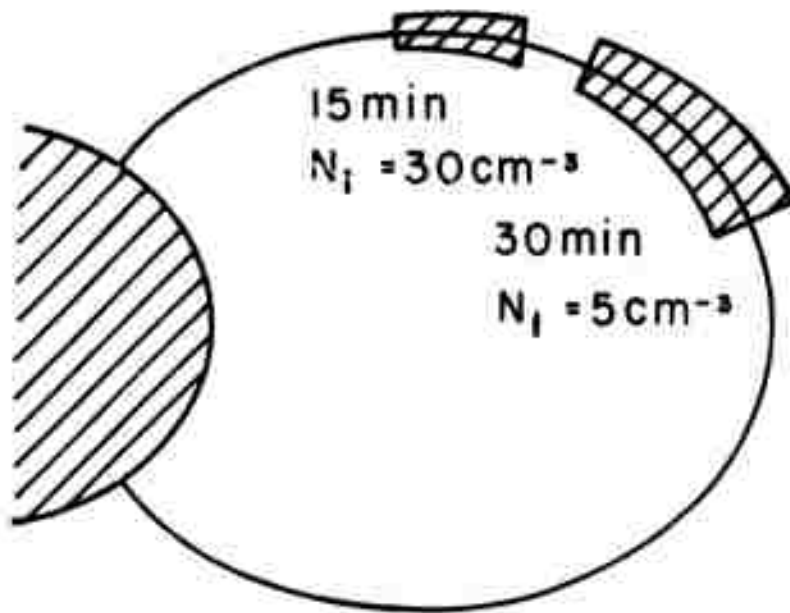
AMBIENT $N = 1.0 (4/R)^3$ (cm^{-3})

Fig. 5 Rocket injection of a barium shaped-charge along the L = 4 field line. The barium jet is assumed to consist of 1 kgm of fully ionized gas. The trajectory is assumed to be in the plasmatrough, where N_0 = 1 electron/cm^{-3} and N varies as R^{-3}.

An important aspect of the problem that is not included explicitly in the amplification calculation is the diameter of the barium ion jet relative to the size of the VLF wave front. As noted in the theoretical section, it is important that any enhancement be comparable to or larger than a wavelength in all of its dimensions. Using the experimental observation of 15 km as the diameter of the barium ion jet at the equator, the diameter at 15 minutes is approximately 7.5 km and at 30 minutes, 11 km. For a propagation frequency of 6 kHz, which is approximately half of the quatorial electron gyrofrequency at L = 4, the free space wavelength is about 50 km. However, the index of refraction within the barium cloud enhancement is approximately 10 in both cases so that the effective wavelength is somewhat less than the actual diameter of the cloud. Thus, to a first approximation, the cyclotron resonance interaction should not be limited by the width of the jet.

The amplification exponent for the interaction of VLF waves within the barium jet at 15 and 30 minutes is illustrated in Figure 6. Evidently the interaction is strongly enhanced as the jet approaches the geomagnetic equator, which is not unexpected due to the smaller Doppler shift that is required. Furthermore, the exponent is strongly enhanced only in the local region of the barium jet. Note the opposite behavior of the exponent, k_i, for the propagation frequencies 0.3 and 0.5 f_{co}^e at 15 and 30 minutes, respectively. This is readily explained by changes in the relative magnitudes of the growth and decay terms in expression (2). The hot plasma which provides the energy for the amplification is arbitrarily assumed to
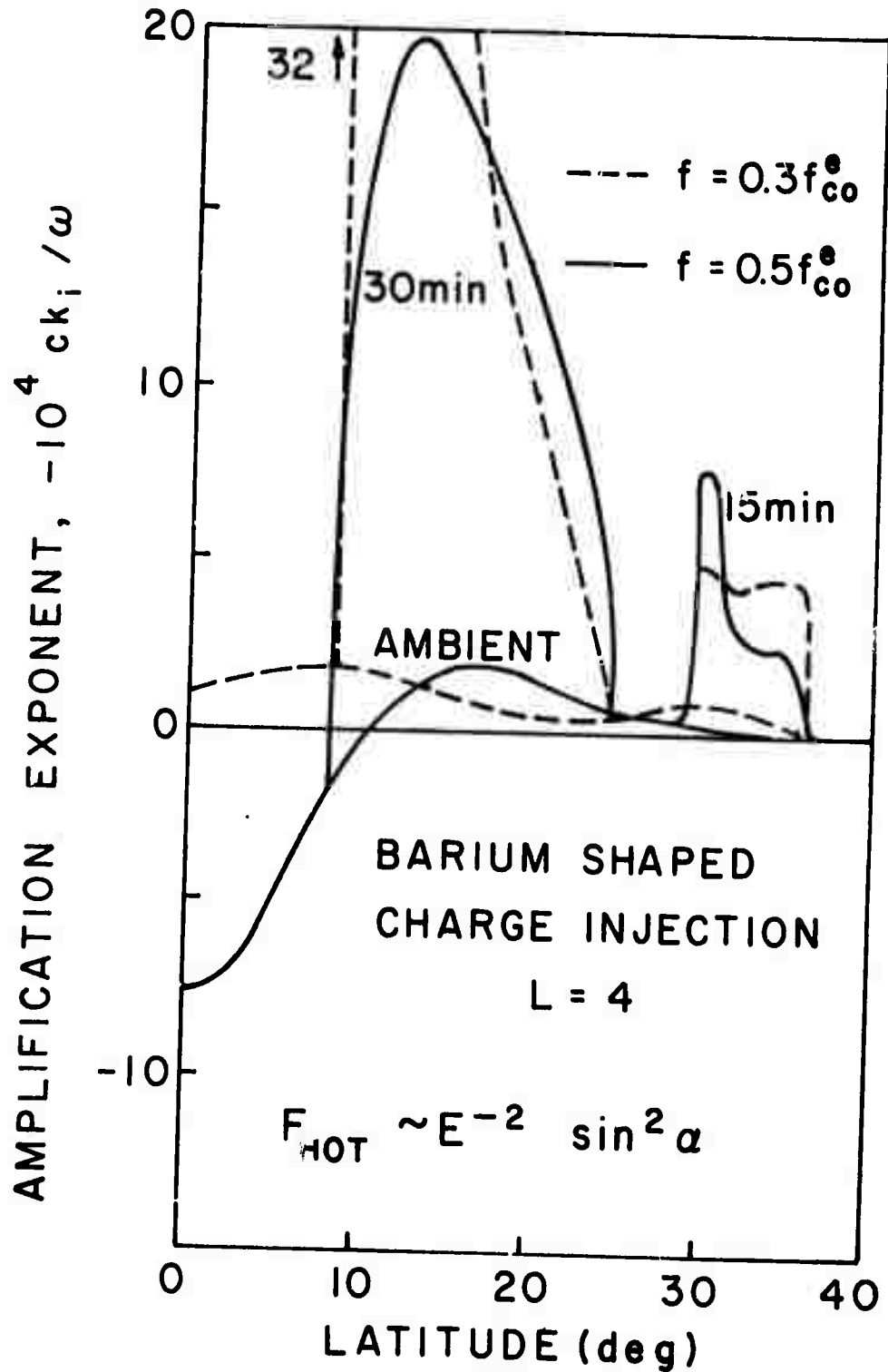
Fig. 6 Amplification exponent for VLF waves propagating through the barium shaped-charge injection along $L = 4$. The hot electrons are assumed to have the distribution $E^{-2} \sin^2\alpha$ (see Figures 1 and 2).
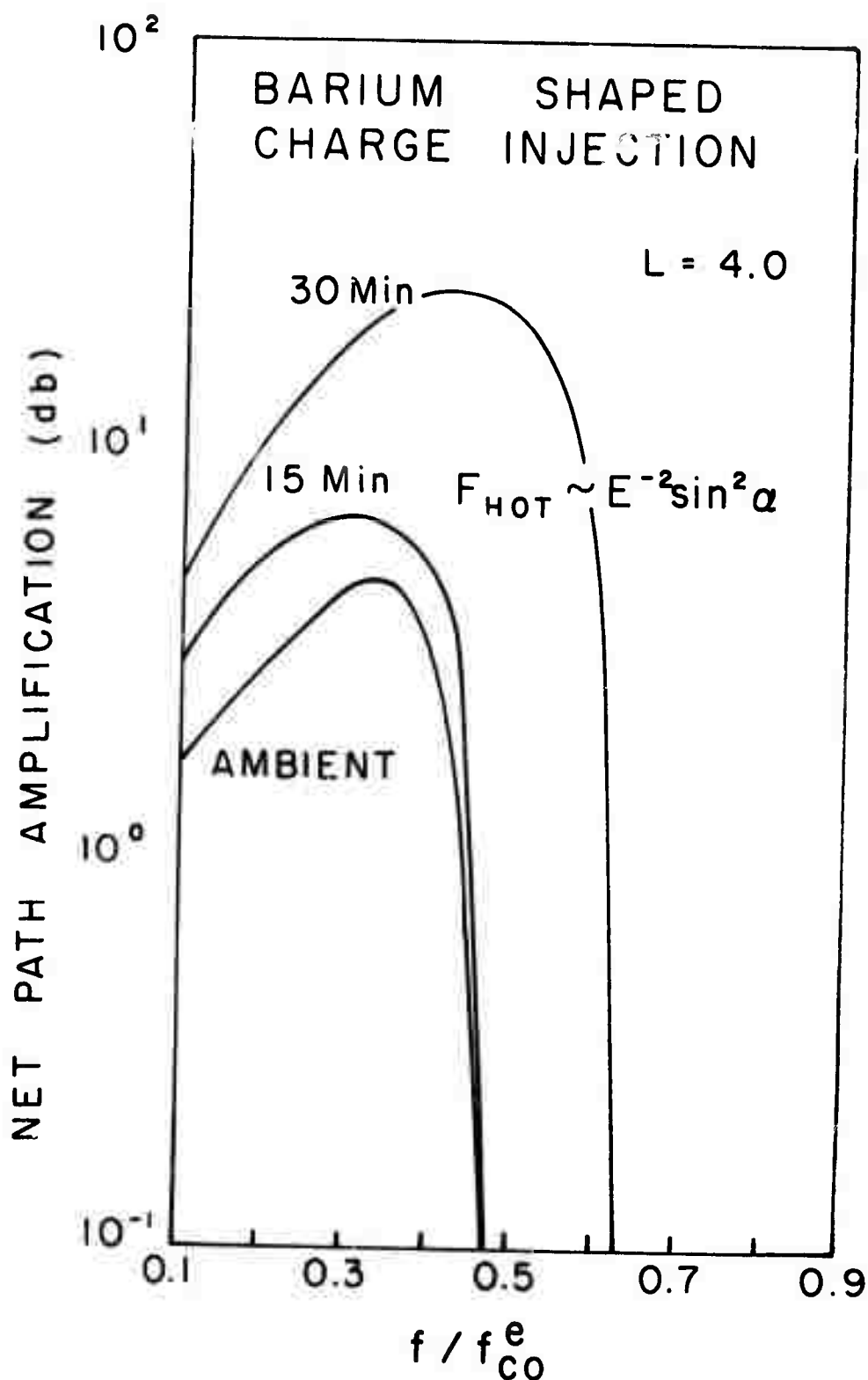
Fig. 7   Net path amplification for VLF waves propagating through the
barium shaped-charge injection along L = 4. The hot electrons
are assumed to have the distribution $E^{-2} \sin^2\alpha$ (see Figures 1
and 2).

have the form $E^{-2} \sin^2 \alpha$ which is a reasonable approximation for the electron energy distribution in the plasmatrough during a geomagnetic storm.

The net power that can be transferred from the energetic electron distribution to VLF waves by the barium shaped-charge enhancement is illustrated in Figure 7. Evidently the amplification some 15 minutes after the injection is still negligible below f_{co}^{e}, but after 30 minutes the amplification has increased 20-30 db and the bandwidth has been expanded somewhat. At L = 4, it has been noted that f_{co}^{e} = 13.6 kHz, so that the 30 minute amplification band is between 4 and 8 kHz.

Geosynchronous Lithium Clouds. One of the more promising methods for inducing strong amplification of waves in the magnetosphere is by injection of a cloud of lithium at the geosynchronous orbit. Lithium has a relatively slow rate of ionization in solar ultraviolet so that the cloud of neutral atoms can diffuse radially for approximately an hour before most of it is ionized and trapped by the geomagnetic field. Although this slow rate of lithium-ion generation does not permit its application as a communication method, the diameter of the cloud makes it a strong contender for a quantitative test of the theory. Furthermore, the large area that would be illuminated with VLF noise at the ground makes it attractive from an observational standpoint.

The distribution of the geosynchronous lithium injection has been modeled by the solution of the diffusion equation for a point source of particles. The density, N, is given as a function of radial distance, r, (from the source point) and time, t (measured from an arbitrary instant of the release), by the equation,

$$N = N_1 \exp (-r^2/4D^2t^2)/(4\pi D^2t^2)^{3/2} \qquad (20)$$

where N_1 is the number of lithium ions injected and D is the diffusion coefficient for the cloud of particles. In such a solution no attempt is made to include the dynamic process for ionization of the lithium atoms; instead, it is assumed that N describes the current number of ions in the cloud at time t.

For this application the value of N_1 is assumed to be 8.5×10^{25} molecules corresponding to 1 kgm of fully ionized lithium. The diffusion coefficient, D, is assumed to be 1 km^2/sec, which gives cloud diffusion rates in good agreement with observations. The induced amplification has been evaluated for distributions corresponding to 10 minutes after release and 50 minutes after release of the lithium charge. The electron density enhancements corresponding to these release times are illustrated in Fig. 8 as a function of geomagnetic latitude. The natural background density is arbitrarily assumed to be 1 electron/cm^3 which is a reasonable limit at the geosynchronous orbit (L = 6.6). Since it requires approximately one hour for sunlight to fully ionize the lithium atoms in the cloud, it requires at least five times as much lithium to achieve one kilogram of ionization in 10 minutes as it does in 50 minutes. If the lithium release from the canister is only 10 percent efficient, as some researchers have suggested (Cornwall private communication), then the amplification enhancement at 10 minutes requires a lithium payload of 50 kgm plus a detonating charge whereas the amplification at 50 minutes requires only 10 kgm of lithium plus charge.
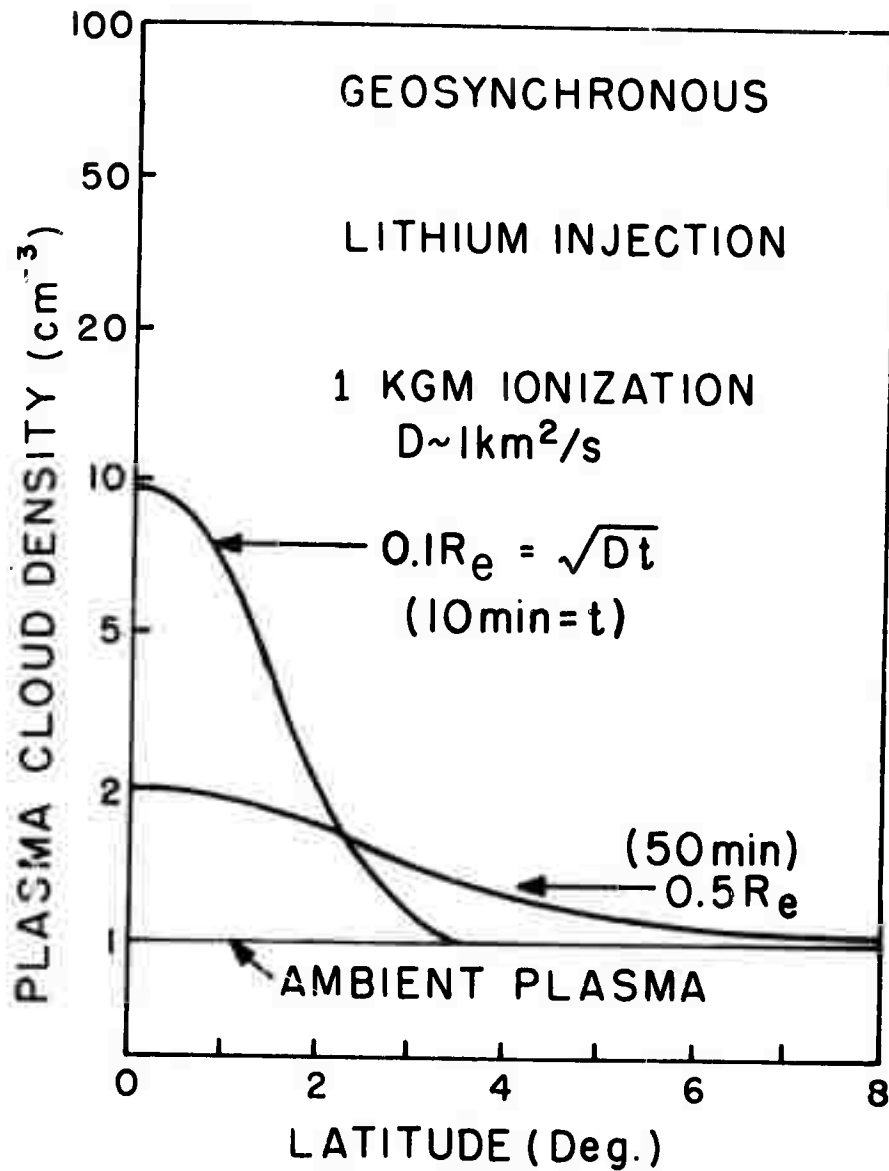
Fig. 8 Injection of lithium from a point source (cannister) in geo-
synchronous orbit (L = 6.6). One kgm of total ionization is
assumed to be diffusing spherically from the source with a
diffusion coefficient D ~ 1 Km²/s. The ambient background
plasma is assumed to be in the plasmatrough where N_o = 1 cm^{-3}.

The effect of this geosynchronous lithium injection on VLF wave amplification is illustrated for two hot plasma distributions in Figures 9-12. For one case, the hot electron distribution is assumed to have the form $E^{-1.5} \sin \alpha$ (see Fig. 2) which is taken to represent conditions at the geosynchronous altitude during geomagnetically quiescent conditions. The second case is modelled after experimental observations of a typical substorm (DeForest and McIlwain, 1971) and is denoted by the functional form $(dN/dE)_{"A"} \sin \alpha$ (see Fig. 2). The VLF amplification results for these two distributions are discussed together in order to emphasize the physical aspects of the interaction.

The first and most obvious effect of the lithium injection is the concentrated enhancement of the amplification exponent, k_i, in the vicinity of the geomagnetic equator (see Figures 9 and 11), which is entirely attributable to the geometry of the enhancement. The second point of interest is the similar magnitudes of k_i for the two hot electron distributions, but note, however, that the frequencies are significantly lower for the distribution $E^{-1.5}$. Outside the frequency bands shown, the enhancement in the amplification is relatively negligible. Since all other parameters are held constant, the entire effect is attributable to the shape of the energy distribution, and points out the need for detailed observations of the phase-space distribution for an adequate quantitative test of the cyclotron resonance amplification.

The net path amplification from these two hot electron distributions are illustrated in Figures 10 and 12. The distribution, $E^{-1.5}$, provides strong amplification at frequencies below $0.35 \, f_{co}^e$. After 10 minutes
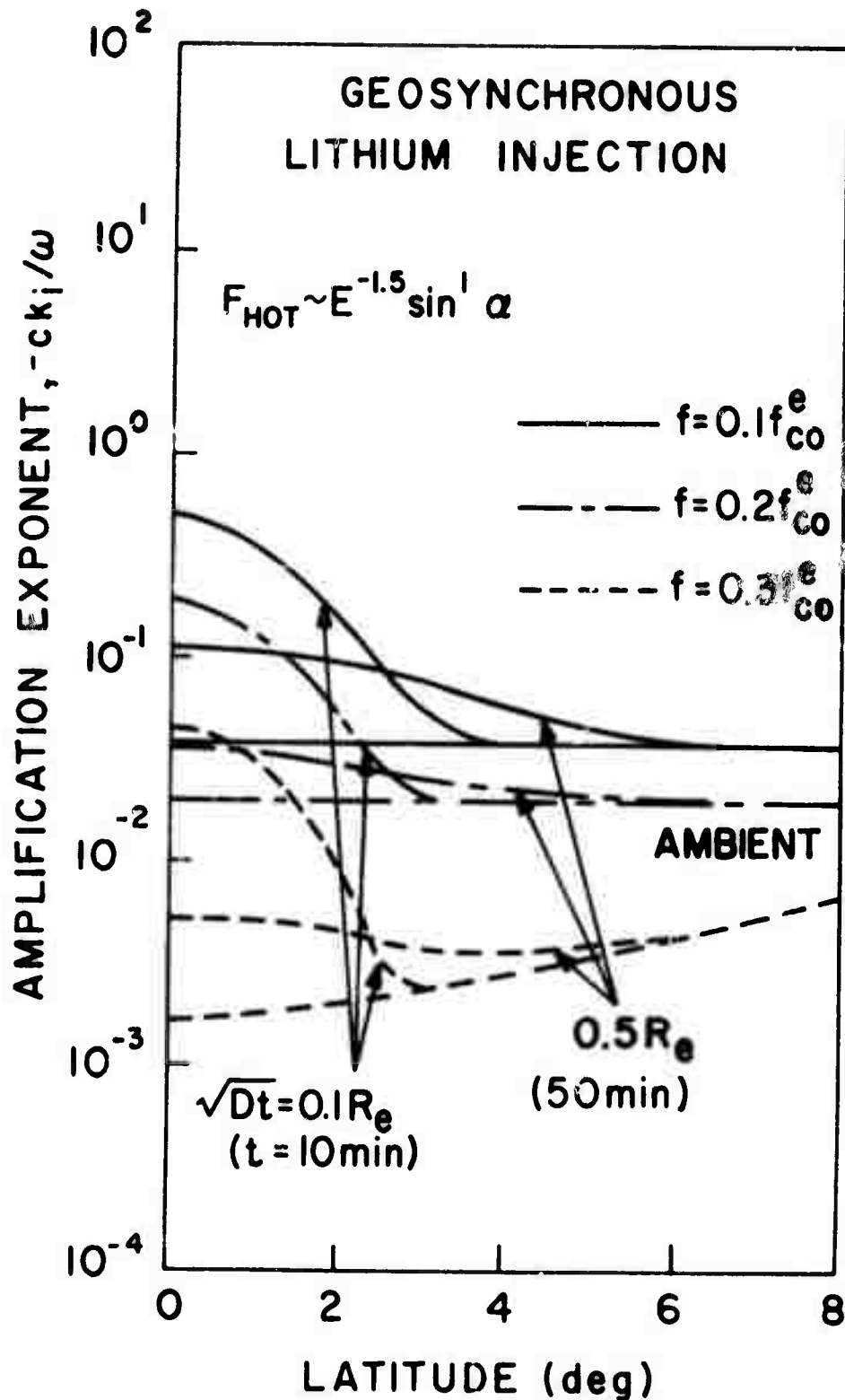
Fig. 9 Amplification exponent for VLF waves propagating through the geosyncrhonous lithium injection. The exponent is sharply peaked in the equatorial enhancement which has a mean diameter of about 6400 km at 50 minutes after injection. The hot electrons are assumed to have the distribution $E^{-1.5} \sin \alpha$.
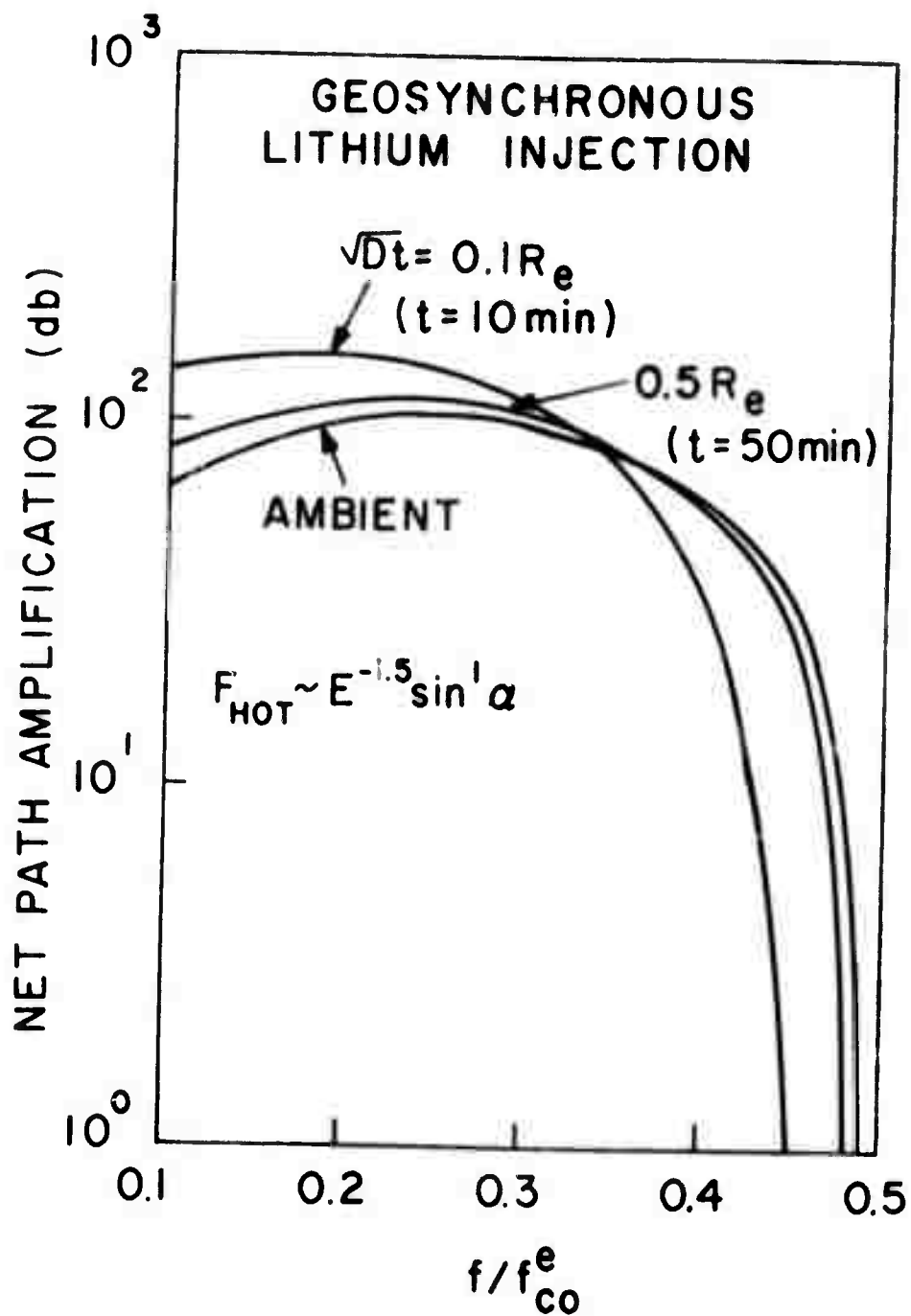
Fig. 10 Net path amplification for VLF waves propagating through a
geosynchronous lithium injection. The enhancement is entirely
attributable to the lithium bubble. The hot electrons are
assumed to have the distribution $E^{-1.5} \sin \alpha$.
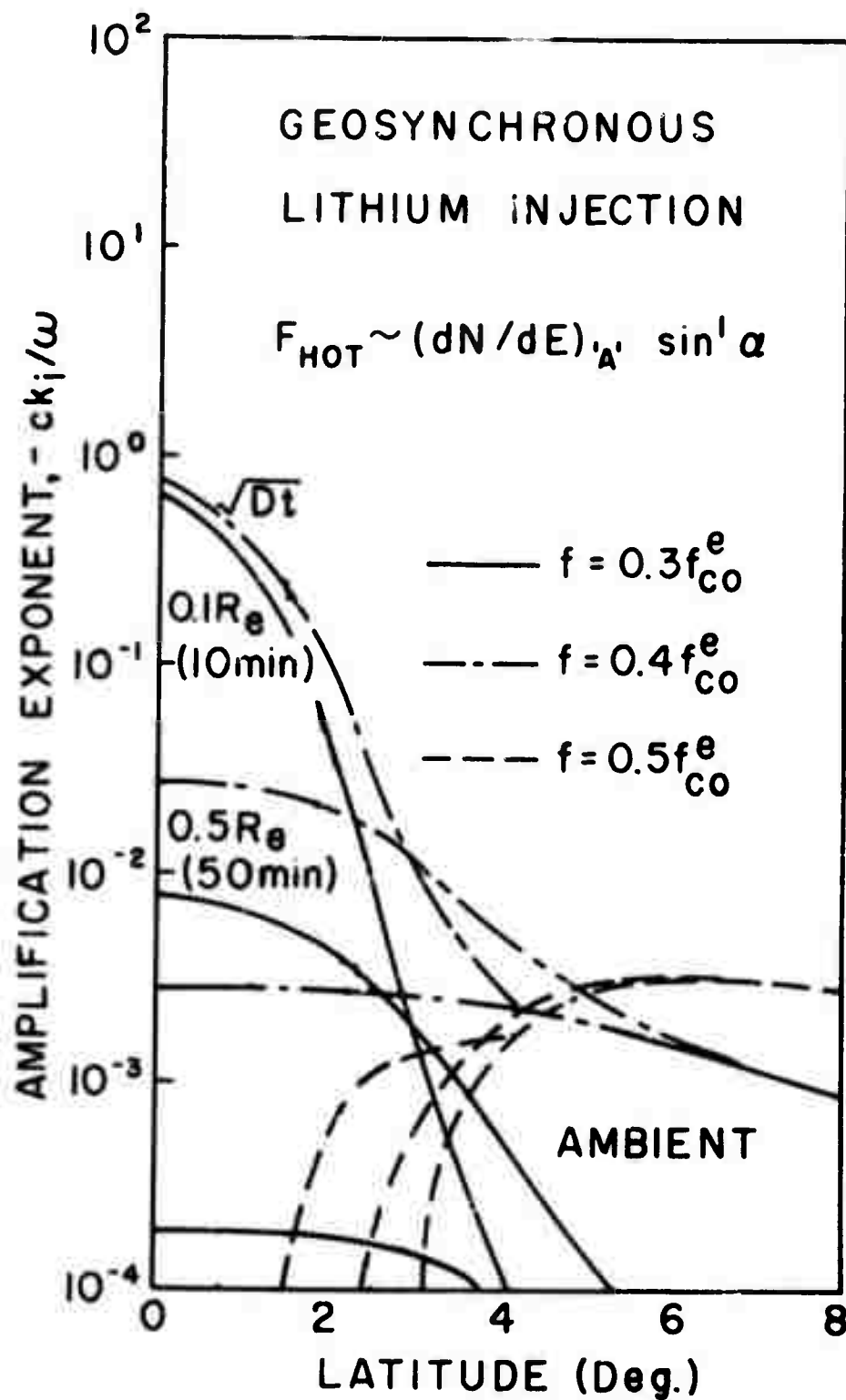
Fig. 11 Amplification exponent for VLF waves propagating through a geosynchronous lithium bubble. The hot electron distribution is based on Model 'A' for a typical geomagnetic substorm (see Fig. 2).
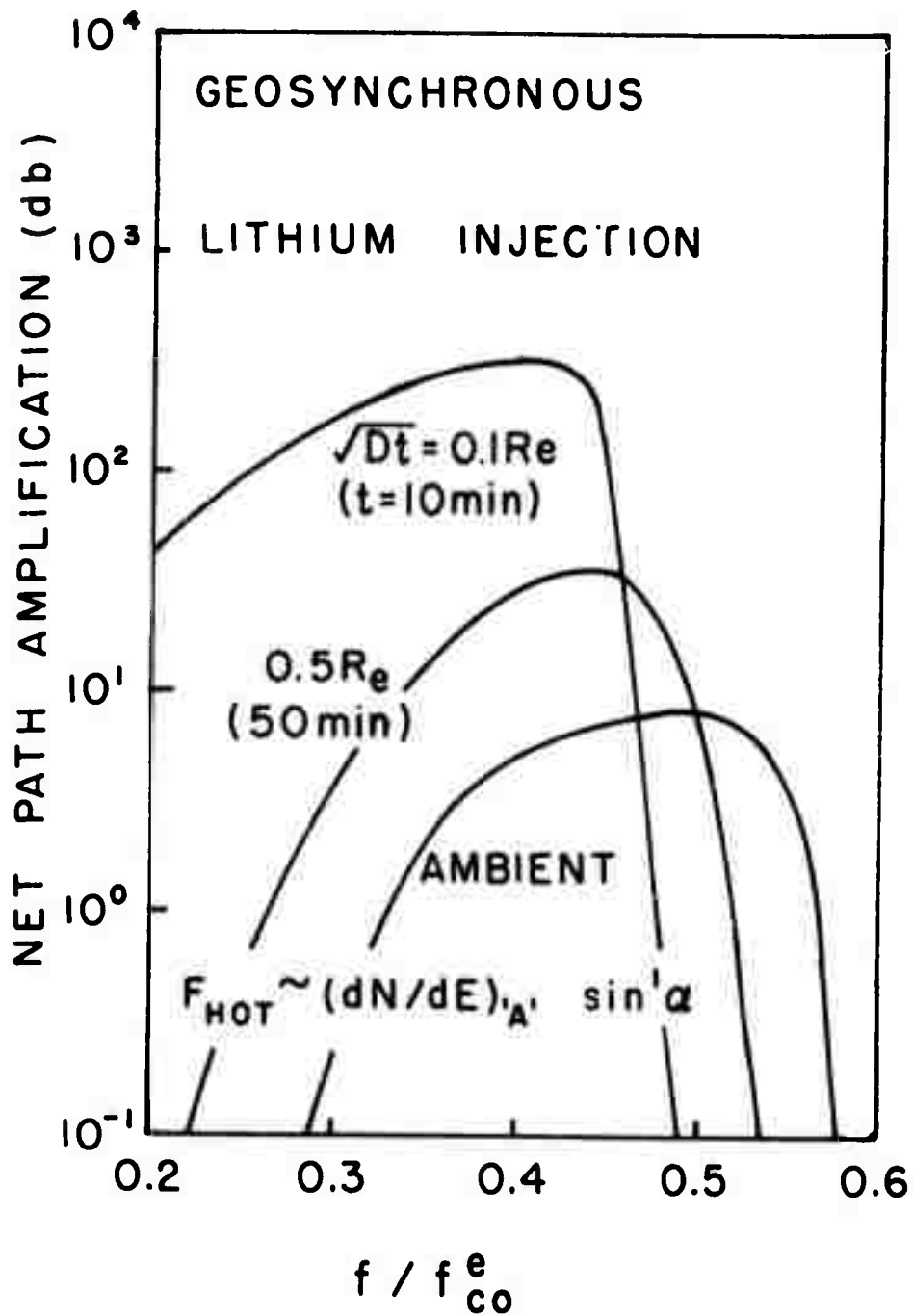
Fig. 12 Net path amplification of VLF waves propagating through a geosynchronous lithium bubble. The hot electron distribution is based on Model 'A' for a typical geomagnetic substorm.

the injection does provide about 30 db of enhanced amplification at
$0.1 - 0.2$ f_{co}^e, but after 50 minutes no appreciable enhancement is
discernible. This is to be contrasted with the amplification for the
substorm "A" where the ambient amplification is shifted to the frequency
band $0.4 - 0.55$ f_{co}^e. This frequency shift and the reduction in ambient
amplification by a factor of 20 is attributable to the depletion of
low-energy particles in F_{HOT} for distribution "A". For this substorm,
the amplification after 10 minutes is extremely high, on the order of
200 db. Such an amplification level could only be realized if the VLF
source is low-power incoherent particle emissions; normal VLF emissions
subject to this much amplification would become nonlinear and distort
the hot plasma phase-space distribution suppressing the net amplification.
From practical considerations, the most important result is the
amplification obtained 50 minutes after injection during a substorm.
For this case, the amplification has been enhanced some 40 db at a
frequency around 1.5 kHz. Such an effect should be readily discernible
from ground-based observations of VLF in the vicinity of the geosynchronous
conjugate points.

Energetic Electron Beams. The prospect of amplifying VLF waves
by direct injection of hot electron beams is attractive because the
net amplification is relatively insensitive to the state of geomagnetic
activity. The state of the natural background plasma is relatively
unimportant since the energy for wave growth is to be derived entirely
from the injected beam of particles. Thus, the process is no longer
catalytic in the sense of utilizing the hot electrons that are trapped
in the geomagnetic field, but rather is a direct stimulation of the
cyclotron resonance interaction. The entire process is quite analogous to
transmitting waves from an antenna on board a spacecraft. The amount
of amplification is obviously proportional to the intensity of the
beam.

In the analysis presented here, the beam is assumed to be launched
by a spacecraft along the geomagnetic field line at L = 4 which is
assumed to be inside the plasmasphere where N_0 = 232 electrons/cm^3.
The natural hot plasma background is assumed to have a distribution of
the form $E^{-1.5}$ sin α. These quantities merely serve to define the local
propagation conditions and the natural amplification along the propagation
path.

The electron gun is assumed to have a power level of 0.5 kilowatts.
For definiteness, the gun is assumed to generate 100 millisecond pulses
of electron current with a beam energy of 10 keV. At this energy,
the electrons have a speed of 6 x 10^4 km/sec and an equatorial gyro
radius (at L = 4) of approximately 1 km, depending of course on the
local pitch angle. Initially, such a beam would appear to be a helix
that is wrapped around the injection field line at the appropriate pitch
angle. However, electrostatic forces and plasma instabilities are

expected to smear out this geometrical form within 100 km or so from the injection point (Pellat, private communication), and the beam is more appropriately described as a flux-tube-column of electrons. Assuming an order of magnitude inflation in the cross section of the beam, the volume of the column is 2×10^5 km^3. Since 0.8×10^{18} electrons are contained in the pulse, the density of the beam is 0.004 electrons/cm^3. If the beam has an effective spread of 2 keV, this density corresponds to a differential energy spectrum of 0.002 electrons/cm^3 keV.

The foregoing considerations were employed to derive the electron beam model shown in Figure 13. The pitch angle distribution H_0 is normalized to unity and has a pitch angle spread of 10° corresponding a limited amount of scattering. The energy distribution, dN/dE, has been normalized to the value derived above with an appropriate energy spread which is attributable to scattering. In order to assess the effect of injection location and injection pitch angle, three values of the equatorial pitch angle are arbitrarily assumed for the beam model. For α_0 = 85° the beam mirrors at a latitude of $\pm$ 3°, for 55° the latitude is $\pm$ 18°, and for 25° the latitude is $\pm$ 37°. Of course the beams must be injected above these corresponding mirror point latitudes in order to achieve the model parameters.

The size of the beam cross section relative to the wavelengths of interest determines the effectiveness of the interaction. Near the geomagnetic equator at L = 4, the electron gyro frequency is 13.7 kHz and for a plasma density N_0 = 232 electrons/cm^3. The corresponding plasma frequency is 137 kHz. For a propagation frequency at half the gyro frequency, 7 kHz, the index of refraction is approximately 20,

ELECTRON   BEAM
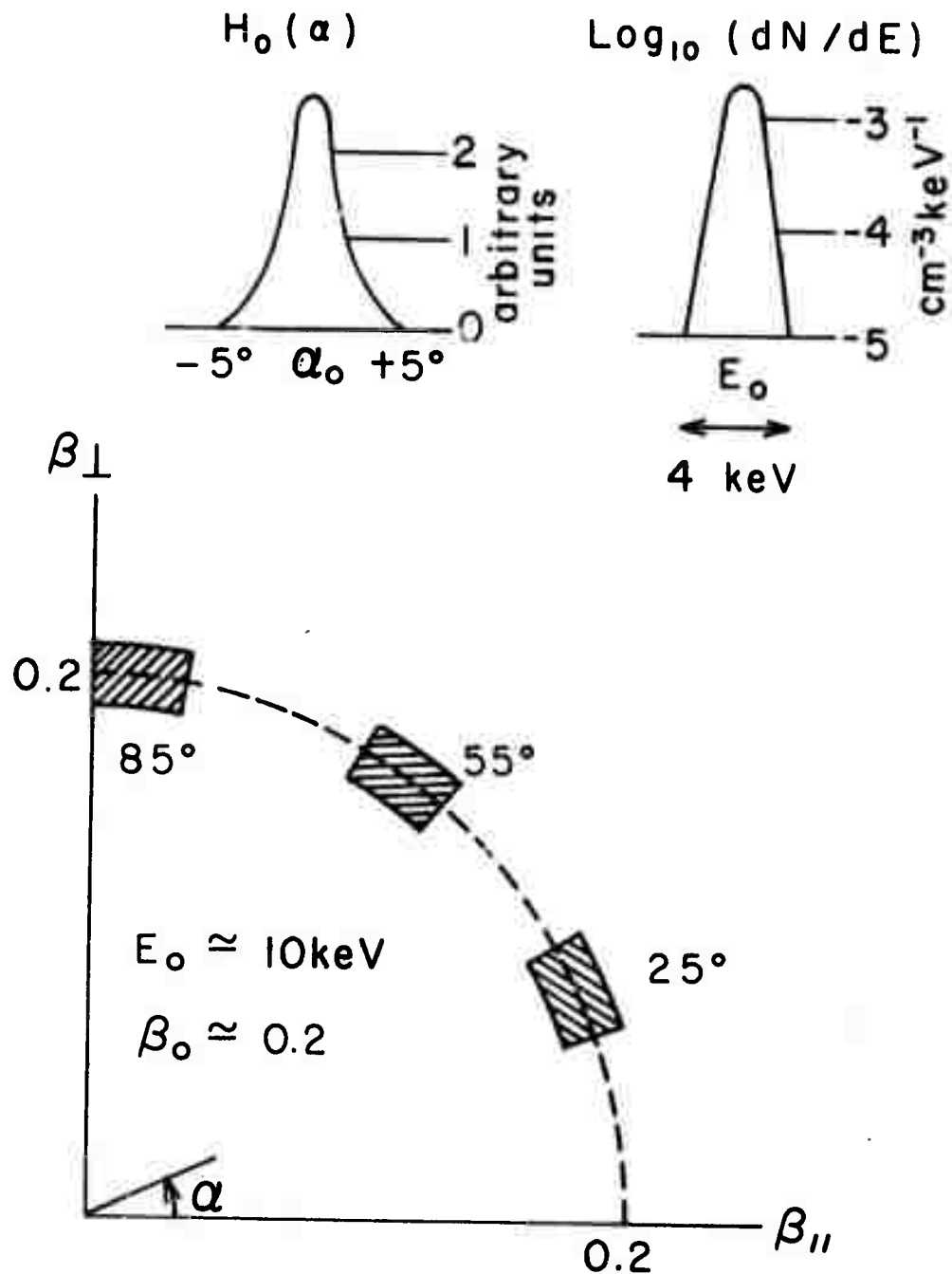
Fig. 13   Electron beam model distributions for pitch angle, H_0, and
differential energy, dN/dE.   The beam distributions
are sharply peaked in pitch angle and energy assuming a
particle gun deploys the beam from a satellite or very high
altitude rocket.

and the wavelength is 2.5 km. This is to be compared with a beam injection diameter of about 2 km. If the beam cross section expands by a factor of 10, as assumed, the cyclotron-resonance interaction between the beam and ambient VLF signals could be quite effective. However, it must be remembered that the interaction flux tube maps onto a very small region in the ionosphere so that the actual VLF energy flux may still be extremely small.

As noted in the introduction, electron beams with the foregoing properties have been generated experimentally (Hendrickson et al, 1971; Cartwright and Kellogg, 1971; and Hess et al, 1971). These beam experiments behaved qualitatively as expected, but many questions remain about the the quantitative aspects of their behavior. One important conclusion is that the well-known two-stream plasma instability does not effectively break up the beam as might be expected. Evidently there is enough spread in the thermal energy of the beam to quench the electrostatic waves that are predicted on the basis of delta-function beam distributions. These experiments and their analyses are continuing.

The cyclotron-resonance interaction between electron beams and VLF waves has some unusual properties due to the shape of the phase-space distribution. Adjacent to the central pitch angle and energy values of the beam, the distribution has exceedingly large derivatives which play a dominant role in the integrand of the amplification exponent, k_i, displayed in equation (2). Thus, in the vicinity of the resonance, there is strong absorption on one side and strong amplification on the other due to the change in sign of the derivative. This behavior is clearly illustrated in Fig. 14 for the case $\alpha_0 = 55°$ and $E_0 = 10$ keV. For a
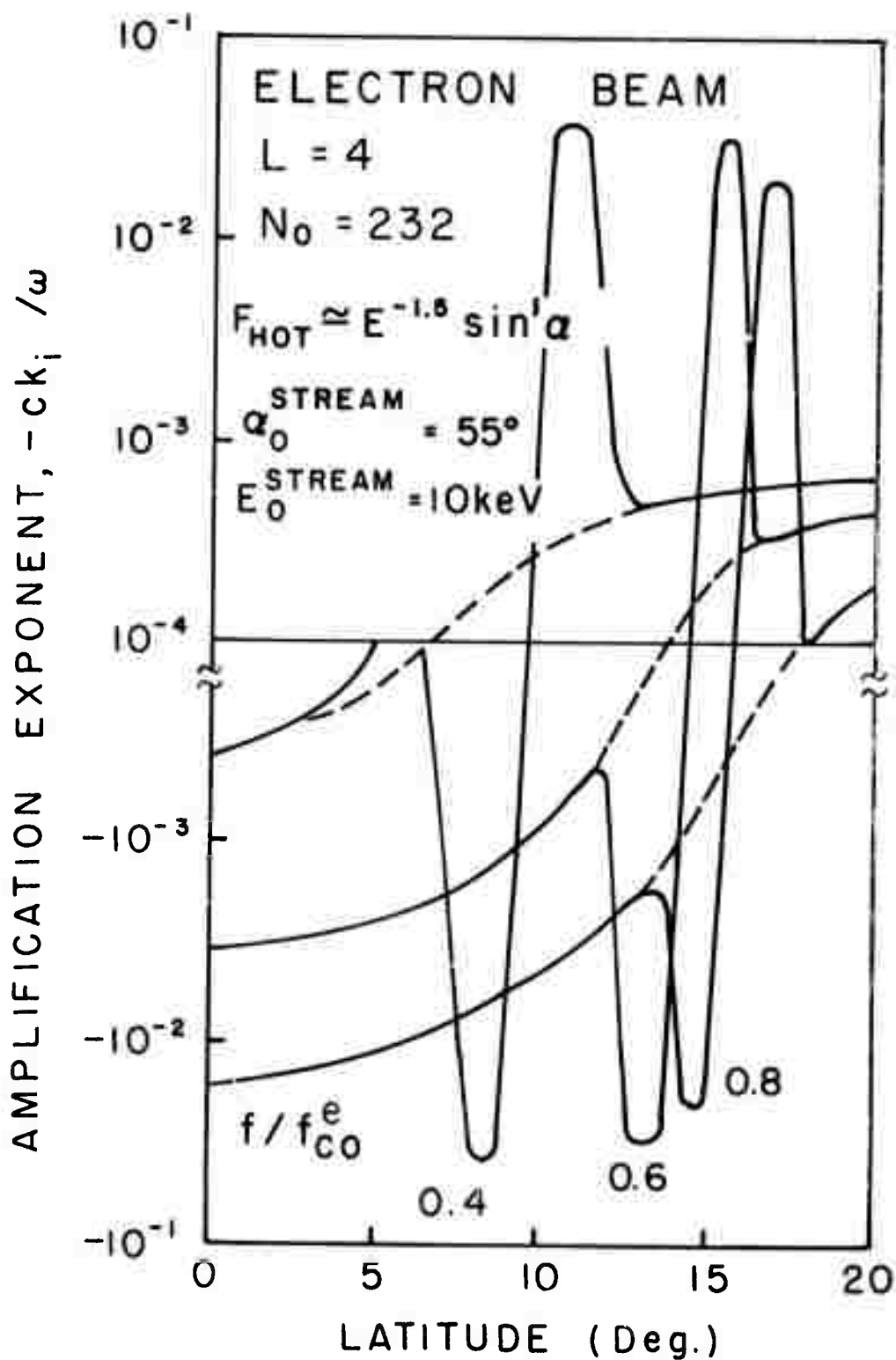
Fig. 14 Amplification exponent for VLF waves propagating tnrough an
electron beam along the field line at L = 4 inside the
plasmapause. The electron beam parameters are an equatorial
pitch angle of 55° and a particle beam energy of 10 keV. See
the text for an explanation of the shape of these curves.

given frequency the interaction is confined to a narrow band of geo-magnetic latitude where the parallel component of the beam velocity matches the resonance velocity given by equation (3). The fact that the absorption occurs on the equatorward side and the amplification on the earthward side of the interaction region is simply due to the values of the derivatives in k_i at the local resonance velocity. The location of the resonance region is further from the equator at the higher frequencies; this is wholly attributable to a reduction in the parallel velocity component of the beam as it progresses toward its mirror point and necessitates frequencies closer to the local gyrofrequencies to achieve resonance.

For the beam energy chosen in this analysis, the pitch angle distributions centered at 85° and 25° do not contribute significant effects. At 85° the entire interaction is extremely close to the geomagnetic equator and the parallel velocity component is relatively small demanding a frequency very close to the local cyclotron frequency where the amplification is also small. At 25° the beam has more parallel than perpendicular energy in the region of interaction so that the wave energy is absorbed by the particles, but again the interaction is relatively small.

The net path amplification for the three cases is illustrated in Fig. 15. Evidently, the interaction at 25° and 85° is essentially neutralized, that is, the absorption of VLF energy just balances the amplification. However, at 55° the absorption is clearly significant above 0.3 f_{co}^e. For this pitch angle the interaction is strongly dominated by the equatorward absorption.
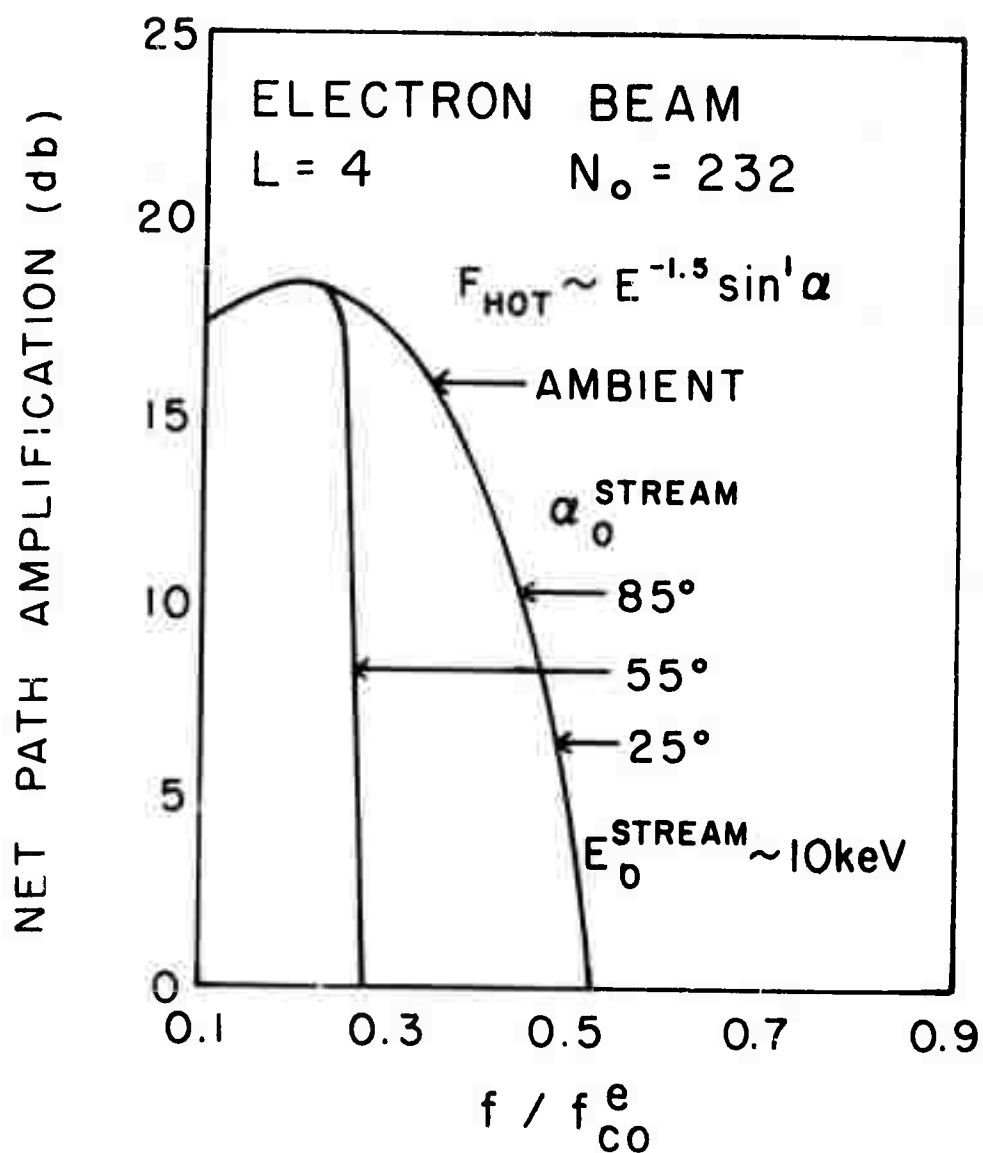
Fig. 15   Net path amplification for VLF waves propagating through an
electron beam at L = 4 inside the plasmapause. Equatorial
pitch angles for the beam are 25°, 55°, and 85° and the beam
energy is 10 keV. See the text for an explanation of the
shape of these curves.

These foregoing properties of the beam amplification provide an
unusual method for generation of narrow band VLF noise pulses. If the
beam is launched from its mirror point toward the equator, it is possible
for VLF noise to build up on the earthward side of the interaction
region and subsequently propagate toward the ionosphere. Since the
equatorward side of the interaction region is absorbing energy more
strongly, no signals from the equatorial region can penetrate through
the beam. Consequently, for any signals to be available for amplification
the electron beam and the natural background plasma must be spontaneously
emitting copious amounts of incoherent VLF noise. Our current under-
standing of this inchoherent noise source (Liemohn, 1965; and Trulsen
and Fejer, 1970) suggests that it is wholly inadequate. For example,
in Fig. 14 the amplification region alone can provide about 35 db but
the incoherent VLF signal is only 10^{-30} watts/Hz from each electron.
Nevertheless, it is intriguing to consider the possibility of generating
a succession of descending tone pulses with an electron beam.

Low-Energy Ion Beams. For this case, the attractive feature of injecting cold plasma to stimulate amplification by catalytic means is coupled with the advantages for direct control that are offered by the beam concept. In the magnetosphere a low-energy (eV) ion is subject to the forces of both gravity and geomagnetic gradients. The individual ions are reflected at low altitude by the geomagnetic gradient and driven toward the equator where gravitational forces take over and pull them earthward again. Thus, these ions are caught in intra hemisphere orbits which are nonlinear but quite repetitive. Such an orbit is illustrated in Figure 16 for a proton with energy 0.32 eV, and argon ion with energy 13 eV, or a cesium ion with energy 43 eV.

Such a beam does not interact with VLF waves, but it is accompanied by a cloud of neutralizing electrons that stimulate strong amplification by the hot (keV) electron plasma. The generation of such an ion beam by a particle gun on board a satellite or rocket requires a neutralizing source of negative charge such as a hot cathode emitting an electron current. If the ions follow a well-established trajectory, the electron gas will be dragged along with the ions by the ambipolar electric field. It is this cloud of electrons that actually enhances the cold plasma density and induces catalytic amplification of VLF waves along the field-line trajectory of the ions. The shape of the electron cloud is assumed to emulate that of the ion beam since the ambipolar field is localized and the ions are so much more massive.

Before undertaking a discussion of the beam interaction with VLF waves, the details of the individual ion motion in the gravitational and

MAGNETIC - GRAVITATIONAL TRAPPING

ION TRAJECTORY

E (H) = 0.32 eV

E (A) = 13 eV

E (Cs) = 43 eV

L = 4

INJECTION PITCH ANGLE = 90°

INJECTION LEVEL = 1600 KM
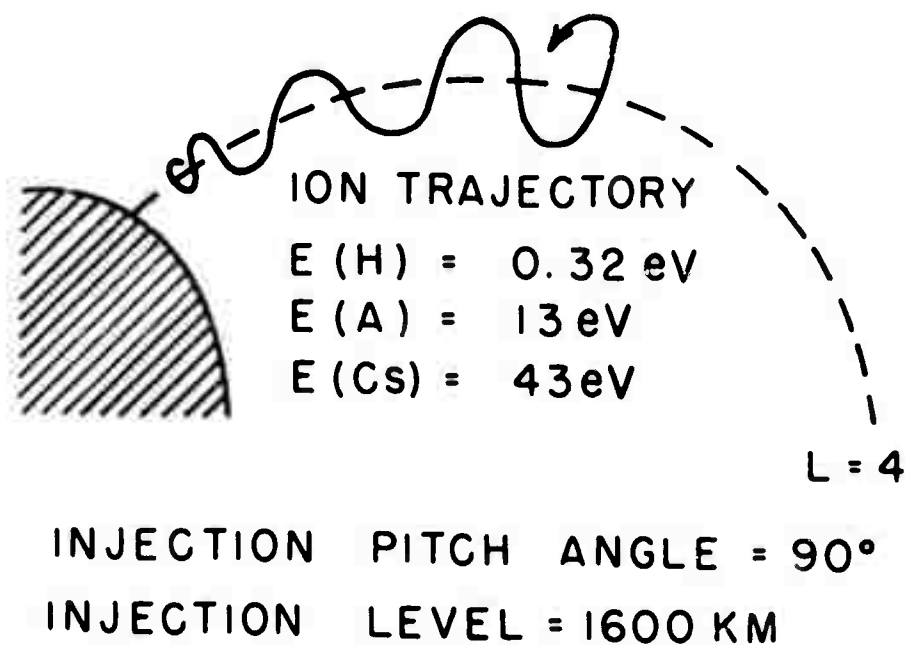
Fig. 16   Schematic diagram of magnetic-gravitational trapping of low
energy ions on an intra-hemisphere trajectory. Injection of
these low-energy ions above the ionosphere can produce a
sharp density enhancement along a portion of the flux tube.

magnetic field must be considered. The important forces acting on the ion are the gravitational component parallel to the local geomagnetic field and the field-aligned geomagnetic gradient force,

$$F_{GRAV} = m^1 \ g \ sin \ \psi/R^2 \tag{21}$$

$$F_{MAG} = -\frac{1}{2} \frac{e \ \nabla_{\parallel} \ B}{m^1 c} \frac{v_{\perp}^2}{\omega_c} \tag{22}$$

where g is the acceleration of gravity at the surface of the earth, ψ is the angle between the radial direction and the field-line normal, and $\nabla_{\parallel}$ is the gradient operator along the local geomagnetic field direction. These force components coupled with the first adiabatic invariant, $v_{\perp}^2/B$ = constant, and the geometry of the geomagnetic field are sufficient to fully identify the ion trajectories. However, since the forces are conservative, it is entirely permissible to use the conservation of total energy to arrive at the end points of the orbit without deriving the full solution for the trajectory. The energy equation has the simple form

$$v_{\parallel I}^2 + v_{\perp I}^2 - 2g/R_I = v_{\perp M}^2 - 2g/R_M \tag{23}$$

where subscript I refers to the injection location and M refers to the mirror or turning points of the trajectory along the flux tube. This formulation of the problem follows that used previously (Eviatar et al, 1964; and LeMarie and Scherer, 1970), but the results are displayed in an entirely different manner.

The solution for the mirror points of typical ion trajectories are illustrated in Fig. 17. The injection level is specified at 1600 km (R = 1.25) along the geomagntic field line L = 4. The mirror point, R_M, is plotted as a function of ion energy for hydrogen, argon, and cesium with the injection pitch angle α as a parameter. For example, an argon ion with an energy of 13 ev and an injection pitch angle of 90° bounches back and forth between R = 1.25 and R = 3 as shown in Fig. 16 as well. An extreme example is a 4 eV argon ion injected upward parallel to the local field (α = 0°) which is reflected at R = 1.6 by gravity and falls directly back into the atmosphere at R = 1. Similar cases have been worked out for a variety of injection levels and geomagnetic field lines; all of them have very similar curves and nearly identical energy regimes. The presence of a natural electric field parallel to the local geomagnetic field can seriously distort the shape of the trapping region, however, and it may play a significant role during disturbed conditions, but it must be ignored here due to lack of evidence.

In order to illustrate the effectiveness of these low-energy ion beams to stimulate VLF wave amplification, the specific case of 43 eV cesium ions with an injection pitch angle of 90° at the rocket altitude of
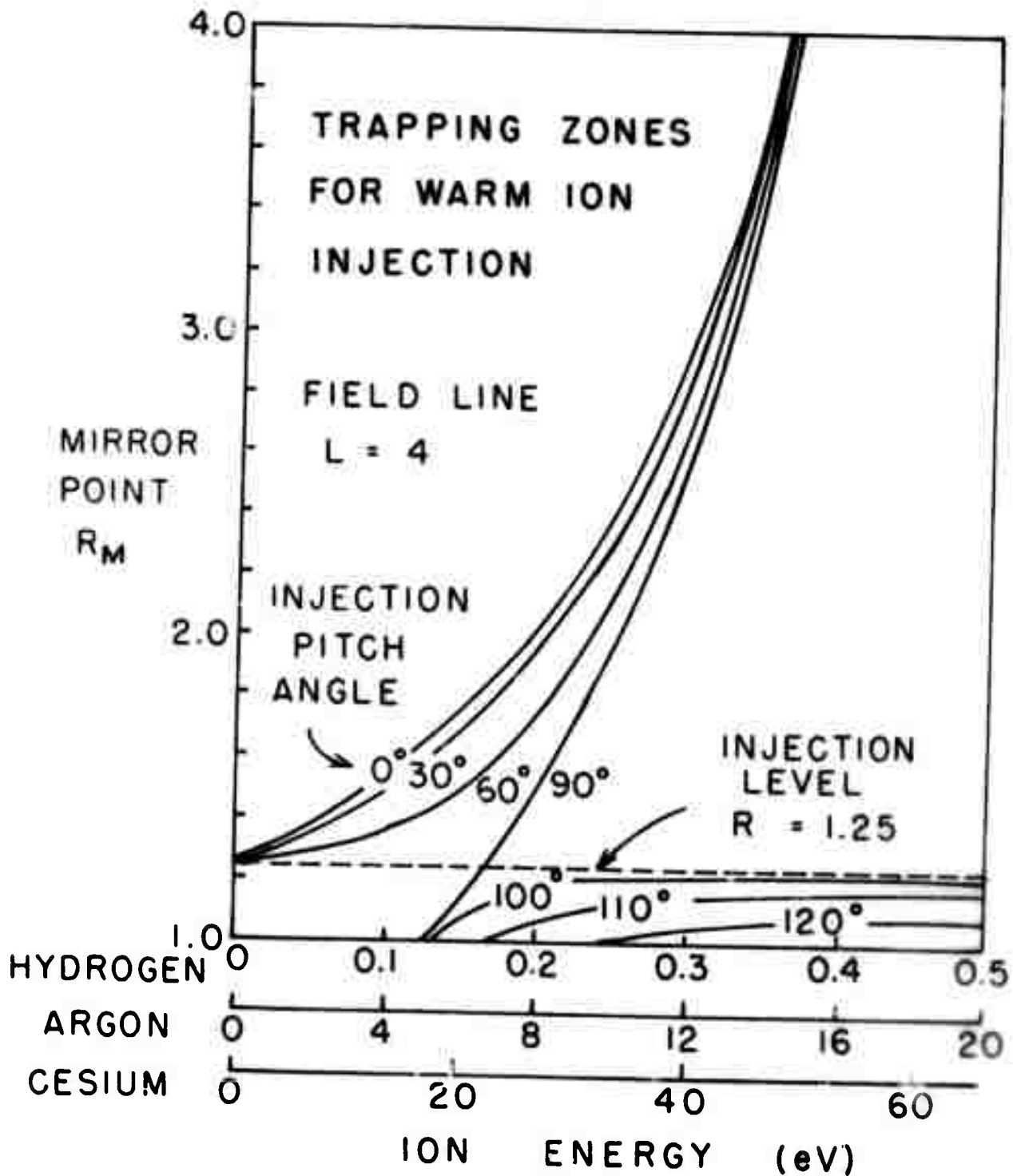
Fig. 17 Trapping zones for warm ion injection above the ionosphere.
The end points of particle orbits for the various ions are
displayed as a function of energy. The injection level is
at an altitude of 1600 km along the field line at L = 4.

1600 km will be considered explicitly. At the injection location these ions have a speed of 7.5 km/sec and a gyro radius of 0.2 km. Due to scattering mechanisms, the beam helix is expected to expand into a column about 1 km^2 in cross-sectional area which is 10 times the gyro-area. If the beam runs continuously for 100 seconds, an initial column length of 50-100 km might be anticipated since most of the particle speed is perpendicular to the field line. Thus, an initial plasma density enhancement of 500 cesium ions/cm^3 may be achieved with a beam current of only 0.05 amps which corresponds to a gun power of just 2 watts.

Such an enhancement of cesium ions and cold electrons drawn up by ambipolar diffusion is not particularly effective inside the plasmasphere but is a remarkably strong enhancement in the plasmatrough. The effect is graphically illustrated in Fig. 18 along the geomagnetic field line $L = 4$ where the ambient plasma density is normalized to unity at the equator and varies as R^{-3}. Such a natural density corresponds to conditions during and immediately following a geomagnetic substorm. Since the ion beam is confined to a geomagnetic flux tube, its density falls off only as $R^{-3/2}$. Consequently, the enhancement is even more effective at the higher altitudes.

Such a beam enhancement stimulates amplification of VLF waves along its field-line path at frequencies near the local electron gyrofrequency. The local amplification exponent for selected frequencies is displayed in Fig. 19 along the field line $L = 4$. The hot electron plasma that supplies the energy for wave amplification is assumed to have the form $E^{-2} \sin^2 \alpha$ (see Figs. 1 and 2). As noted in the figure, the region of enhancement
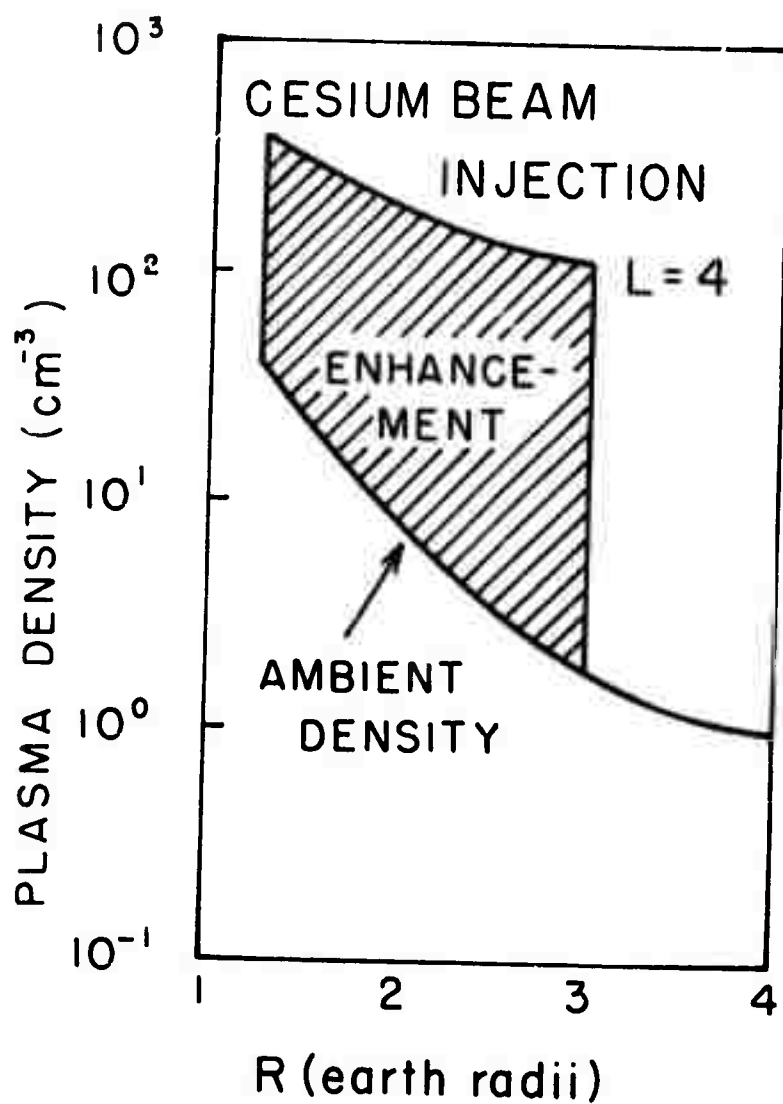
Fig. 18 The net plasma density enhancement produced by a warm (43 eV) cesium beam. The ambient background plasma is assumed to be in the plasmatrough where $N_0 = 1$ ion-electron/cm^3.
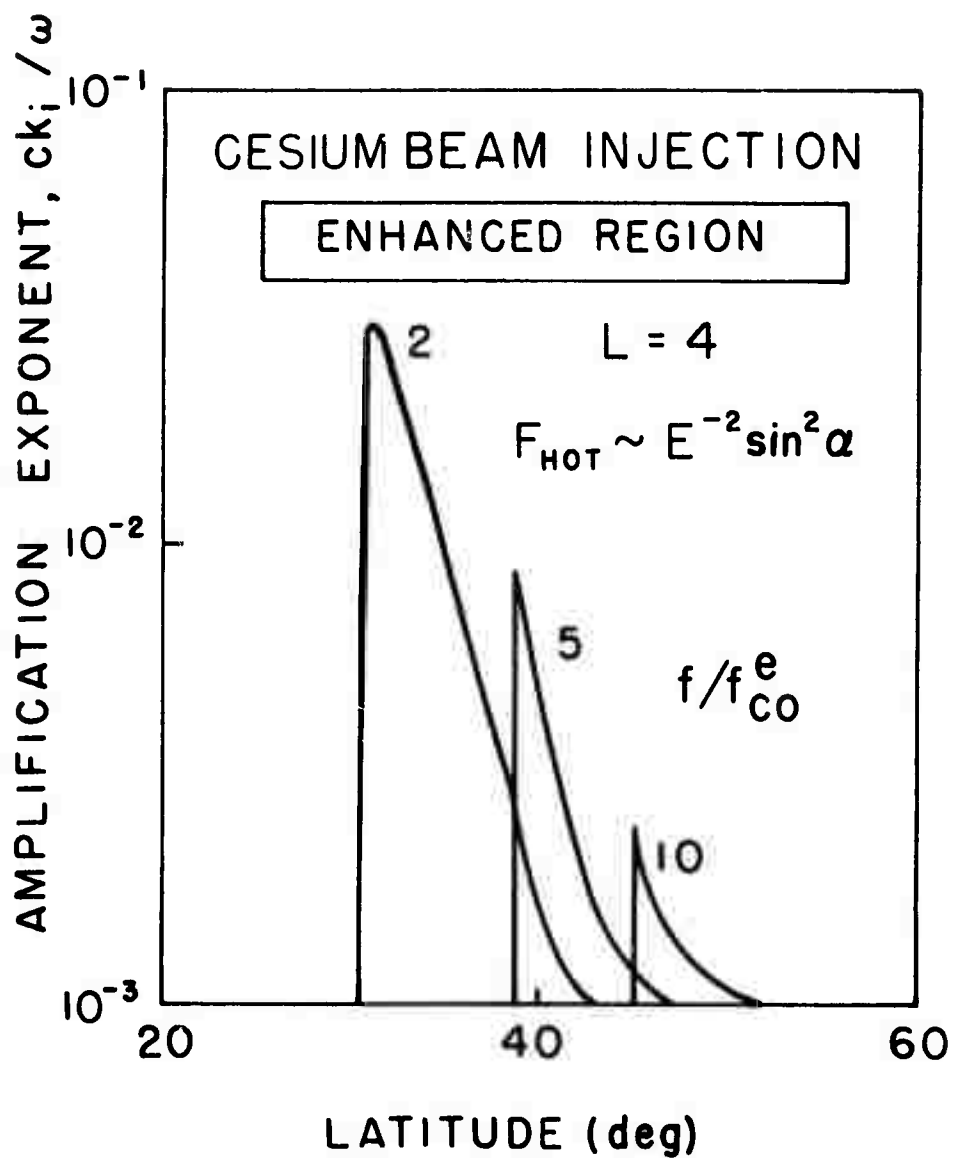
Fig. 19 Amplificatic.i exponent for VLF waves propagating through the warm (43 eV) cesium beam. The hot electrons are assumed to have the distribution $E^{-2} \sin^2 \alpha$. Note these frequencies are above the equatorial value f_{co}^e.

covers the geomagnetic latitude band from 25° to 56°. The amplitude exponent, k_i, has been evaluated for frequencies *above* the equatorial electron gyro frequency f_{co}^e but the actual energy exchange between the hot electrons and VLF waves takes place below the local electron gyro frequency. Since f_{co}^e = 13.7 kHz, the amplification actually occurs in the LF band over most of the interaction region.

The net amplification induced by the cesium-electron beam along the field line path L = 4 is displayed in Fig. 20. Amplifications of 30-40 db may be expected at frequencies between 60 and 150 kHz. Near the equatorial zone where the cyclotron resonance interaction is very strong, amplifications of 100 db or more apparently can be expected for frequencies in the range 20-30 kHz. One should be reminded that this amplification power is derived catalytically from the natural hot electron plasma in the energy range 10-100 keV; it is not derived from the 2 watts of beam power.

Certain properties of the cesium beam make it rather attractive as a stimulator of VLF and LF radio noise. The size of the beam column is adequate to interact with an appreciable wave front of VLF-LF energy. At 50 kHz the free space wave length is 6 km and the index of refraction is 10-30 so that the effective wavelength is significantly less than 1 km. The gyroradius for cesium ions at R = 2-3 is 0.6-1.0 km and any scattering that occurs will expand the beam column well beyond these values. Since a column of 50-100 kilometers in length can be anticipated for 100 second bursts from the ion gun, there is an adequate interaction zone extending over many wavelengths. A single plasma beam generates a
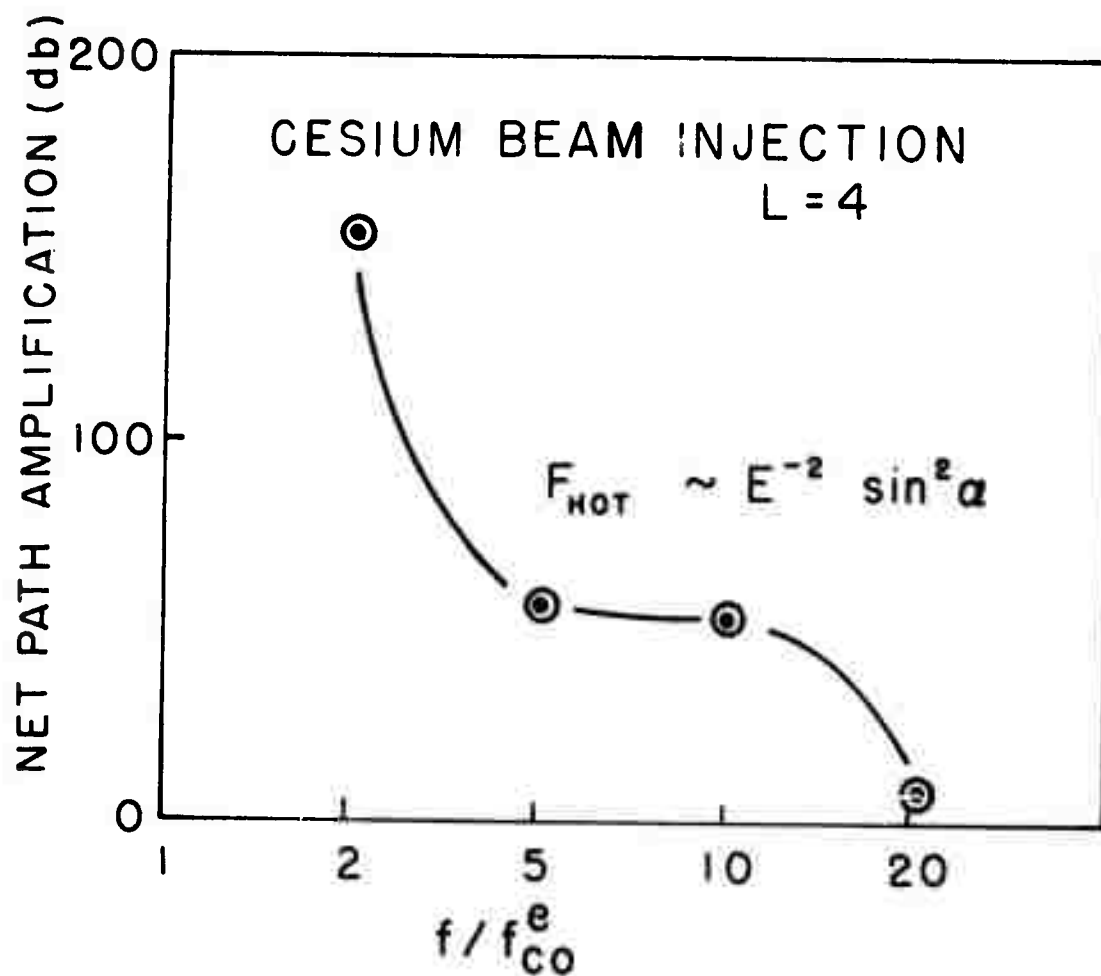
Fig. 20 Net path amplification for VLF waves propagating through a warm cesium beam. The hot electrons are assumed to have the distribution $E^{-2} \sin^2 \alpha$.

relatively narrow band VLF-LF descending noise tone as it proceeds up the field line to its mirror point and an ascending noise tone as it returns toward the injection point. Similar tone patterns might be generated on adjacent field lines by the release of other beam columns. The bandwidth and noise amplitude obviously depends on the geomagnetic field line and altitude of the injection as well as the natural hot electron plasma that is available to interact with the waves.

ULF AMPLIFICATION

Stimulated amplification of ULF waves in the magnetosphere is more difficult than its VLF counterpart for two reasons. First, the cyclotron resonance interaction is inherently weaker at ULF because the index of refraction for the medium is relatively smaller requiring a relatively higher value of the resonance velocity (see Eq. (3)). Second, the injection of clouds of proton plasma which would provide the most efficient means for catalytic stimulation of the interaction are simply not feasible; less convenient types of ion injection must be substituted. Despite these limitations, significant amounts of amplification can be stimulated by the techniques that will be described in the following subsections.

For ULF wave amplification the critical consideration is the pitch angle and energy distributions of the hot protons (1-100 keV). Pitch angle distributions of the form $\sin^m \alpha$ are quite applicable to the proton plasma as well. Distributions with $m = 1$ or 2 are frequently encountered in the magnetosphere and will be used in the analyses that follow.

As in the preceding electron cases, the energy distributions of the protons may be subdivided into a cold plasma and a hot plasma. The cold plasma contains most of the charge density and its distribution defines the propagation characteristics of ULF waves. The cold protons are assumed to have energies on the order of 0.1 eV. The main source of the hot proton plasma is the ring current that waxes and wanes with geomagnetic activity. Some typical hot proton distributions as well as the cold plasma distribution are displayed in Fig. 21. The ring
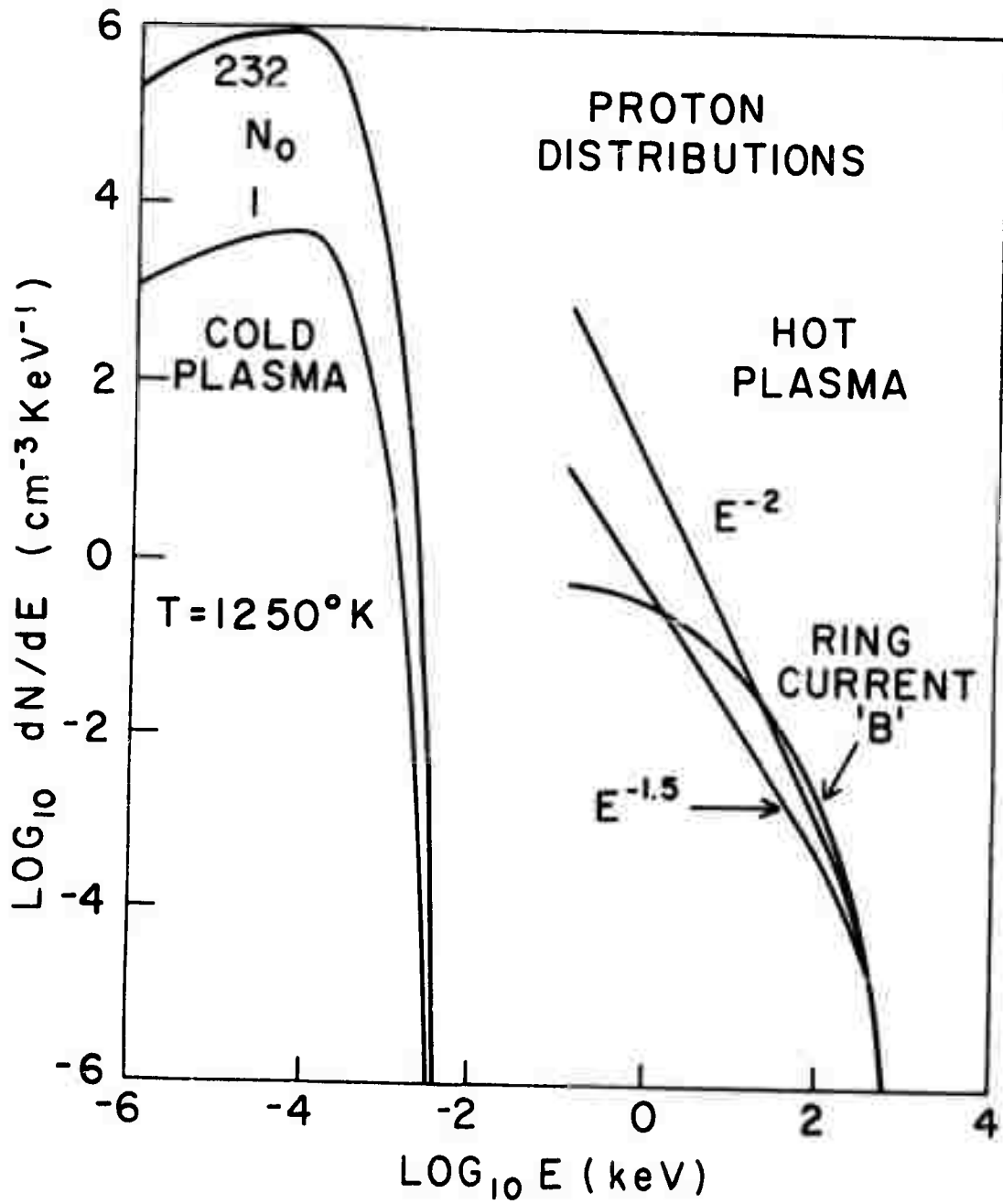
Fig. 21 Typical proton energy distributions in the magnetosphere. The calculations are based on distributions of the form E^{-n} which are commonly encountered by spacecraft. The ring current distribution 'B' is based on OGO-5 observations (Pizzella and Frank, 1971).

current distribution "B" is based on data derived from several satellite observations (Pizzella and Frank, 1971) beyond the plasmapause. The distributions E^{-n} have also been used extensively for quiet periods in the magnetosphere. The excessively high values of these distributions below 1 keV does not play a significant role in the cyclotron resonance interaction since the resonance energy at frequencies of interest is well above this level.

Lithium Jet in the Plasmatrough. During strong geomagnetic storms the plasmapause frequently comes inside L = 3.5 and the proton ring current develops a strong maximum at L = 3.5 - 4.5 which might be tapped for ULF amplification. In this case, the plasmatrough has an unusually low density (~ 1 proton/cm^3) and the hot proton ring current is exceptionally dense (≥ 0.02 protons/cm^3). Such conditions allow artificial stimulation of ULF amplification by injection of a cloud of lithium ions (Cornwall and Schulz, 1971). One source for lithium clouds at L = 3 - 4 (Hoch, private communication) is a shaped-charge injection of a neutral lithium jet from a low altitude rocket. By choosing a launch time and location that avoids sunlight for part of the ballistic trajectory to the equatorial region at L = 3.5, an appreciable fraction of the initial jet might be deposited as an ion cloud in the plasmatrough near the ring current maximum. The process is illustrated schematically in Figure 22. Owing to the ballistic trajectories there is a moderate amount of focusing that can be achieved by proper injection velocities and orientation of the jet.

A detailed model of the injection characteristics has been developed in order to assess its amplification potential. A jet velocity band of 10-15 km/sec may be assumed at the source (experimentally observed for

LITHIUM   INJECTION
L = 3.5   EQTRL

SHAPED
CHARGE
BALLISTIC
TRAJECTORY
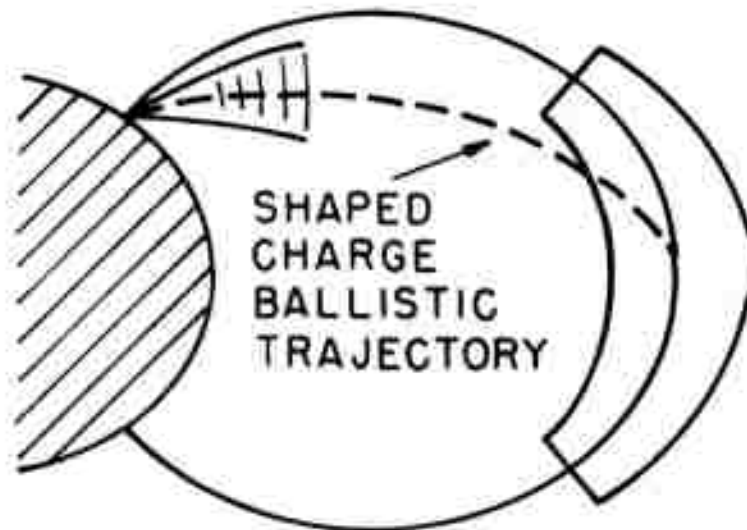
AMBIENT $N = 1.0 \ (3.5/R)^3 \ (cm^{-3})$
LITHIUM $N = 10 \ (cm^{-3})$

Fig. 22   Shaped-charge injection of lithium to the equatorial region
at L = 3.5.   The neutral lithium jet of approximately 1 kgm
is expected to follow a ballistic trajectory across the
magnetic field until solar radiation ionizes it and deposits
approximately 10 lithium-ion electron pairs/cm^{-3}.   The ambient
background plasma is assumed to be in the plasmatrough where
N_o = 1 proton-electron pair/cm^{-3}.

barium injections by Peek, private communication). Since the jet is slowed by the gravitational forces on the neutral atoms, it is estimated to require 30-40 minutes for the lithium cloud to travel about 2.5 earth radii from the injection point to the equatorial region at L = 3.5. The velocity spread of 5 km/sec corresponds to a radial dispersion of about 6,000 km. If the jet is sprayed in a narrow range of latitudes and is carefully columnated along the geomagnetic meridian plane, the lithium ions at L = 3.5 can be confined to a latitude band of 10,000 km across the geomagnetic equator and perhaps only 2,000 km spread in longitude. This corresponds to a volume of 10^{26} cm^3.

Since the ionization of lithium atoms by solar ultraviolet is a continuous process with a characteristic ionization time of 60 minutes, perhaps only 10% of the initial jet is available in the lithium ion cloud. Only 10^{26} ions of lithium are available in 1 kgm so that 100 kgm of lithium is required to deposit a density of 10 lithium ions/cm^3 in the enhancement region. These numbers are obviously debatable, but they serve as a basis for judging the usefulness of this method. Obviously, a total payload weight of 1,000 kgm including the explosive charge is not out of the question with certain rockets that might be considered for this experiment.

According to equation (4), ULF propagation characteristics are sharply modified in a lithium ion cloud. Below the lithium gyro-frequency the phase velocity is reduced appreciably whereas above it, the propagation is evanescent. This alteration from the normal proton plasma propagation characteristics allows the cyclotron resonance

interaction to proceed with lower energy particles which are normally more numerous and consequently the interaction is appreciably enhanced.

In accordance with Fig. 22 the lithium injection at L = 3.5 is assumed to have a density of 10 lithium ions/cm^3 and the ambient plasma trough is assumed to have a density $N = N_o (3.5/R)^3$ where $N_o = 1$ cm^{-3}. The amplification exponent, k_i, for ULF waves propagating through this lithium ion cloud is illustrated in Fig. 23. The hot proton plasma for the ring current is assumed to have the distribution $E^{-2} \sin^2 \alpha$ which is consistent with experimental observations at these relatively low L shells. The curves for the exponent are entirely attributable to the lithium cloud; the ambient (cold) proton plasma causes a negligible amount of natural amplification at these frequencies. The sharp cutoff in the exponent at 5° and 15° is due to the propagation cutoff above the local lithium gyro frequency. Evidently, there is significant non-equatorial amplification that allows strong enhancements at frequencies above the equatorial lithium gyro frequency $f_{co}^{Li} = 0.143 \, f_{co}^{p}$. This is more vividly illustrated in Fig. 24 where the net path amplification actually has its maximum above f_{co}^{Li}. Obviously ULF waves above f_{co}^{Li} cannot penetrate the evanescent zone at the geomagnetic equator, so that the ULF band from 0.143-0.22 f_{co}^{p} is restricted to intrahemisphere propagation. Despite the high lithium ion density that is proposed for injection, the net amplification is only a few decibels. Consequently, this method for stimulation of ULF amplification is not particularly effective.
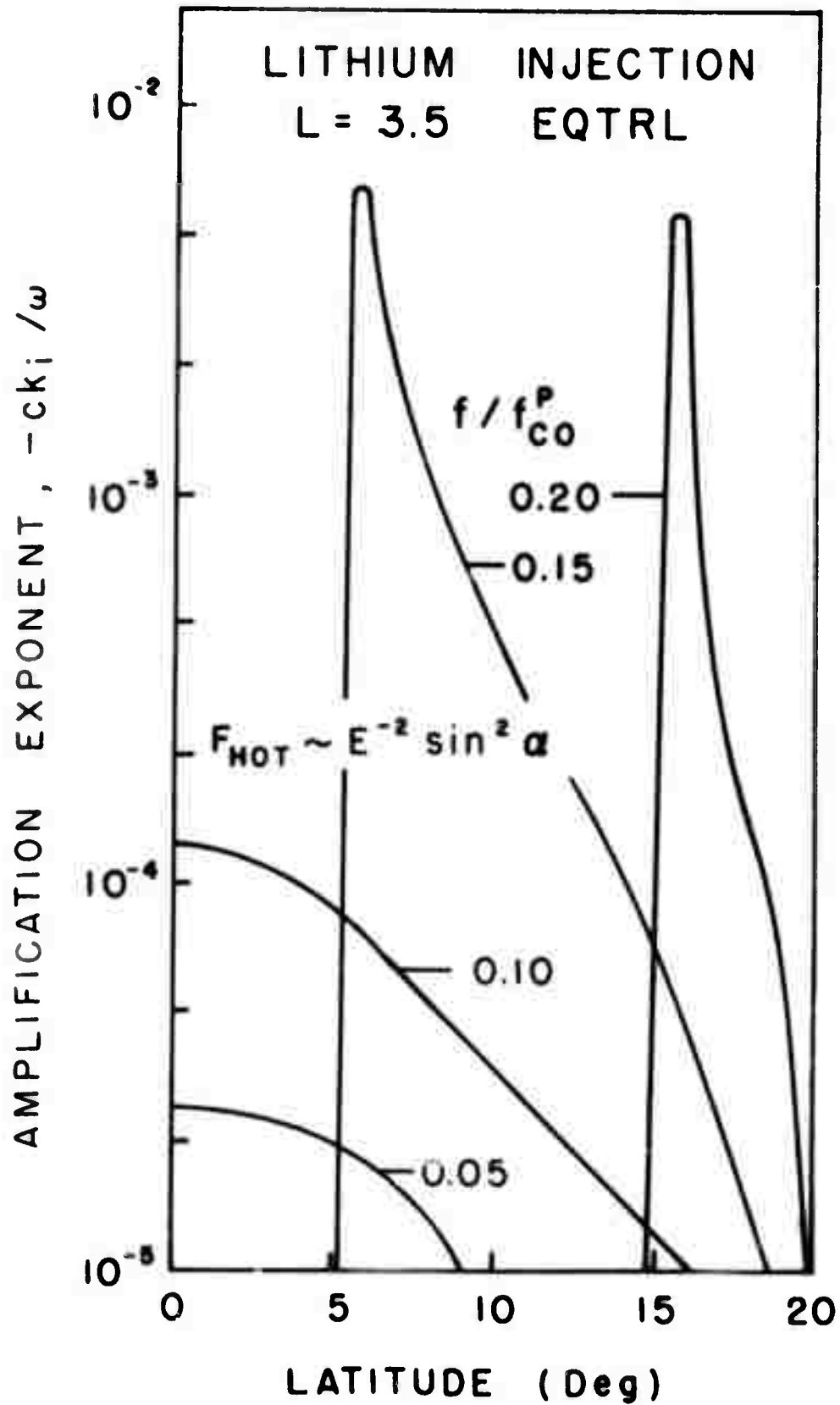
Fig. 23 Amplification exponent for ULF waves propagating through the lithium shaped-charge injection along L = 3.5. The hot protons are assumed to have the distribution $E^{-2} \sin^2\alpha$ (see Figs. 1 and 21).
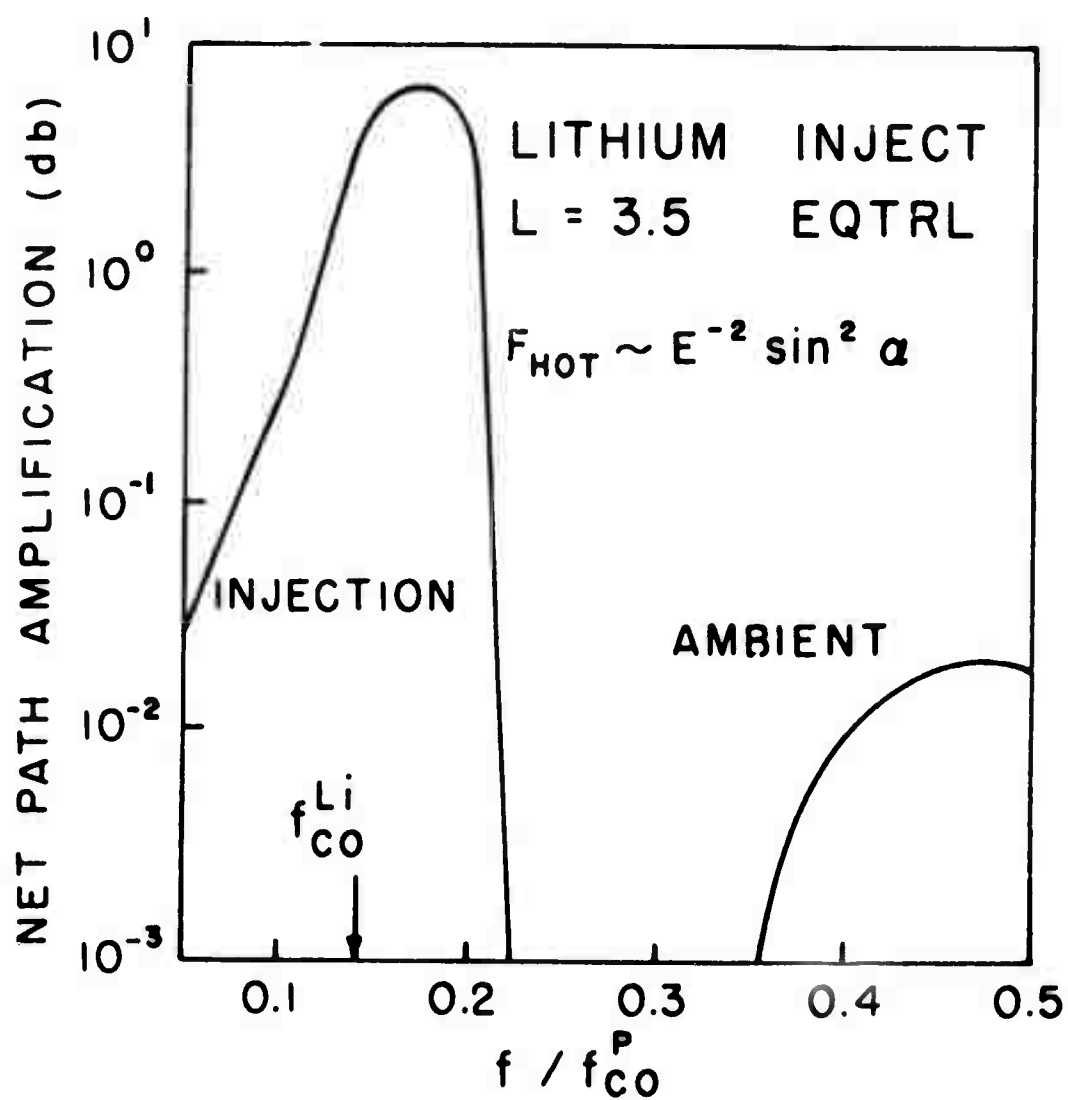
Fig. 24 Net path amplification for ULF waves propagating through the lithium shaped-charge injection along L = 3.5. The hot protons are assumed to have the distribution $E^{-2} \sin^2 \alpha$ (see Figs. 1 and 21).

Geosynchronous Lithium Clouds. The injection of lithium ion clouds from satellites at geosynchronous altitudes has already been discussed by others (Cornwall and Shultz, 1971; and Cornwall, 1972), but it is included here in order to corroborate their findings and perhaps elaborate upon them. The amplification analysis performed here is based on the two cloud models depicted in Fig. 8. Details of the injection requirements and diffusion properties are described in the section on VLF amplification. In one case the 1 kgm cloud of lithium ions is confined to a radius of 0.1 R_e which corresponds to 10 minutes of diffusion from a point source, whereas the other case has a radius 0.5 R_e corresponding to 50 minutes of diffusion.

As before, it is important to recognize that the lithium injection alters the local propagation characteristics. Above the lithium gyrofrequency, ULF waves are evanescent whereas below the phase velocity is strongly reduced. The latter effect gives rise to the enhanced cyclotron resonance interaction.

The ULF amplification that is stimulated by these two injection models is illustrated in Figs. 25-28 for two models of the hot proton distribution function. The model $E^{-1.5} \sin \alpha$ represents quiescent conditions in the magnetosphere when the proton ring current is very weak. The second case is the ring current model "B" which has been experimentally observed during geomagnetic storm conditions; it is denoted by the functional form $(dN/dE)_{"B"} \sin \alpha$ (see Fig. 21).

As expected, the ULF amplification enhancement is restricted to the narrow equatorial region where the lithium injection dominates the total plasma density. The injection region is restricted to
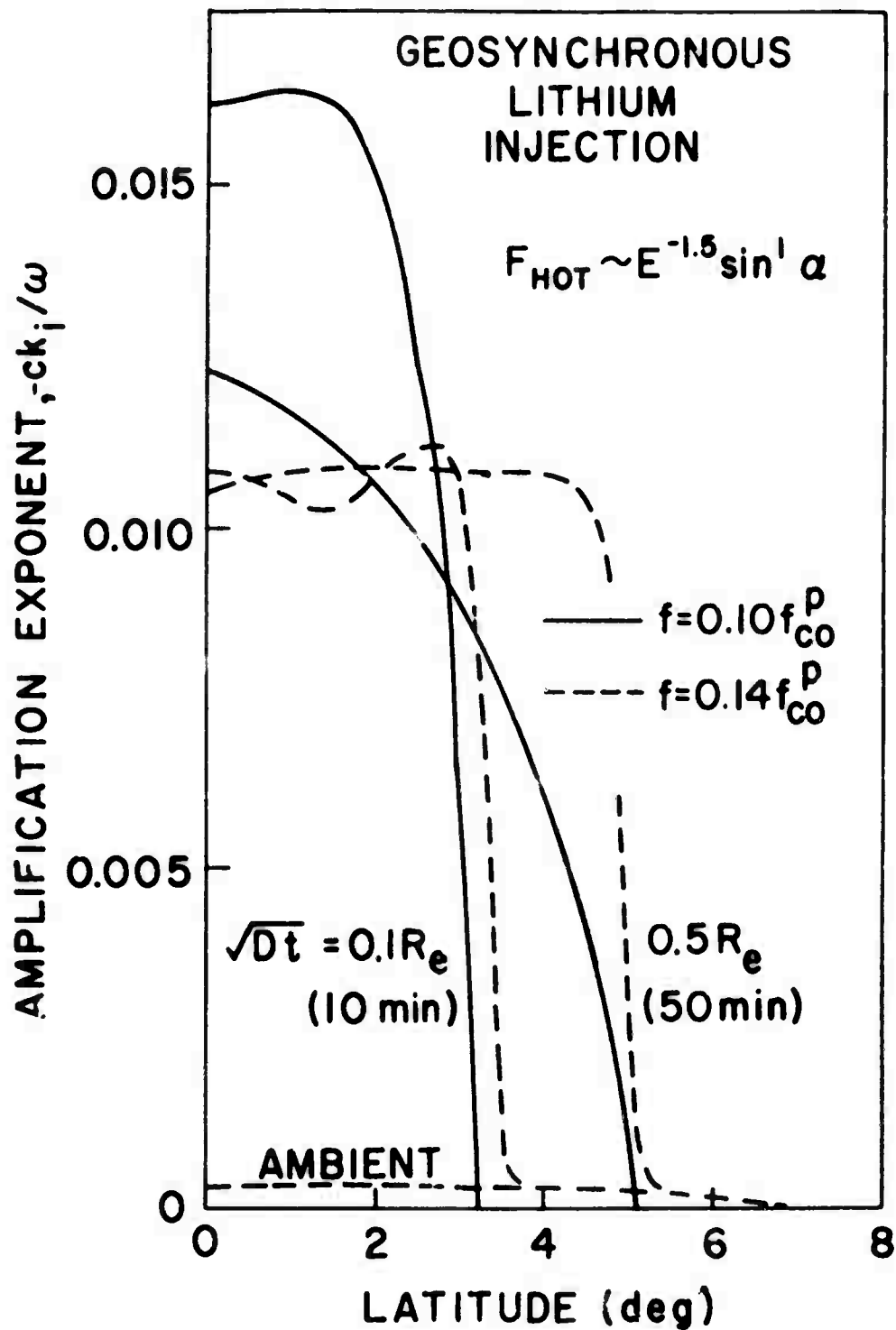
Fig. 25 Amplification exponent for ULF waves propagating through the geosynchronous lithium injection (see Fig. 8). The exponent is sharply peaked in the equatorial enhancement which have mean diameters of 1280 and 64 km. The hot protons are assumed to have the distribution $E^{-1.5} \sin \alpha$.
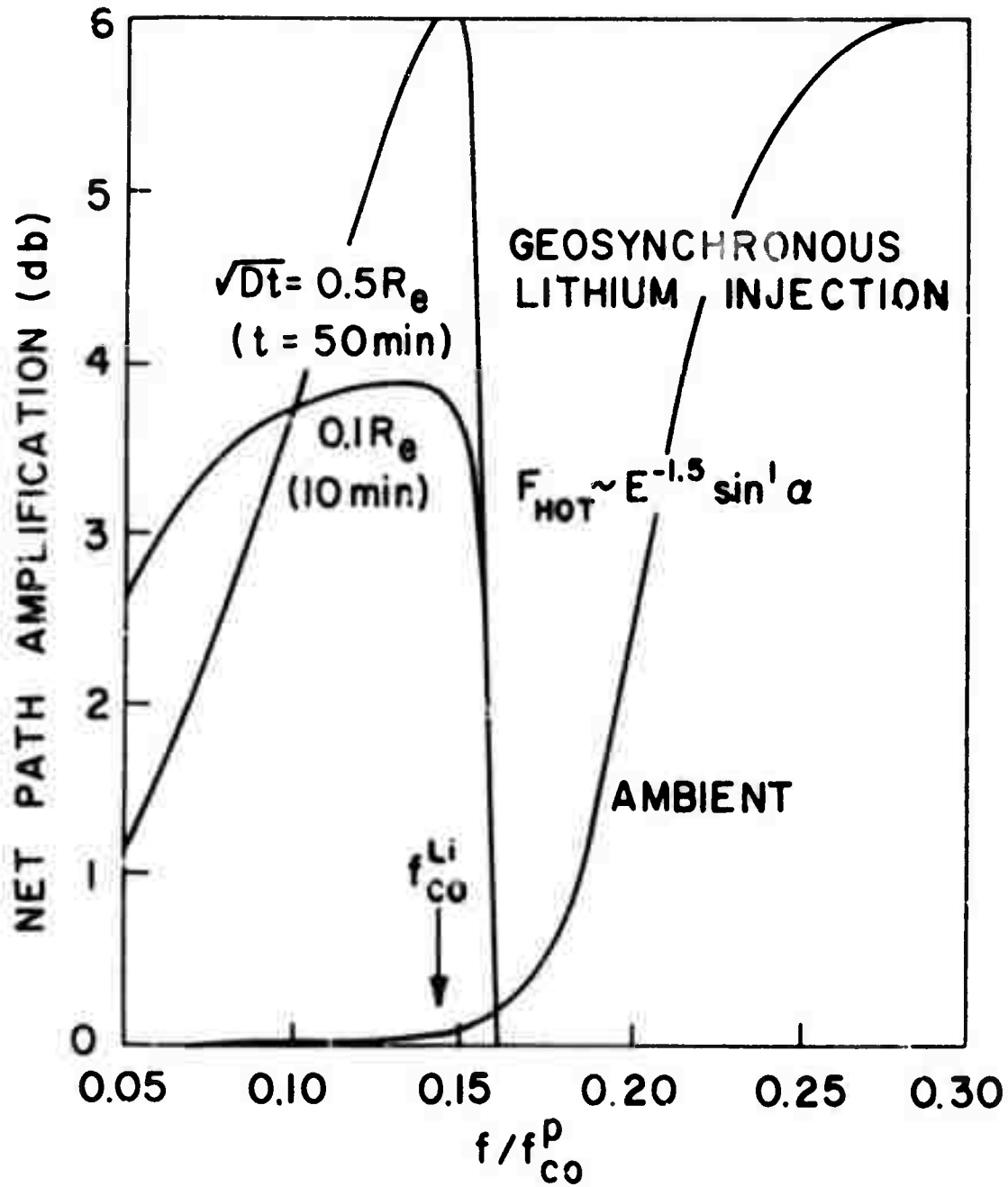
Fig. 26 Net path amplification for ULF waves propagating through a
geosynchronous lithium injection (see Fig. 8). The enhance-
ment is entirely attributable to the lithium bubble. The hot
protons are assumed to have the distribution $E^{-1.5} \sin \alpha$.
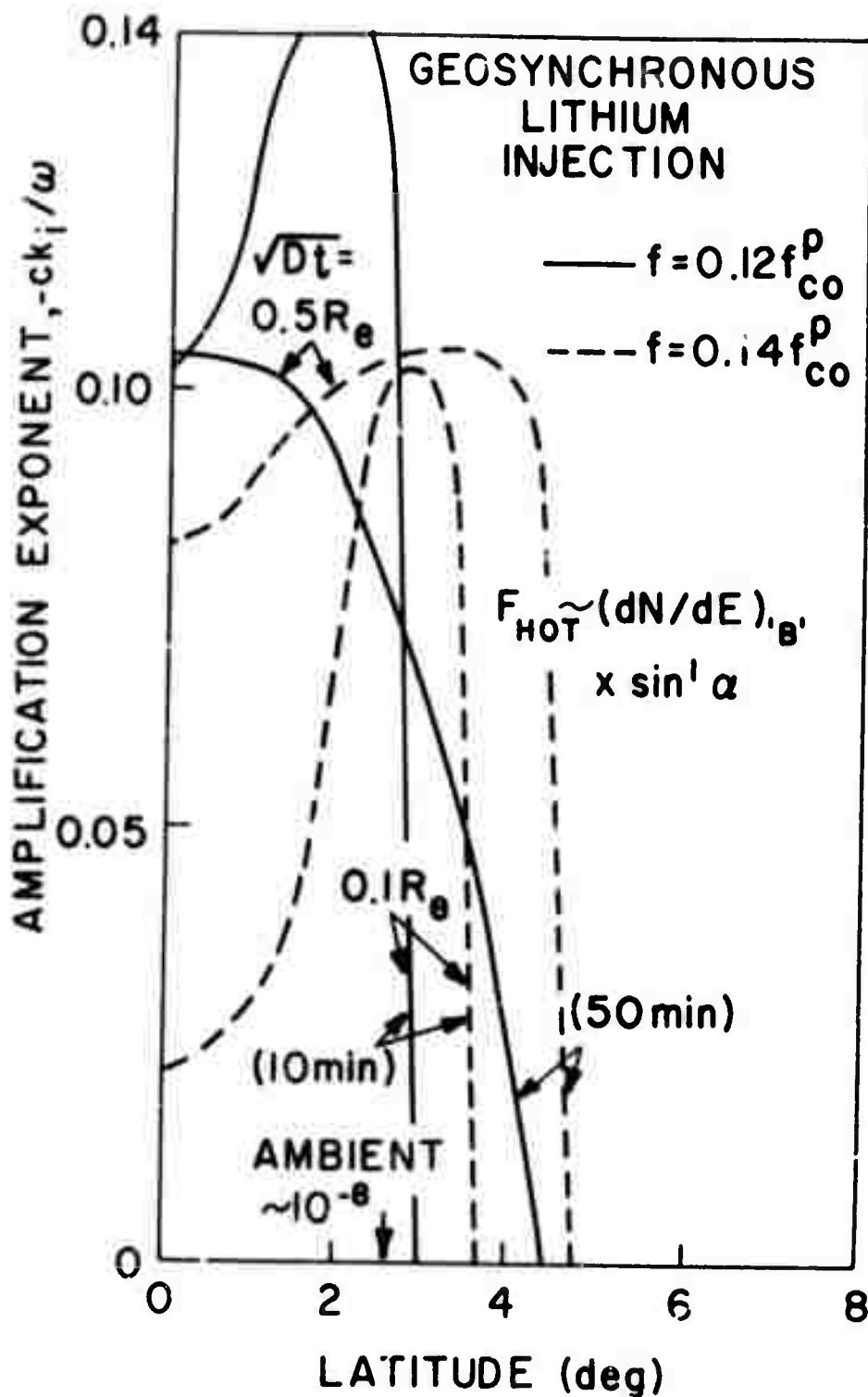
Fig. 27 Amplification exponent for ULF waves propagating through a geo-
synchronous lithium injection (see Fig. 8). The exponent is
sharply peaked in the equatorial enhancement which have mean
diameters of 1280 and 6400 km. The hot proton distribution is
based on Model 'B' for the ring current of a typical geomagnetic
substorm (see Fig. 21).
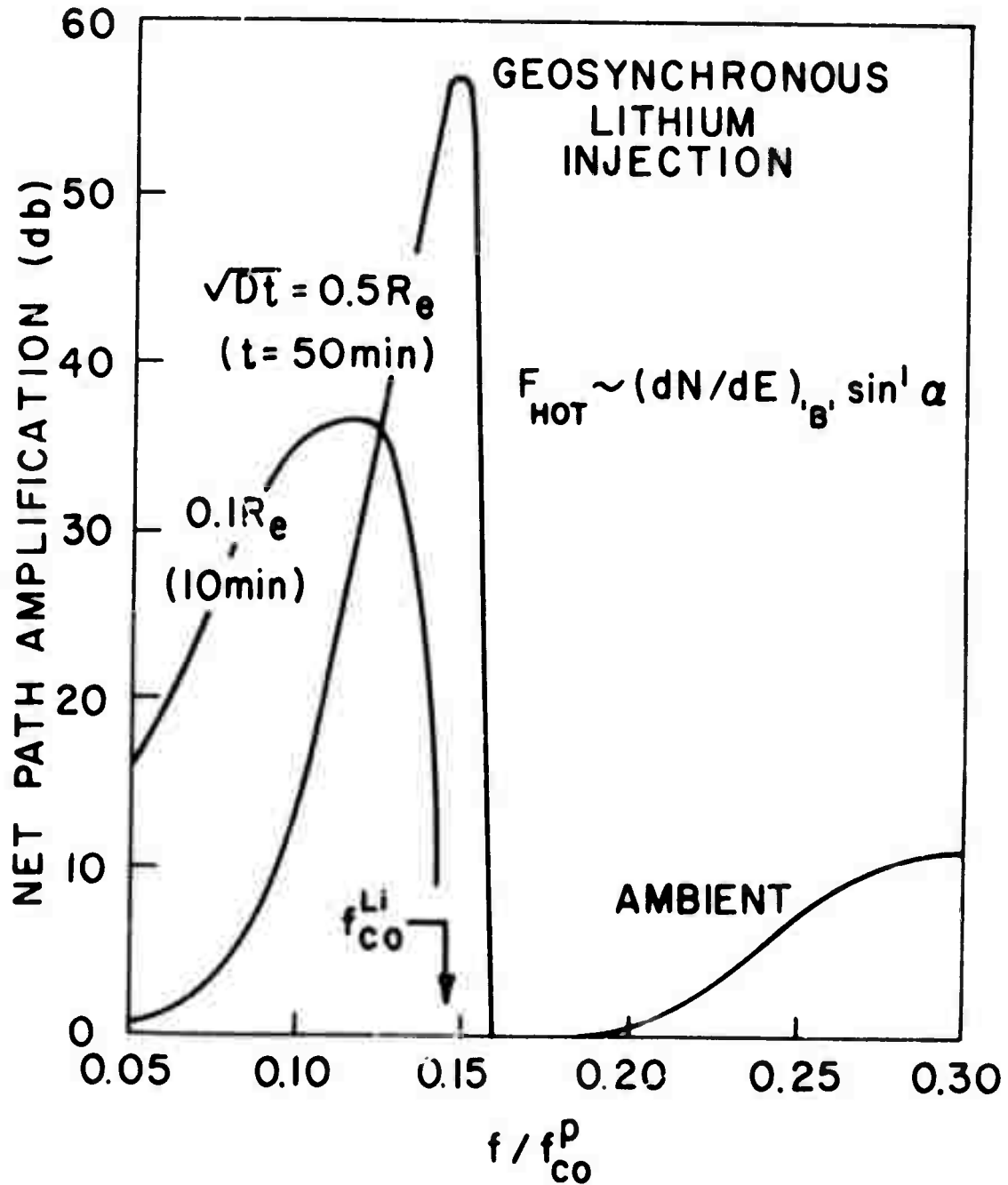
Fig. 28 Net path amplification for ULF waves propagating through a geosynchronous lithium injection. The enhancement is entirely attributable to the lithium bubble. The hot proton distribution is based on Model 'B' for the ring current of a typical geomagnetic substorm (see Fig. 21).

$\pm\ 3°$ geomagnetic for the 10 minute case and $\pm\ 5°$ for the 50 minute case. Since the interaction is dominated by the lithium gyrofrequency cutoff in the propagation, ULF frequencies above 0.143 f_{co}^{p} simply do not get amplified significantly. An important distinction between the results in Figures 25 and 27 is the order of magnitude increase in the value of k_i during disturbed conditions.

The dependence on the shape of the energetic particle distribution manifests itself more explicitly in the net path amplification illustrated in Figures 26 and 28. The quiescent conditions yield an amplification of 4-6 db whereas the ring current conditions provide 35-55 db. This remarkable difference is attributable to the higher value of the ring current density (Figure 21) at those energies where the resonance energy exchange is most effective (2 - 200 keV). Another important conclusion is that the amplification is stronger at 50 minutes after injection than at 10 minutes. This is attributable to the longer propagation path over which amplification is enhanced.

The amplification achieved by injection of a lithium ion cloud at geosynchronous altitude is comparable to the earlier predictions (Cornwall and Schultz, 1971). Perhaps what has not been emphasized as strongly by previous research is the relatively sharp amplification maximum that is nearly centered on the equatorial lithium gyrofrequency f_{co}^{Li} which has the value 0.■ Hz at L = 6.6. The duration of the lithium-ion cloud depends of course on the strength of the local electric fields in the magnetosphere, but it is expected to survive for several hours as a discernible entity. The ULF noise generated by the cloud will also have a distinctive characteristic. According to the results in Figure 28,

the noise consists of an ascending tone of increasing amplitude maximizing at f_{co}^{Li} along the injection field line and subsequently broadening over a narrow range of frequencies corresponding to the L shells covered by the lithium cloud. If a convective electric field is present, the cloud may drift radially causing a change in the frequency corresponding to the change in the local gyrofrequency.

Energetic Proton Beams. Amplification of ULF waves by direct injection of energetic proton beams is obviously more desirable than the preceding methods because it is not subject to the vagaries of geomagnetic activity. The wave growth that is achieved by beam injection is derived entirely from the energy of the beam particles. The process is not catalytic in the sense that the natural background of hot protons in the magnetosphere has a negligible effect. The amount of amplification is proportional to the intensity of the beam as expected and the frequency band depends on the beam pitch angle at the injection location.

The beam is assumed to be launched during geomagnetically quiet conditions along the field line at L = 4 which is assumed to be inside the plasmasphere where N_0 = 232 protons/cm^3. For completeness, the natural hot proton distribution is assumed to have the form $E^{-1.5} \sin \alpha$, although it does not contribute appreciable amplification.

The proton gun is arbitrarily assumed to have a power level of 10 kilowatts, and the beam current consists of 100 millisecond pulses of 10 keV protons. In so far as the author is aware, no one has developed a proton gun for use on spacecraft. The foregoing gun characteristics

are probably very difficult to achieve due to the high current level (10 amps). These beam parameters were chosen intentionally so that the proton beam could be modelled quantitatively by the same pitch angle and energy distributions that are used for the electron beam (see Fig. 13). The protons have a speed of 1.5×10^3 km/sec and an equatorial gyro-radius of approximately 30 km, depending as before on the local pitch angle. Electrostatic forces and plasma instabilities undoubtedly break up the initial helix trajectory so that the beam is smeared into a plasma column. Assuming an order of magnitude inflation in the cross section of the beam, the column volume is $\sim 4 \times 10^6$ km^3. In each pulse there are 1.6×10^{19} protons, so that the density of the beam is 0.004 protons/cm^3. Thus, for an effective beam energy spread of 2 keV, the differential energy spectrum is 0.002 protons/cm^3 keV (as shown in Fig. 13).

The pitch angle distribution H_o is normalized to unity with a spread of 10° corresponding to a limited amount of scattering. As in the electron case, the pitch angle distributions are centered on 85 55° and 25° corresponding to mirror points at $\pm 3^o$, $\pm 18^o$, and $\pm 37^o$, respectively.

The effectiveness of the beam for stimulation of the cyclotron resonance interaction depends on its diameter and length relative to the ULF wavelengths involved in the interaction. Near the geomagnetic equator at L = 4 the ULF index of refraction is 500-600 for propagation frequencies around 3Hz which corresponds to 0.5 f_{co}^p. The corresponding wavelength at 3 Hz is 160-200 km which is comparable to the dimensions of the plasma beam column. Since the beam should be several wavelengths

in each dimension, its effectiveness as an amplifier is very questionable even at the large beam power levels proposed. Nevertheless, it is worthwhile to investigate the amplification potential assuming that ways may be found to increase the size of the beam while maintaining its internal density.

The amplification exponent for a beam with $\alpha^{STREAM} = 55^\circ$ is shown in Fig. 29. The sharp peaks in k_i are due to the large gradients in the proton beam energy and pitch angle distributions which cause strong interactions in limited regions where the beam energy happens to match the local cyclotron-resonance interaction energy. On the earthward side of the interaction region, the beam strongly amplifies ULF waves whereas on the equatorward side it strongly absorbs. Curiously the frequency at 0.4 f_{co}^p is strongly amplified around the geomagnetic equatorial region; evidently, the resonance energy never gets low enough to permit significant absorption.

This result is more clearly demonstrated in Fig. 30 where the net path amplification at 0.4 f_{co}^p has a sharp peak of 50-60 db for the stream at 55°. There are other unexpected results as well. The 55° has another maximum around 0.9 f_{co}^p which must be attributed to the local interaction characteristics at a geomagnetic latitude around 20°. The beam with $\alpha_0^{STREAM} = 85^\circ$ has a sharp maximum at 0.7 f_{co}^p which is attributable to a narrow equatorial band interaction where the absorption portion of the distribution never has an opportunity to enter the interaction. Finally, the beam at 25° is simply too weakly interacting in the equatorial region
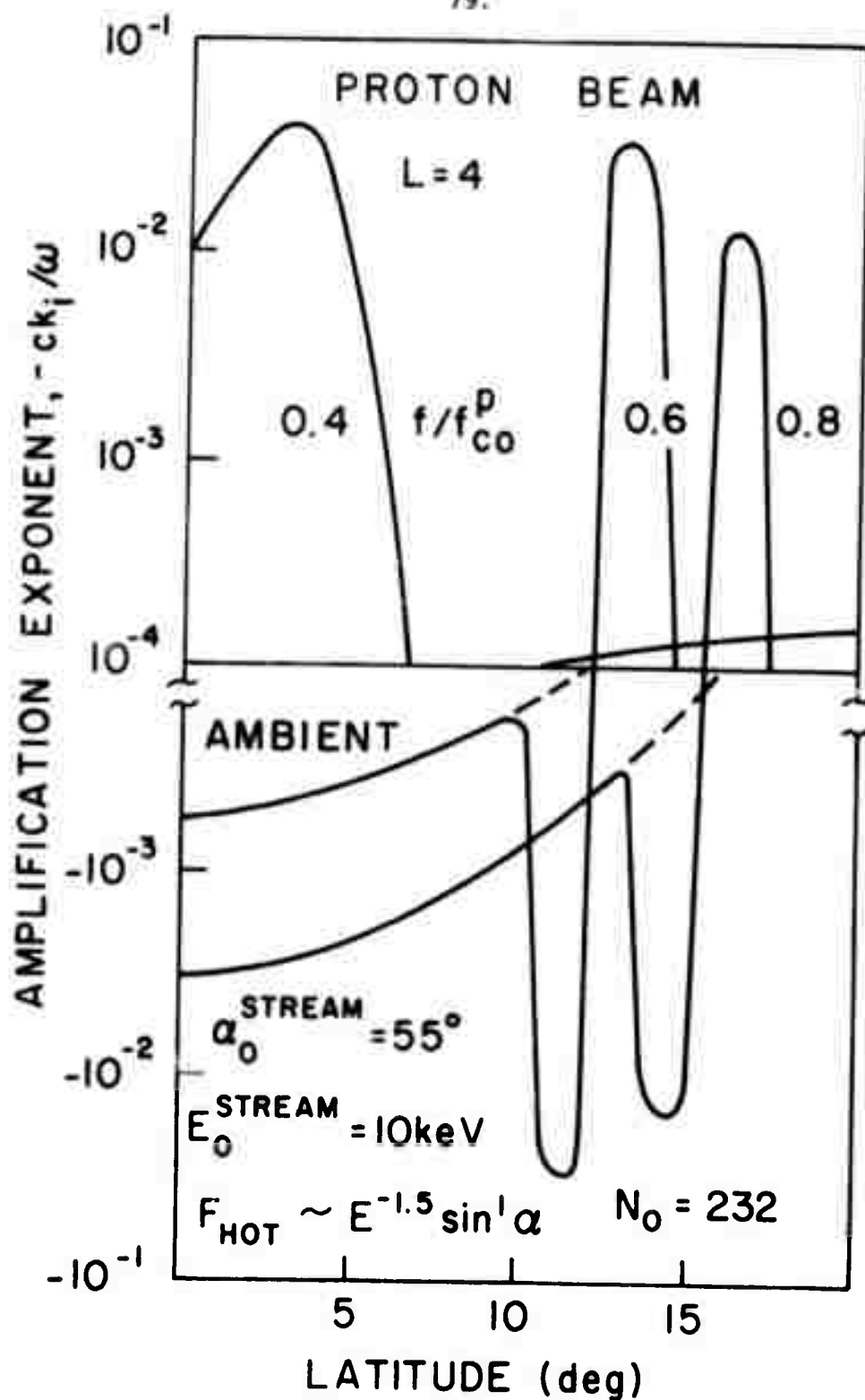
Fig. 29 Amplification exponent for ULF waves propagating through a proton beam along the field line at L = 4 inside the plasma-pause. The beam model has the same distributions as for electrons (see Fig. 13). The beam has an equatorial pitch angle of 55° and a particle beam energy of 10 keV.
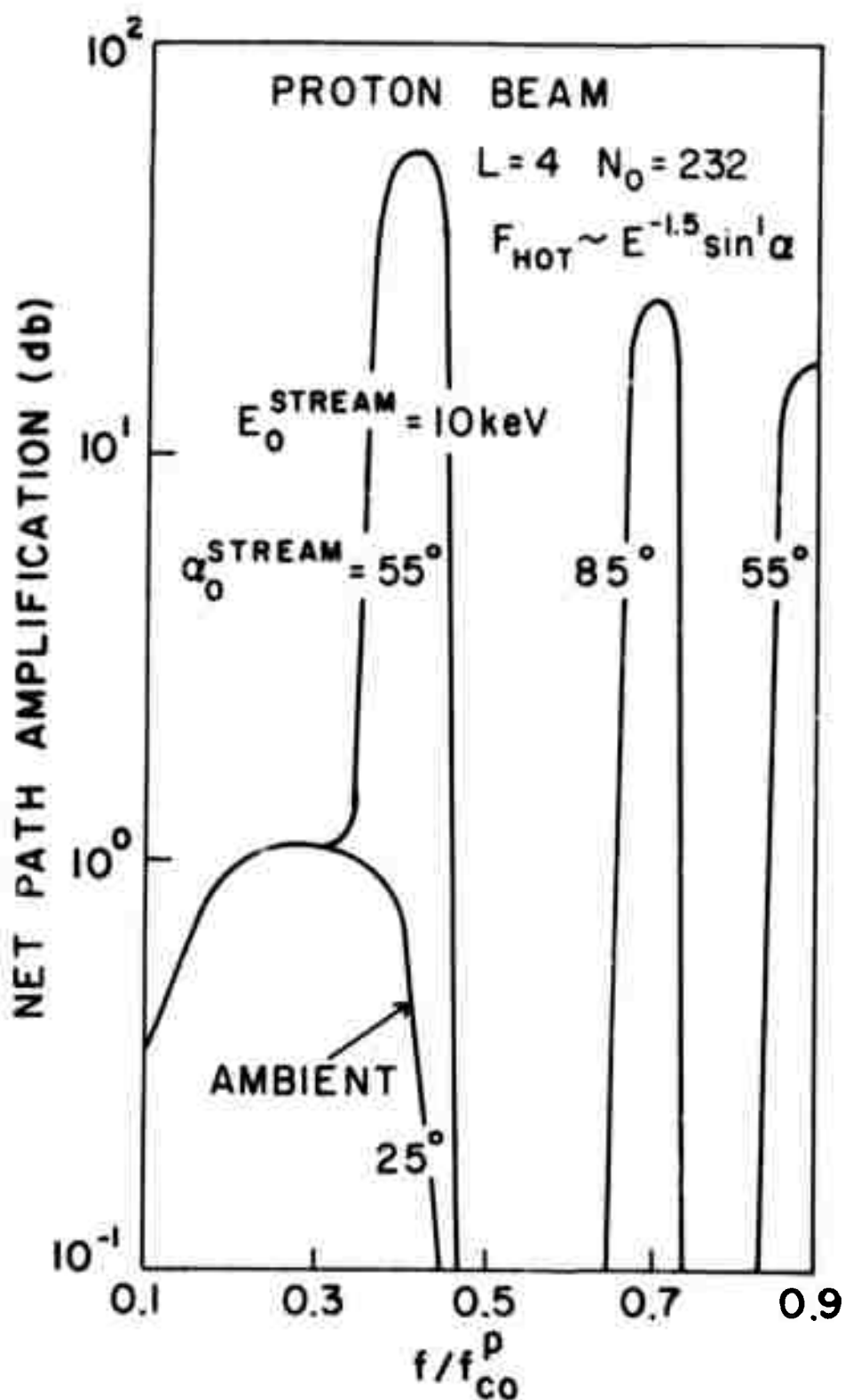
Fig. 30 Net path amplification for ULF wave propagating through a proton beam along the field line at L = 4 inside the plasma-pause. Equatorial pitch angles for the beam are 25°, 55°, and 85° and the beam energy is 10 keV.

to provide much net exchange of energy. The reader is referred to the section on the electron beam amplification of VLF waves for more details about the general physics of the interaction.

If proton beams of sufficient energy can be generated from rocket or satellite platforms, they may prove to be useful generators of ULF noise. From the cursory results displayed in Figs. 29 and 30, it seems clear that certain noise frequencies will be strongly amplified depending on the source location and injection pitch angle. Unlike the electron beam-VLF noise interaction which provided little net amplification, the proton beam ULF noise interaction yields a net amplification that may produce a recognizable signature. Much more research is needed to verify these results.

CONCLUSIONS

The foregoing methods for enhancement of the cyclotron-resonance interaction to amplify VLF and ULF waves in the magnetosphere were chosen for analysis because they showed potential for stimulation of amplification. Generally the models for the interaction are based on current state-of-the-art knowledge about injection methods and charged particle guns. Conditions in the magnetosphere were arbitrarily chosen to represent either a disturbed or a quiescent state with an arbitrary ambient plasma density. The parameters are not necessarily the most likely conditions that will be encountered, but they are typical and provide a uniform basis for comparison of the different methods for stimulation of the cyclotron resonance instability. A much more thorough investigation of those methods that show promise is advisable in order to assess the variety of results that can be anticipated for a wide range of conditions.

Perhaps the most immediate question concerns the validity of the linear theory in these applications. It clearly is a useful starting point for these investigations because a wide variety of injection methods may be studied parametrically for a relatively small expenditure of computer time. However, most of the useful results do penetrate the bounds of linear validity in some way. There are at least three levels of nonlinear sophistication that may be applied. First, the Taylor series expansion used to derive equations (4) and (5) requires $|k_i| \ll k_r$ which is frequently violated in the foregoing applications. An asymptotic solution for $|k_i| \gg k_r$ is readily derived and numerical solutions of (1) are possible when $|k_i| \simeq k_r$. Numerical solutions for the acoustic mode (Liemohn and Scarf, 1964) suggest that

the qualitative behavior for $|k_i| \doteq k_r$ is described by the linear expressions above, but the quantitative results are open to question.

Second, the linear theory is based on the assumption that the phase space distribution F_{HOT} is not perturbed significantly by the electromagnetic fields. The extent of this distortion depends on the magnitude of the fields and the repetitive interaction rate. These effects are difficult to estimate quantitatively, because the field amplitudes are not well known and the repetition depends on the size of the injection and the local resonance energy. The quasi-linear theory describes the equilibrium distortion of F_{HOT} rather well for the natural conditions in the magnetosphere, but it is inappropriate for these transient applications. The conclusion is that a full-blown nonlinear solution is needed to properly assess the linear results. Hopefully, existing nonlinear theory (Roux and Solomon, 1971; Bud'ko et al., 1972; Istomin and Karpman, 1972 a, b; and Brinca, 1972) can be adapted to these applications.

Based on the linear analysis, a few cases show considerable promise for stimulation of significant amplification; one or two may be appropriate for further study if a breakthrough in injection methods can be achieved, and some cases simply did not have the desired properties. For example, at VLF the barium shaped-charge injection gave a moderate mount of amplification only after 30 minutes had passed and its effectiveness was further limited by the experimentally observed striations that separated the jet of particles. Consequently, it appears

to be a relatively weak candidate using the current technology that was modeled in the case presented above. However, the advent of a larger payload at higher injection velocities which may produce a denser cloud, does offer real promise of strong amplification.

The geosynchronous lithium injection is currently the most promising method for stimulating either VLF or ULF radio noise. The conditions modeled some 10-minutes after injection are unrealistic at the present time due to the large payload required to achieve the plasma density; however, the conditions modeled at 50 minutes after injection appear to be readily achievable with current technology and a modest payload. These cases do require a nonlinear investigation, however, because $k_i \gtrsim k_r$ when amplification is appreciable (above 20-30 db).

The electron and proton beams have attractive characteristics for communication applications. But they do not appear to be feasible due to beam-current limitations. At VLF the electron beam has the property that it produces as much absorption as amplification so net wave growth is negligible. At ULF the net amplification appears to be much stronger, but for significant amplification a major breakthrough is required for the proton gun. Thus neither type of beam looks promising. Furthermore, no other parameter regimes look hopeful.

The low-energy cesium beam shows considerable potential both for stimulation of amplification and as a flux tube for earthward propagation. This somewhat radical concept should not be difficult to test because the technology is well established in laboratory plasma systems. The beam of electrons that is assumed to follow the cesium is of course somewhat

uncertain, but ambipolar diffusion in the plasma media is well recognized. An interesting sidelight is that the amplification exponent in Fig. 19 satisfies the requirements for application of the linear theory. The only remaining question is whether the helical beam expands into a larger plasma column as assumed in the analysis.

The lithium injection at L = 3.5 that is proposed to stimulate ULF waves fails miserably but it has important consequences for understanding the natural interaction at the plasmapause. Ignoring the injection for the moment, the important quantity is the index of refraction just inside and outside the plasmapause. Inside the index is at least an order of magnitude greater than outside because the plasma density is correspondingly lower in the plasmatrough. Thus the resonance speed for the cyclotron resonance interaction (equation (7) is an order of magnitude larger outside than inside the plasmapause, and the resonance energy is two orders of magnitude greater. Consequently, there is no appreciable amplification in the plasmatrough immediately outside the plasmapause and the proton ring current is relatively unaffected until it diffuses radially inward across this discontinuity (Cornwall et al., 1971). Returning to the lithium injection, it is now clear that huge densities of lithium are necessary to induce significant cyclotron resonance interactions below the local lithium gyro frequency just outside the plasmapause. The best place to inject lithium ion clouds for stimulation of amplification is at geosynchronous altitudes where only modest amounts of lithium are required and the proton ring current is still adequate.

Future studies must investigate the nonlinear aspects of the cyclotron resonance interaction for those cases that show promise of stimulating significant amplification. At VLF, improvements in the

shaped-charge barium jet must be investigated theoretically for its nonlinear limitations, and the low-energy cesium beam results should be independently corroborated. At ULF the only case that appears realistically feasible is geosynchronous injection of a lithium cloud. While these cases may not fulfill the immediate objective for communications, they do represent demonstrable ways to test the cyclotron-resonance interaction quantitatively. When this has been verified more exotic means of transmitting information can be explored.

REFERENCES

Brice, N., Artificial enhancement of energetic particle precipitation through cold plasma injection: A technique for seeding substorms?, J. Geophys. Res., 75, 4890-4892, 1970.

Brice, N., and C. Lucas, Influence of magnetospheric convection and polar wind on loss of electrons from the outer radiation belt, J. Geophys. Res., 76, 900-908, 1971.

Brinca, A. L., Whistler side-band growth due to nonlinear wave particle interaction, J. Geophys. Res., 77, 3508-3523, 1972.

Bud'ko, N. I., V. I. Karpman, and O. A. Pokhotelov, Nonlinear theory of the monochromatic circularly polarized VLF and ULF waves in the magnetosphere, Cosmic Electrodynamics, 3, 147-164, 1972.

Carpenter, D. L., Whistler studies of the plasmapause in the magnetosphere, 1. Temporal variations in the position of the knee and some evidence on plasma motions near the knee, J. Geophys. Res. 71, 693-709, 1966.

Carpenter, D. L., C. G. Park, H. A. Taylor, Jr., and H. C. Bunton, Multi-experiment detection of the plasmapause from EOGO satellites and Antarctic ground stations, J. Geophys. Res. 74, 1837-1847, 1969.

Cartwright, D. G., and P. J. Kellogg, Controlled experiment on wave-particle interactions in the ionosphere, Nature Physical Science, 231, No. 18, 11-12, May 3, 1971.

Cocke, W. B., and J. M. Cornwall, Theoretical simulation of micro-pulsations, J. Geophys.Res., 69, 2843-2856, 1967.

Cornwall, J. M., Micropulsations and the outer radiation zone, J. Geophys. Res., 71, 2185-2199, 1966.

Cornwall, J. M., Precipitation of auroral and ring-current particles by artificial plasma injection, Reviews of Geophys. and Space Science 10, 993-1002, 1972.

Cornwall, J. M., F. V. Coroniti, and R. M. Thorne, Unified theory of SAR arc formation at the plasmapause, J. Geophys. Res., 76, 4428-4445, 1971.

Cornwall, J. M. and M. Schulz, Electromagnetic ion-cyclotron instabilities in multicomponent magnetospheric plasmas, J. Geophys. Res., 76, 7791-7796, 1971.

Cuperman, S., and Y. Salu, Magnetospheric implications of nonlinear whistler instability obtained in a computer experiment, Preprint Tel-Aviv University, Israel.

DeForest, S. E., and C. E. McIlwain, Plasma clouds in the magnetosphere, J. Geophys. Res., 76, 3587-3611, 1971.

Derfler, H., Growing wave and instability criteria for hot plasmas, Phys. Letters 24A, 763-764, 1967.

Derfler, H., Frequency cusp, a means for discriminating between convective and nonconvective instability, Phys. Rev., A1, 1467-1471, 1970.

Eviatar, A., A. M. Lenchek, and S. F. Singer, Distribution of density in an ion-exosphere of a non-rotating planet, Phys. Fluids, 7, 1775-1779, 1964.

Frank, L. A., Several observations of low-energy protons and electrons in the earth's magnetosphere with OGO 3, J. Geophys. Res., 72, 1905-1916, 1967.

Frank, L. A., Recent observations of low-energy charged particles in the earth's magnetosphere, in Physics of the Magnetosphere, eds. R. L. Carovillano, J. F. McClay, and H. R. Radoski, Reidel, Dordrecht, Holland, 271-289, 1968.

Gendrin, R., Pitch angle diffusion of low energy protons due to gyro-resonant interaction with hydromagnetic waves, J. Atmospheric Terrest. Phys., 30, 1313-1330, 1968.

Helliwell, R. A., Whistlers and Related Pheonomena, Stanford University Press, Calif., 1965.

Hendrickson, R. A., R. W. McEntire, and J. R. Winckler, The electron echo experiment: A new magnetospheric probe, Nature, 230, No.5296, 564-566. April 30, 1971.

Hess, W. N., N. C. Trichel, T. N. Davis, W. C. Beggs, G. E. Kraft, E. Stassinopoulos, and E. J. R. Maier, Artificial aurora experiment: experiment and principal results, J. Geophys. Res., 76, 6067-6081, 1971.

Ho, H. S. and H. B. Liemohn, Some algebraic solutions of the cyclotron-resonance interaction, Plasma Physics, 14, 11-26, 1972.

Istomin, J. N., and V. I. Karpman, Nonlinear evolution of the quasi-monochromatic whistler mode packet, propagating along the magnetic field, Preprint #5, Inst. of Terrest. Mag. Ionosphere, and Radio Propag. Acad. Sci., USSR, 1972.

Istomin, J. N. and V. I. Karpman, Dispersion effects in the nonlinear evolution of quasimonochromatic helical waves in the magnetosphere, Preprint #17, Inst. Terrest. Mag., Ionosphere, and Radio Propag. Acad. Sci. USSR, 1972.

Jackson, J. D., Longitudinal plasma oscillations, J. Nucl. Energy, Part C: Plasma Phys, 1, 171-189, 1960.

Jacobs, J. A., and T. Watanabe, Micropulsation whistlers, J. Atmospheric Terrest. Phys., 26, 825-829, 1964.

Kennel, C. F., and H. Petschek, Limit on stably trapped particle fluxes, J. Geophys. Res., 71, 1-28, 1966.

Kennel, C. F., Low frequency whistler mode, Phys. Fluids, 9, 2190-2202, 1966.

Kennel, C. F., and R. M. Thorne, Unstable growth of unducted whistlers propagating at an angle to the geomagnetic field, J. Geophys. Res., 72, 871-878, 1967.

Kennel, C. F., and H. V. Wong, Resonantly unstable off-angle hydromagnetic waves, J. Plasma Phys., 1, 810104, 1967 (b).

Kitamura, T. and J. A. Jacobs, Ray paths of PC 1 waves in the magnetosphere, University of British Columbia, Institute of Earth Sciences, Scientific Report No. 14, April 19, 1967.

LeMaire, J., and M. Scherer, Model of the polar ion-exosphere, Planet. Space Sci.,18, 103-120, 1970.

Liemohn, H. B., Radiation from electrons in magnetoplasma, Radio Sci., 69D, 741-766, 1965.

Liemohn, H. B., Cyclotron-resonance amplification of VLF and ULF whistlers, J. Geophys. Res., 72, 39-55, 1967.

Liemohn, H. B., Cyclotron-resonance amplification of whistlers in the magnetosphere, in Plasma Waves in Space and in the Laboratory, eds. J. O. Thomas and B. J. Landmark, Edinburgh University Press, 437-449, 1969.

Liemohn, H. B., and F. L. Scarf, Whistler determination of electron energy and density distributions in the magnetosphere, J. Geophys. Res., 69, 883-904, 1964.

Montgomery, D. C., and D. A. Tidman, Plasma kinetic theory, McGraw-Hill, New York, 1964.

O'Brien, B. J., Review of studies of trapped radiation with satellite-borne apparatus, Space Science Revs., 1, 415-484, 1963.

Ossakow, S. L., E. Ott, and I. Haber, Theory and computer simulation of whistler turbulence and velocity space diffusion in the magneto-spheric plasma, NRL Memo Rpt. 2432, Wash. D. C., 1972.

Pizzella, G., and L. A. Frank, Energy spectrums for proton (200 eV $\leq$ E $\leq$ 1 meV) intensities in the outer radiation zone, J. Geophys. Res., 76, 88-91, 1971.

Rosenberg, T. J.,,R. A. Helliwell, and J. P. Katsufrakis, Electron precipitation associated with discrete very low frequency emissions, J. Geophys. Res., 76, 8445, 1971.

Roux, A., and J. Solomon, Self-consistent solution of the quasi-linear theory: Application to the spectral shape and intensity of VLF waves in the magnetosphere, J. Atmos. & Terrest. Physics, 33, 1457-1471, 1971.

Scarf, F. L., Landau damping and the attenuation of whistlers, Phys. Fluids, 5, 6-13, 1962.

Smith, R. L , R. A. Helliwell, and I. W. Yabroff, A theory of trapping of whistlers in field-aligned columns of enhanced ionization, J. Geophys. Res., 65, 815-823, 1960.

Smith, R. L., Propagation characteristics of whistlers trapped in field-aligned columns of enhanced ionization, J. Geophys. Res., 66, 3699-3707, 1961.

Thorne, R. M., and C. F. Kennel, Relativistic electron precipitation during magnetic storm main phase, J. Geophys. Res., 76, 4446-4453, 1971.

Trulsen, J., and J. A. Fejer, Radiation from a charged particle in magnetoplasma, J. Plasma Physics, 4, 825-841, 1970.

CYCLOTRON RESONANCE AMPLIFICATION OF
ULF AND VLF WHISTLER-MODE WAVES IN THE MAGNETOSPHERE

Computer Program Description

Programmer: R. J. Kerr
                     Applied Physics Laboratory
                     University of Washington

Scientist: H. B. Liemohn
                     Geophysics Program
                     University of Washington

August 1972

Cyclotron Resonance Amplification of ULF and VLF Whistler-Mode Waves in the Magnetosphere.

Mathematical Models

Net Amplitude Exponent (dimensionless)

$$XNIXY = n_{imag} = ck_i/\omega$$

For other models, see text.

INPUT VALUES

Card No.	Columns	Format	Symbol	Definition
1	1-2	I2	MONTH	Month, i.e., February enter 02.
1	3-4	I2	NDAY	Day of month.
1	5-6	I2	NYR	Year, i.e., 1972 enter 72
2	1-80	80H	--	Identification title for the data set immediately following.
3	1-10	F10.1	THO	Surface latitude (deg).
3	11-20	F10.0	XNO	Equatorial density (cm^{-3}).
3	21-25	I5	NTYPEQ	Indicator for cold plasma density model. See text for list of available models.
3	26-30	F5.0	YS	Lower band limit of range of propagation frequency/equatorial cyclotron frequency.
3	31-35	F5.0	YE	Upper band limit (as above).
3	36-40	F5.0	DELY	Step size (as above).
3	41-45	I5	NALPHA	Number of integration steps over pitch angle range.
3	46-50	I5	NX	Number of integration steps over latitude range.
3	51-55	I5	NBETAP	Number of integration steps over perpendicular velocity range.
3	56-50	F5.0	PORE	Indicator PORE = 1 for electron plasma particles. PORE ≈ 1836 for ion plasma particles.
4	1-5	I5	NUMHQ	Number of cards to be read for the quiescent pitch angle and distribution values.
4	6-10	I5	NUMNQ	Number of cards to be read for the quiescent normal energy and distribution values.
4	11-15	I5	NUMHS	Number of cards to be read for the streaming normal energy and distribution values.

Magnetosphere.

Input Values, cont.

Card No.	Columns	Format	Symbol	Definition
4	16-20	I5	NUMNS	Number of cards to be read for the streaming normal energy and distribution values.
5	1-10	F10.3	ALPHAQ$_{(1)}$	First value of quiescent pitch angle array (deg).
5	11-25	F15.3	HQ$_{(1)}$	First value of distribution array (relative).
			.	.
			.	.
			.	.
1 + NUMHQ	1-10	F10.3	ALPHAQ$_{(NUMHQ)}$	NUMHQ value of quiescent pitch angle array.
1 + NUMHQ	11-25	F15.3	HQ$_{(NUMHQ)}$	NUMHQ value of quiescent distribution array.
5 + NUMHQ	1-10	F10.3	EMCQ$_{(1)}$	First value of quiescent normal energy array (LOG_{10} (keV).
5 + NUMHQ	11-25	F15.3	XNQ$_{(1)}$	First value of distribution array (LOG_{10} (cm^{-3}).
			.	.
			.	.
			.	.
4 + NUMHQ + NUMNQ	1-10	F10.3	EMCQ$_{(NUMNQ)}$	NUMNQ value of quiescent normal energy array.
4 + NUMHQ + NUMNQ	11-25	F15.3	XNQ$_{(NUMNQ)}$	NUMNQ value of quiescent distribution array.

If values for streaming arrays are to be read, they are punched in the same manner as given for the quiescent arrays and follow immediately behind. Values for pitch angle and normalized energy must be in ascending order.

To run more than one set of data, repeat instructions starting at Card #2.

SAMPLE OUTPUT

M=1.0 N=1.5   ELECTRON TEST
SURFACE LATITUDE (THQ) =   60.00   PLASMA PARTICLE (PORE) =   1
EQUATORIAL DENSITY (XNO) =   232.00   DENSITY MODEL (NTYPEQ) =   2
PROPAGATION FREQ./EQUATORIAL CYCLOTRON FREQ. (DELY) = .100
BAND LIMITS (YS) =   .100   (YE) =   .900

QUIESCENT DISTRIBUTIONS

PITCH ANGLE (ALPHAQ)	DISTRIBUTION (HQ)	NORM. ENERGY (LOG(E/MCQ))	DISTRIBUTION (LOG(DNQ/(DE/MCQ)))
10.000	.000	-5.000	4.750
12.000	.060	-4.500	4.000
14.000	.150	-4.000	3.250
16.000	.210	-3.500	2.500
18.000	.260	-3.000	1.750
20.000	.310	-2.500	1.000
22.000	.350	-2.000	.250
24.000	.390	-1.500	-.500
26.000	.430	-1.000	-1.250
29.000	.470	-.500	-2.000
30.000	.500	0.000	-3.000
32.000	.530	.500	-5.000
34.000	.559	1.000	-10.000
36.000	.588	1.500	-40.000
38.000	.616	2.000	-200.000
40.000	.643		
42.000	.669		
44.000	.695		
46.000	.719		
48.000	.743		
50.000	.766		
52.000	.768		
54.000	.809		
56.000	.829		
58.000	.845		
60.000	.866		
62.000	.883		
64.000	.899		
66.000	.914		
68.000	.927		
70.000	.940		
72.000	.951		
74.000	.961		
76.000	.970		
78.000	.978		
80.000	.985		
82.000	.990		
84.000	.994		
86.000	.998		
88.000	.999		
90.000	1.000		

ELECTRON BEAM

$$\alpha_0 = 55^\circ \quad E_0 = 10 \text{ keV}$$

INTEGRATION STEPS   PITCH ANGLE (NALPHA) =   20
                      LATITUDE (NX) =   40
        PERPENDICULAR VELOCITY (NBETAP) =   50

STREAMING DISTRIBUTIIONS

PITCH ANGLE (ALPHAS)	DISTRIBUTION (HQ)	NORM. ENERGY (LOG(E/MCS))	DISTRIBUTION (LOG(DNS/(DE/MCS)))
50.000	0.000	-2.000	-40.000
51.000	.200	-1.900	-8.000
52.000	.600	-1.800	-2.000
53.000	1.200	-1.700	0.000
54.000	2.000	-1.600	-2.000
55.000	2.500	-1.500	-8.000
56.000	2.000	-1.400	-40.000
57.000	1.200		
58.000	.600		
59.000	.200		
60.000	0.000		

PROPAG. FREQ./EQTRL. CYCLOTRON FREQ.   (LOCAL) = .3000

| LOCAL B/EQTRL B | REFRACTIVE INDEX**2 | LOCAL AMPLITUDE EXPONENT | | | SINE (LATITUDE) |
| | | STREAMING | QUIESCENT | NET | |
(B)	(XN2)	(XJS)	(XJQ)	(XN1XY)	(X)
1.0000E+00	4.7853E+02	3.2770E-03	-2.6933E-05	3.7339E-02	.0000
1.0021E+00	4.7726E+02	3.5918E-03	-2.8394E-05	4.1062E-02	.0217
1.0085E+00	4.7348E+02	4.1488E-03	-3.2265E-05	4.7865E-02	.0433
1.0192E+00	4.6729E+02	3.2387E-03	-3.8732E-05	3.7767E-02	.0650
1.0343E+00	4.5882E+02	-1.8430E-03	-3.9715E-05	-2.2687E-02	.0866
1.0541E+00	4.4826E+02	-3.3646E-03	-4.6085E-05	-4.2204E-02	.1083
1.0787E+00	4.3583E+02	-6.6772E-04	-5.0457E-05	-9.1766E-03	.1299
1.1085E+00	4.2178E+02	-1.5896E-05	-5.4378E-05	-9.3226E-04	.1516
1.1439E+00	4.0638E+02	-2.8354E-08	-5.8282E-05	-8.0735E-04	.1732
1.1854E+00	3.8988E+02	0.	-6.2214E-05	-9.0362E-04	.1949
1.2335E+00	3.7255E+02	0.	-6.3038E-05	-9.6519E-04	.2165
1.2889E+00	3.5463E+02	0.	-6.3147E-05	-1.0241E-03	.2382
1.3524E+00	3.3635E+02	0.	-6.1553E-05	-1.0622E-03	.2598
1.4251E+00	3.1791E+02	0.	-5.6646E-05	-1.0449E-03	.2815
1.5081E+00	2.9950E+02	0.	-5.4277E-05	-1.0748E-03	.3031
1.6029E+00	2.8127E+02	0.	-4.9667E-05	-1.0605E-03	.3248
1.7113E+00	2.6336E+02	0.	-4.3521E-05	-1.0063E-03	.3464
1.8354E+00	2.4587E+02	0.	-3.9196E-05	-9.8574E-04	.3681
1.9777E+00	2.2889E+02	0.	-3.4397E-05	-9.4495E-04	.3897
2.1414E+00	2.1249E+02	0.	-2.9170E-05	-8.7927E-04	.4114
2.3305E+00	1.9673E+02	0.	-2.5360E-05	-8.4259E-04	.4330
2.5498E+00	1.8165E+02	0.	-2.1449E-05	-7.8929E-04	.4547
2.8054E+00	1.6727E+02	0.	-1.7366E-05	-7.1129E-04	.4763
3.1050E+00	1.5360E+02	0.	-1.4007E-05	-6.4199E-04	.4980
3.4584E+00	1.4067E+02	0.	-1.1228E-05	-5.7913E-04	.5196
3.8783E+00	1.2846E+02	0.	-8.4184E-06	-4.9158E-04	.5413
4.3812E+00	1.1698E+02	0.	-5.9441E-06	-3.9557E-04	.5629
4.9889E+00	1.0622E+02	0.	-3.9268E-06	-3.0013E-04	.5846
5.7305E+00	9.6173E+01	0.	-2.3847E-06	-2.1077E-04	.6062
6.6459E+00	8.6817E+01	0.	-1.2300E-06	-1.2689E-04	.6279
7.7900E+00	7.8145E+01	0.	-4.8726E-07	-5.9255E-05	.6495
9.2405E+00	7.0142E+01	0.	-1.1588E-07	-1.6796E-05	.6712
1.1109E+01	6.2796E+01	0.	-1.6409E-08	-2.8708E-06	.6928
1.3563E+01	5.6096E+01	0.	-9.8203E-10	-2.1039E-07	.7145
1.6853E+01	5.0034E+01	0.	-1.4679E-11	-3.9164E-09	.7361
2.1377E+01	4.4609E+01	0.	0.	0.	.7578
2.7785E+01	3.9829E+01	0.	0.	0.	.7794
3.7188E+01	3.5723E+01	0.	0.	0.	.8011
5.1601E+01	3.2354E+01	0.	0.	0.	.8227
7.4921E+01	2.9861E+01	0.	0.	0.	.8444
1.1538E+02	2.6559E+01	0.	0.	0.	.8660

PROPER. FREQ./ZCTRL. CYCLOTRON FREQ.   (LOCAL) = .4000

LOCAL B/CNTRL B	REFRACTIVE INDEX**2	LOCAL AMPLITUDE EXPONENT			SINE (LATITUDE)
		STREAMING	QUIESCENT	NET	
(B)	(XN2)	(XJS)	(XJQ)	(XNIXY)	(X)
1.6003E+00	4.1884E+02	9.9491E-37	5.6106E-05	4.1421E-04	.0000
1.6021E+00	4.2752E+02	1.3480E-30	5.2469E-05	3.8875E-04	.0217
1.3065E+00	4.1306E+02	6.5073E-25	4.2025E-05	3.1915E-04	.0433
1.6192E+00	4.0720E+02	7.1810E-17	2.8365E-05	2.1610E-04	.0650
1.0343E+00	3.9893E+02	4.2235E-09	1.2107E-05	9.4523E-05	.0866
1.3541E+00	3.8773E+02	3.1454E-06	-2.3752E-06	6.1977E-06	.1083
1.6767E+00	3.7517E+02	5.3532E-04	-1.5356E-05	4.3298E-03	.1299
1.1065E+00	3.6113E+02	4.0354E-03	-2.8472E-05	3.4931E-02	.1516
1.1439E+00	3.4590E+02	-1.8558E-03	-3.9248E-05	-1.7349E-02	.1732
1.1654E+00	3.2980E+02	-1.9987E-03	-4.7311E-05	-1.9761E-02	.1949
1.2335E+00	3.1310E+02	-1.0340E-05	-5.1601E-05	-6.3538E-04	.2165
1.2389E+00	2.9606E+02	-6.6507E-16	-5.5956E-05	-6.0699E-04	.2382
1.352E+00	2.7892E+02	0.	-5.8868E-05	-6.8908E-04	.2598
1.4251E+00	2.6137E+02	0.	-6.0137E-05	-7.5611E-04	.2815
1.5061E+00	2.4536E+02	0.	-5.7719E-05	-7.8571E-04	.3031
1.6029E+00	2.2603E+02	0.	-5.2737E-05	-7.7910E-04	.3248
1.7113E+00	2.1277E+02	0.	-4.9043E-05	-7.8954E-04	.3464
1.8354E+00	1.9744E+02	0.	-4.4218E-05	-7.7892E-04	.3681
1.3777E+00	1.8275E+02	0.	-3.8417E-05	-7.4353E-04	.3897
2.1414E+00	1.6873E+02	0.	-3.3141E-05	-7.0767E-04	.4114
2.3305E+00	1.5543E+02	0.	-2.8800E-05	-6.8146E-04	.4330
2.5498E+00	1.4279E+02	0.	-2.4117E-05	-6.3566E-04	.4547
2.8054E+00	1.3088E+02	0.	-2.0253E-05	-5.9632E-04	.4763
3.1053E+00	1.1968E+02	0.	-1.6295E-05	-5.3915E-04	.4980
3.4564E+00	1.0915E+02	0.	-1.3095E-05	-4.8950E-04	.5196
3.8783E+00	9.9346E+01	0.	-1.0065E-05	-4.2750E-04	.5413
4.3812E+00	9.0173E+01	0.	-7.3594E-06	-3.5740E-04	.5629
4.9563E+00	8.1636E+01	0.	-5.0593E-06	-2.8287E-04	.5846
5.7305E+00	7.3718E+01	0.	-3.2836E-06	-2.1298E-04	.6062
6.5459E+00	6.6393E+01	0.	-1.8539E-06	-1.4068E-04	.6279
7.7960E+00	5.9642E+01	0.	-8.7571E-07	-7.8487E-05	.6495
9.2405E+00	5.3443E+01	0.	-2.6852E-07	-2.8733E-05	.6712
1.1109E+01	4.7780E+01	0.	-5.1797E-08	-6.6993E-06	.6928
1.3563E+01	4.2636E+01	0.	-4.4549E-09	-7.0634E-07	.7145
1.6853E+01	3.7999E+01	0.	-1.1672E-10	-2.3065E-08	.7361
2.1377E+01	3.3862E+01	0.	0.	0.	.7578
2.7785E+01	3.0228E+01	0.	0.	0.	.7794
3.7188E+01	2.7113E+01	0.	0.	0.	.8011
5.1601E+01	2.4501E+01	0.	0.	0.	.8227
7.4921E+01	2.2075E+01	0.	0.	0.	.8444
1.1535E+02	2.1688E+01	0.	0.	0.	.8660

PROPAG. FREQ./CNTR. CYCLOTRON FREQ.   (LOCAL) = .5000

LOCAL B/=CNTRL B (B)	REFRACTIVE INDEX**2 (XN2)	LOCAL AMPLITUDE EXPONENT			SINE (LATITUDE) (X)
		STREAMING (XJS)	QUIESCENT (XJQ)	NET (XNIXY)	
1.0000E+00	4.0212E+02	0.	2.0426E-04	1.3988E-03	.0000
1.0021E+00	4.0053E+02	0.	2.7706E-04	1.3694E-03	.0217
1.0085E+00	3.9600E+02	0.	2.5531E-04	1.2778E-03	.0433
1.0192E+00	3.8855E+02	0.	2.2035E-04	1.1260E-03	.0650
1.0343E+00	3.7851E+02	0.	1.7430E-04	9.1658E-04	.0866
1.0541E+00	3.6622E+02	0.	1.3359E-04	7.2839E-04	.1083
1.0787E+00	3.5236E+02	0.	9.3844E-05	5.3438E-04	.1299
1.1085E+00	3.3645E+02	4.0716E-14	5.7823E-05	3.4619E-04	.1516
1.1439E+00	3.1977E+02	3.9515E-05	1.5623E-05	3.4927E-04	.1732
1.1854E+00	3.0242E+02	3.4846E-03	-9.0470E-06	2.3429E-02	.1949
1.2335E+00	2.8472E+02	-2.1070E-03	-2.9715E-05	-1.5411E-02	.2165
1.2889E+00	2.6697E+02	-1.6139E-03	-4.5990E-05	-1.2919E-02	.2382
1.3524E+00	2.4942E+02	-2.4294E-07	-4.7192E-05	-3.9740E-04	.2598
1.4251E+00	2.3226E+02	0.	-5.0052E-05	-4.7312E-04	.2815
1.5081E+00	2.1563E+02	0.	-5.5085E-05	-5.4544E-04	.3031
1.6029E+00	1.9900E+02	0.	-5.4653E-05	-5.9185E-04	.3248
1.7113E+00	1.8440E+02	0.	-5.0888E-05	-6.0498E-04	.3464
1.8354E+00	1.6992E+02	0.	-4.7047E-05	-6.2416E-04	.3681
1.9777E+00	1.5624E+02	0.	-4.2840E-05	-6.2067E-04	.3897
2.1414E+00	1.4330E+02	0.	-3.6771E-05	-5.9144E-04	.4114
2.3305E+00	1.3127E+02	0.	-3.1397E-05	-5.6281E-04	.4330
2.5490E+00	1.1997E+02	0.	-2.7145E-05	-5.4450E-04	.4547
2.8054E+00	1.0941E+02	0.	-2.2470E-05	-5.0652E-04	.4763
3.1050E+00	9.9592E+01	0.	-1.8127E-05	-4.6130E-04	.4980
3.4584E+00	9.0407E+01	0.	-1.4970E-05	-4.3219E-04	.5196
3.8783E+00	8.2006E+01	0.	-1.1706E-05	-3.8547E-04	.5413
4.3812E+00	7.4177E+01	0.	-8.7604E-06	-3.3176E-04	.5629
4.9889E+00	6.6947E+01	0.	-6.2009E-06	-2.7057E-04	.5846
5.7309E+00	6.0287E+01	0.	-4.1881E-06	-2.1258E-04	.6062
6.6459E+00	5.4135E+01	0.	-2.4770E-06	-1.4745E-04	.6279
7.7900E+00	4.8557E+01	0.	-1.2696E-06	-8.9452E-05	.6495
9.2465E+00	4.3435E+01	0.	-5.1653E-07	-4.3525E-05	.6712
1.1109E+01	3.8777E+01	0.	-1.2137E-07	-1.2430E-05	.6928
1.3563E+01	3.4564E+01	0.	-1.2806E-08	-1.6165E-06	.7145
1.6853E+01	3.0780E+01	0.	-4.7907E-10	-7.4795E-08	.7361
2.1377E+01	2.7410E+01	0.	-2.7229E-12	-5.4050E-10	.7578
2.7785E+01	2.4406E+01	0.	0.	0.	.7794
3.7186E+01	2.1947E+01	0.	0.	0.	.8011
5.1601E+01	1.9880E+01	0.	0.	0.	.8227
7.4921E+01	1.8363E+01	0.	0.	0.	.8444
1.1530E+02	1.7564E+01	0.	0.	0.	.8660

PROPAG. FREQ./ENTRL. CYCLOTRON FREQ.   (LOCAL) = .6000

LOCAL B/ENTRL B (B)	REFRACTIVE INDEX**2 (XN2)	LOCAL AMPLITUDE EXPONENT STREAMING (XJS)	QUIESCENT (XJQ)	NET (XNIXY)	SINE (LATITUDE) (X)
1.0000E+00	4.1884E+02	0.	9.6593E-04	3.1697E-03	.0000
1.0021E+00	4.1679E+02	0.	9.4317E-04	3.1113E-03	.0217
1.0085E+00	4.1075E+02	0.	8.8050E-04	2.9504E-03	.0433
1.0192E+00	4.0101E+02	0.	7.9065E-04	2.7185E-03	.0650
1.0343E+00	3.8653E+02	0.	6.4759E-04	2.3068E-03	.0866
1.0541E+00	3.7233E+02	0.	4.9607E-04	1.8473E-03	.1083
1.0787E+00	3.5467E+02	0.	3.6671E-04	1.5180E-03	.1299
1.1085E+00	3.3551E+02	0.	2.8091E-04	1.1712E-03	.1516
1.1439E+00	3.1548E+02	0.	1.8237E-04	8.1539E-04	.1732
1.1854E+00	2.9509E+02	7.6972E-09	1.0538E-04	5.0561E-04	.1949
1.2335E+00	2.7470E+02	2.1858E-03	4.9102E-05	1.1600E-02	.2165
1.2889E+00	2.5492E+02	3.2323E-03	1.5409E-06	1.6247E-02	.2382
1.3524E+00	2.3593E+02	-2.0759E-03	-2.4463E-05	-1.7866E-02	.2598
1.4251E+00	2.1787E+02	-1.5802E-06	-4.6895E-05	-3.2739E-04	.2815
1.5161E+00	1.9950E+02	0.	-4.4081E-05	-3.2753E-04	.3031
1.6329E+00	1.8305E+02	0.	-5.0341E-05	-4.1291E-04	.3248
1.7113E+00	1.6759E+02	0.	-5.2885E-05	-4.6042E-04	.3464
1.8584E+00	1.5317E+02	0.	-5.0464E-05	-5.0930E-04	.3681
1.9777E+00	1.3970E+02	0.	-4.5581E-05	-5.1269E-04	.3897
2.1414E+00	1.2733E+02	0.	-4.0756E-05	-5.1254E-04	.4114
2.3305E+00	1.1583E+02	0.	-3.4504E-05	-4.6676E-04	.4330
2.5493E+00	1.0522E+02	0.	-2.9435E-05	-4.6747E-04	.4547
2.8054E+00	9.5542E+01	0.	-2.4245E-05	-4.3509E-04	.4763
3.1050E+00	8.6440E+01	0.	-2.0242E-05	-4.1215E-04	.4980
3.4584E+00	7.8154E+01	0.	-1.6530E-05	-3.8359E-04	.5196
3.8763E+00	7.0504E+01	0.	-1.3055E-05	-3.4695E-04	.5413
4.3612E+00	6.3593E+01	0.	-9.9653E-06	-3.0499E-04	.5629
4.9383E+00	5.7230E+01	0.	-7.1552E-06	-2.5373E-04	.5846
5.7305E+00	5.1363E+01	0.	-4.8363E-06	-2.0607E-04	.6062
6.6459E+00	4.6035E+01	0.	-3.1459E-06	-1.5301E-04	.6279
7.7390E+00	4.1182E+01	0.	-1.7028E-06	-9.8233E-05	.6495
9.2469E+00	3.6772E+01	0.	-7.5147E-07	-5.1942E-05	.6712
1.1103E+01	3.2738E+01	0.	-2.1200E-07	-1.7763E-05	.6928
1.3563E+01	2.9150E+01	0.	-2.6376E-08	-2.9211E-06	.7145
1.6853E+01	2.5970E+01	0.	-1.4618E-09	-1.8014E-07	.7361
2.1377E+01	2.3119E+01	0.	-1.5801E-11	-2.5829E-09	.7578
2.7785E+01	2.0629E+01	0.	0.	0.	.7794
3.7165E+01	1.8537E+01	0.	0.	0.	.8011
5.1601E+01	1.6709E+01	0.	0.	0.	.8227
7.4921E+01	1.5489E+01	0.	0.	0.	.8444
1.1533E+02	1.4510E+01	0.	0.	0.	.8660

PROPAG. FREQ./EQTRL. CYCLOTRON FREQ.   (LOCAL) = .7000

LOCAL B/EQTRL B (B)	REFRACTIVE INDEX**2 (XN2)	LOCAL STREAMING (XJS)	AMPLITUDE EXPONENT QUIESCENT (XJQ)	NET (XNIXY)	SINE (LATITUDE) (X)
1.0000E+00	4.7853E+02	0.	3.2284E-03	6.8124E-03	.0000
1.0021E+00	4.7536E+02	0.	3.1553E-03	6.7050E-03	.0217
1.0085E+00	4.6607E+02	0.	2.9192E-03	6.3336E-03	.0433
1.0192E+00	4.5129E+02	0.	2.5593E-03	5.7447E-03	.0650
1.0343E+00	4.3198E+02	0.	2.1839E-03	5.1339E-03	.0866
1.0541E+00	4.0923E+02	0.	1.7386E-03	4.3284E-03	.1083
1.0787E+00	3.8419E+02	0.	1.3257E-03	3.5295E-03	.1299
1.1085E+00	3.5793E+02	0.	9.6282E-04	2.7648E-03	.1516
1.1439E+00	3.3127E+02	0.	6.4341E-04	2.0073E-03	.1732
1.1854E+00	3.0501E+02	0.	4.1044E-04	1.3996E-03	.1949
1.2335E+00	2.7903E+02	2.7339E-10	2.5294E-04	9.4770E-04	.2165
1.2889E+00	2.5551E+02	2.7250E-03	1.2432E-04	1.1780E-02	.2382
1.3524E+00	2.3284E+02	1.4415E-03	4.7243E-05	6.8167E-03	.2598
1.4251E+00	2.1175E+02	-2.5179E-03	-3.6056E-06	-1.2826E-02	.2815
1.5081E+00	1.9225E+02	-1.2003E-08	-2.9129E-05	-1.6513E-04	.3031
1.6029E+00	1.7433E+02	0.	-3.8136E-05	-2.4132E-04	.3248
1.7113E+00	1.5791E+02	0.	-4.6372E-05	-3.2846E-04	.3464
1.8354E+00	1.4291E+02	0.	-5.0271E-05	-3.9949E-04	.3681
1.9777E+00	1.2924E+02	0.	-4.6283E-05	-4.3146E-04	.3897
2.1414E+00	1.1679E+02	0.	-4.3530E-05	-4.3848E-04	.4114
2.3305E+00	1.0545E+02	0.	-3.6360E-05	-4.1391E-04	.4330
2.5498E+00	9.5103E+01	0.	-3.2069E-05	-4.1373E-04	.4547
2.8054E+00	8.5795E+01	0.	-2.7045E-05	-3.9667E-04	.4763
3.1050E+00	7.7279E+01	0.	-2.2088E-05	-3.6959E-04	.4980
3.4584E+00	6.9538E+01	0.	-1.7734E-05	-3.3985E-04	.5196
3.8783E+00	6.2502E+01	0.	-1.4596E-05	-3.2176E-04	.5413
4.3812E+00	5.6109E+01	0.	-1.1301E-05	-2.8801E-04	.5629
4.9889E+00	5.0302E+01	0.	-8.2272E-06	-2.4377E-04	.5846
5.7305E+00	4.5031E+01	0.	-5.5517E-06	-1.9248E-04	.6062
6.6459E+00	4.0253E+01	0.	-3.6195E-06	-1.4789E-04	.6279
7.7900E+00	3.5927E+01	0.	-2.0274E-06	-9.9957E-05	.6495
9.2405E+00	3.2020E+01	0.	-9.9099E-07	-5.7793E-05	.6712
1.1109E+01	2.8502E+01	0.	-3.2162E-07	-2.0770E-05	.6928
1.3563E+01	2.5347E+01	0.	-5.2405E-08	-4.5638E-06	.7145
1.6853E+01	2.2535E+01	0.	-3.2872E-09	-3.5765E-07	.7361
2.1377E+01	2.0051E+01	0.	-5.1424E-11	-7.1208E-09	.7578
2.7785E+01	1.7887E+01	0.	0.	0.	.7794
3.7188E+01	1.6044E+01	0.	0.	0.	.8011
5.1601E+01	1.4543E+01	0.	0.	0.	.8227
7.4921E+01	1.3430E+01	0.	0.	0.	.8444
1.1536E+02	1.2052E+01	0.	0.	0.	.8660

PROPAG. FREQ./CENTRL. CYCLOTRON FREQ.   (LOCAL) = .6600

LOCAL B/CNTRL B (B)	REFRACTIVE INDEX**2 (XN2)	LOCAL AMPLITUDE EXPONENT			SINE (LATITUDE) (X)
		STREAMING (XJS)	QUIESCENT (XJQ)	NET (XNIXY)	
1.0000E+00	5.2776E+02	0.	8.8864E-03	1.0944E-02	.0000
1.0021E+00	6.2142E+02	0.	8.7309E-03	1.0866E-02	.0217
1.0085E+00	6.0313E+02	0.	8.2555E-03	1.0597E-02	.0433
1.0192E+00	5.7479E+02	0.	7.5279E-03	1.0157E-02	.0650
1.0340E+00	5.3900E+02	0.	6.5379E-03	9.4298E-03	.0866
1.0541E+00	4.9833E+02	0.	5.4258E-03	8.4847E-03	.1083
1.0787E+00	4.5062E+02	0.	4.2130E-03	7.2259E-03	.1299
1.1065E+00	4.1451E+02	0.	3.0825E-03	5.8515E-03	.1516
1.1439E+00	3.7401E+02	0.	2.1214E-03	4.4881E-03	.1732
1.1854E+00	3.3603E+02	0.	1.3747E-03	3.2579E-03	.1949
1.2339E+00	3.0105E+02	0.	8.5417E-04	2.2760E-03	.2165
1.2809E+00	2.6925E+02	2.2740E-04	4.5237E-04	2.0419E-03	.2382
1.3524E+00	2.4059E+02	4.4234E-03	2.3976E-04	1.5828E-02	.2598
1.4251E+00	2.1491E+02	-4.3554E-03	1.0406E-04	-1.6311E-02	.2815
1.5081E+00	1.9196E+02	-1.3237E-03	1.7348E-05	-5.6970E-03	.3031
1.6029E+00	1.7155E+02	0.	-1.7430E-05	-8.5812E-05	.3248
1.7113E+00	1.5336E+02	0.	-3.3226E-05	-1.6553E-04	.3464
1.8354E+00	1.3717E+02	0.	-4.2609E-05	-2.7010E-04	.3681
1.9777E+00	1.2274E+02	0.	-4.7102E-05	-3.3933E-04	.3697
2.1414E+00	1.0987E+02	0.	-4.4606E-05	-3.6617E-04	.4114
2.3305E+00	9.8379E+01	0.	-4.0975E-05	-3.8285E-04	.4330
2.5498E+00	8.8101E+01	0.	-3.4358E-05	-3.6657E-04	.4547
2.8054E+00	7.8836E+01	0.	-2.8943E-05	-3.5344E-04	.4763
3.1053E+00	7.0042E+01	0.	-2.3537E-05	-3.2986E-04	.4980
3.4504E+00	5.3227E+01	0.	-1.9630E-05	-3.1076E-04	.5196
3.8783E+00	5.6503E+01	0.	-1.5623E-05	-2.9137E-04	.5413
4.3612E+00	5.3507E+01	0.	-1.2445E-05	-2.6943E-04	.5629
4.9089E+00	4.5169E+01	0.	-8.9504E-06	-2.2627E-04	.5846
5.7303E+00	4.0339E+01	0.	-6.3861E-06	-1.8938E-04	.6062
6.5459E+00	3.5934E+01	0.	-4.1029E-06	-1.4592E-04	.6279
7.7300E+00	3.1999E+01	0.	-2.5441E-06	-1.0625E-04	.6495
9.2409E+00	2.8464E+01	0.	-1.2777E-06	-6.4174E-05	.6712
1.1109E+01	2.5293E+01	0.	-4.4496E-07	-2.7170E-05	.6928
1.3563E+01	2.2470E+01	0.	-1.0262E-07	-7.7182E-06	.7145
1.6895E+01	1.9900E+01	0.	-6.5934E-09	-6.2008E-07	.7361
2.1377E+01	1.7751E+01	0.	-1.3431E-10	-1.6049E-08	.7578
2.7703E+01	1.5531E+01	0.	0.	0.	.7794
3.7100E+01	1.4200E+01	0.	0.	0.	.8011
5.1601E+01	1.2673E+01	0.	0.	0.	.8227
7.4921E+01	1.1696E+01	0.	0.	0.	.8444
1.1530E+02	1.1330E+01	0.	0.	0.	.8660

M=1.J N=1.5   ELECTRON TEST

OPAG. FREQ./ENTRL CYCLOTRON FREQ.	NET AMPLIFICATION (DECIBELS)
.100	1.736683981420E+01
.200	1.850691970669E+01
.300	-4.442368976719E+01
.400	-1.264777731429E+00
.500	-3.606791249726E+00
.600	-5.269851215569E+01
.700	-7.692933324534E+01
.800	-1.345422457571E+02
.900	-2.438744868675E+02

PLASMA DENSITY QUIESCENT/COLD	PITCH ANGLE QUIESCENT NORM.	PLASMA DENSITY STREAMING/COLD	PITCH ANGLE STREAMING NORM.
3.6503E-03	1.0212E-01	1.3812E-15	5.2957E-01

Cyclotron Resonance Amplification of ULF and VLF Whistler-Mode Waves in the Magnetosphere.

Flow Diagram
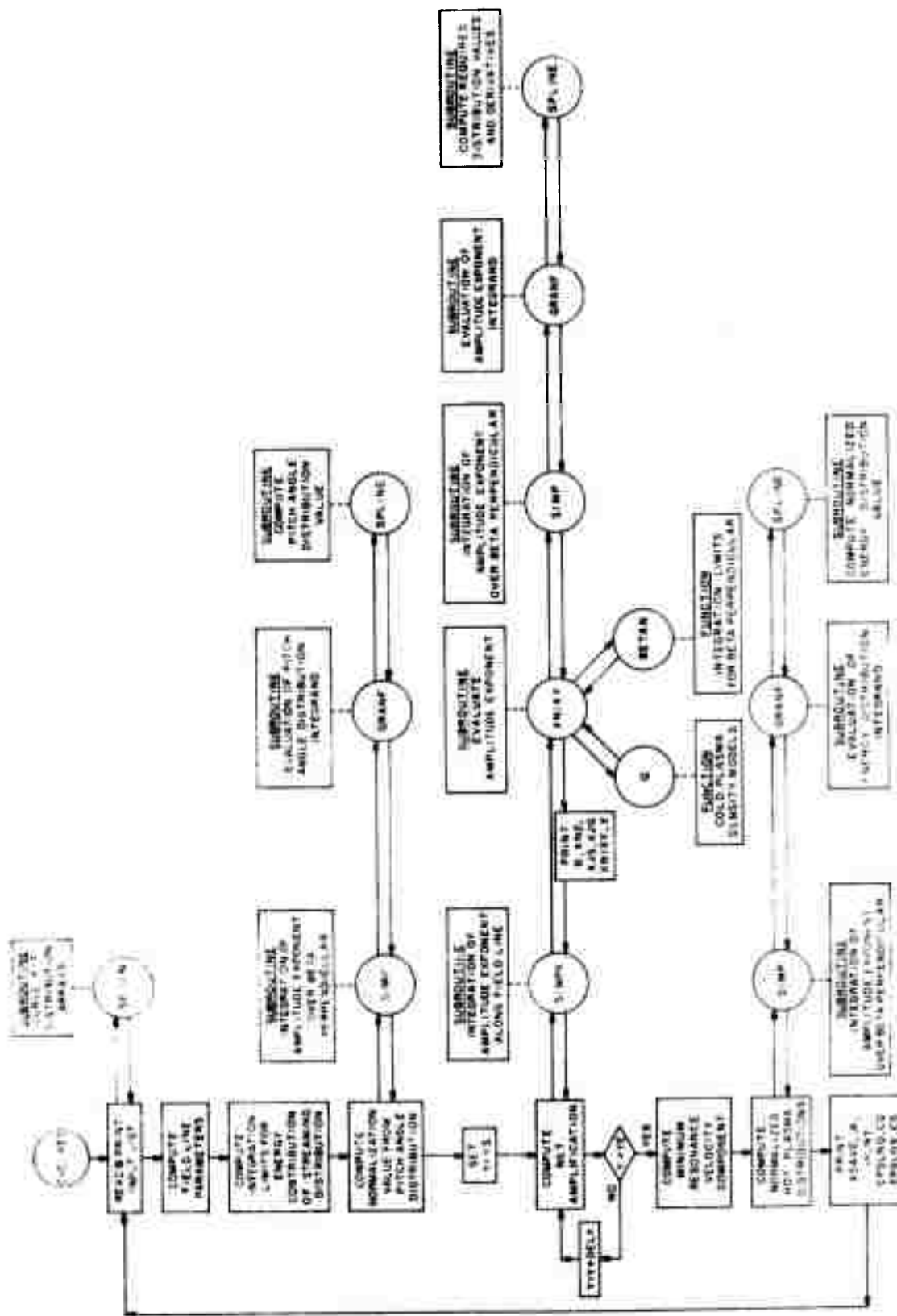
```
      PROGRAM CYCLRES (INPUT,OUTPUT,TAPE1=INPUT,TAPE3=OUTPUT)
      DIMENSION         A(100),P(100),XSAVE(100)
      DIMENSION         HQ(50),HS(50),XNQ(50),XNS(50),ALPHAQ(50),
     1ALPHAS(50),EMCQ(50),EMCS(50),SPLCNS(50),SPLCHQ(4,50),SPLCHS(4,50),
     2SPLCNQ(4,50)
      COMMON HQ,HS,XNQ,XNS,ALPHAQ,ALPHAS,EMCQ,EMCS,SPLCHQ,SPLCHS,SPLCNQ,
     1  SPLCNS,RAD,PI,THO,XNO,CQ,CS,HPO,THOR,COSTH,SINTH,HCO,Y,Y2,HCO2,
     2  B2,XN2,B,XN,DEG,BETAS1,BETAS2,PORE,NUMHQ,NUMHS,NUMNQ,NUMNS,
     3  NTYPEQ,NTYPE,NBETAP,NPAGE,MONTH,NDAY,NYR
C
C
C
C     PROGRAM FOR HAROLD LIEMOHN   ACT 1445   TP41233
C       PROGRAM MODIFIED 2/28/72   ROBERTA KERR
C
C
C     WHISTLER MODE AMPLIFICATION
C
C
      NPAGE=1
      RAD=.0174532925
      PI=3.141592654
      DEG=57.2957795
C
      READ (1,2000)MONTH,NDAY,NYR
C TITLE CARD
    5 READ (1,1030)
      IF(EOF,1) 5000,6
    6 CALL SPRINT
      WRITE (3,1030)
C   INITIAL VALUES AND CONTROL PARAMETERS
      READ (1,1040)THO,XNO,NTYPEQ,YS,YE,DELY,NALFHA,NX,NBETAP,PORE
      WRITE(3,1050)  THO,PORE,NALPHA,XNO,NTYPEQ,NX,DELY,NBETAP,YS,YE
C
C
C   READ PITCH ANGLE DISTRIB(HQ,HS) AND LOG10 OF ENERGY DISTRIB(XNQ,XNS)
      READ (1,1000)NUMHQ,NUMNQ,NUMHS,NUMNS
      IF(NUMHQ.LE.0) GO TO 20
      READ (1,1010) (ALPHAQ(I),HQ(I),I=1,NUMHQ)
      CALL SPLICN(ALPHAQ,HQ,NUMHQ,SPLCHQ)
   20 IF(NUMNQ.LE.0) GO TO 21
      READ (1,1010) (EMCQ(I),XNQ(I),I=1,NUMNQ)
      CALL SPLICN(EMCQ,XNQ,NUMNQ,SPLCNQ)
   21 IF(NUMHS.LE.0) GO TO 22
      READ (1,1010) (ALPHAS(I),HS(I),I=1,NUMHS)
      CALL SPLICN(ALPHAS,HS,NUMHS,SPLCHS)
   22 IF(NUMNS.LE.0) GO TO 23
      READ (1,1010) (EMCS(I),XNS(I),I=1,NUMNS)
      CALL SPLICN(EMCS,XNS,NUMNS,SPLCNS)
   23 WRITE(3,1020)
      MMAX=MAXO(NUMHQ,NUMHS,NUMNQ,NUMNS)
      DO 25 I=1,MMAX
      IF(I.LE.NUMNQ) WRITE(3,1001) ALPHAQ(I),HQ(I)
      IF(I.LE.NUMNQ) WRITE(3,1002) EMCQ(I),XNQ(I)
      IF(I.LE.NUMHS) WRITE(3,1003) ALPHAS(I),HS(I)
      IF(I.LE.NUMNS) WRITE(3,1004) EMCS(I),XNS(I)
   25 CONTINUE
C
```

```
C    FIELD LINE PARAMETERS
C
      THOR=THO*RAD
      COSTH =  COS(THOR)
      SINTH =  SIN(THOR)
      WP0 = 5.65E+04* SQRT(XN0)
      WC0=5.5E+06*COSTH**6
      WC02=WC0**2
      IF(NUMNS.LE.0) GO TO 26
      BETAC1=SQRT(1.-1./((10.**EMCS(1)/PORE+1.)**2))
      BETACS2=SQRT(1.-1./((10.**EMCS(NUMNS)/PORE+1.)**2))
C
C    NORMALIZE PITCH ANGLE DISTRIBUTIONS
C
   26 NTYPE=1
      CALL SIMP(0.,PI/2.,NALPHA,CO)
      CO=CO*4.*PI
      CO=1./CO
      IF(NUMHS.LE.0) GO TO 160
      NTYPE = 2
      CALL SIMP(ALPHAS(1)*RAD,ALPHAS(NUMHS)*RAC,NALPHA,CS)
      CS=CS*4.*PI
      CS=1./CS
C    SET PROPAGATION FREQUENCY
  160 NUMY=0
      Y=YS
C
C    COMPUTE CYCLOTRON RESONANCE AMPLIFICATION AT Y
C
  170 Y2=Y*Y
      CALL SPRINT
      WRITE(3,1110) Y
      WRITE (3,1100)
  410 CALL SIMPX(0.,SINTH,NX,FI)
      NUMY=NUMY+1
      A(NUMY)=-2.03E+06*Y*COSTH**4*FI
      XSAVE(NUMY)=Y
      Y=Y+DELY
      IF (Y-YE)170,170,180
C
C    EVALUATE MINIMUM RESONANCE VELOCITY COMPONENT
C
  180 YA=YS
      IF(PORE.GT.10.) GO TO 362
      ZA=YA
      GO TO 363
  362 ZA=1
  363 XN2=1.+WP0**2/(WC02*ZA*(1.-YA))
      XN= SQRT(XN2)
      YA2=YA*YA
      C1=1./(XN2*YA2)
      BETAR=1.- SQRT(1.-(1.+C1)*(1.-1./YA2))
      BETAC=BETAR/(XN*(1.+C1))
C    NORMALIZE HOT PLASMA DISTRIBUTIONS
      NTYPE=5
      IF (BETAR-.001)500,502,501
```

```
  500 CALL SIMP(BETAR,.001,NBETAP,EPSLQ1)
  502 STRT=.001
      GO TO 503
  501 STRT=BETAR
      EPSLQ1=0.0
  503 CALL SIMP(STRT,.999,NBETAP,EPSLQ2)
      EPSLNQ=EPSLQ1+EPSLQ2
      IF(NUMHS.GT.0) GO TO 504
      EPSLNS=0.
      CS=0.
      GO TO 505
  504 NTYPE=6
      CALL SIMP(BETAS1,BETAS2,NBETAP,EPSLNS)
  505 CALL SPRINT
      WRITE(3,1030)
      WRITE(3,1060)
      WRITE(3,1070) (XSAVE(I),A(I),I=1,NUMY)
      WRITE(3,1121) EPSLNQ,CQ,EPSLNS,CS
      GO TO 5
 5100 STOP
 1000 FORMAT (4I5)
 1001 FORMAT(F10.3,F15.3)
 1002 FORMAT (1H+ 25X 2F15.3)
 1003 FORMAT (1H+ 65X 2F15.3)
 1004 FORMAT (1H+ 95X 2F15.3)
 1010 FORMAT (2F10.0)
 1020 FORMAT(1H0 18X *QUIESCENT DISTRIBUTIONS* 42X *STREAMING DISTRIBUTI
     -IONS*//* PITCH ANGLE     DISTRIBUTION    NORM. ENERGY    DISTRIBUTIO
     -N* 11X *PITCH ANGLE    DISTRIBUTION    NORM. ENERGY   DISTRIBUTION*
     -  / 3X *(ALPHAQ)* 10X *(HQ)* 7X *(LOG(E/MCQ))* 2X *(LOG(DNQ/(DE/MC
     -Q)))* 5X *(ALPHAS)* 10X *(HQ)* 7X *(LOG(E/MCS))* 2X *(LOG(DNS/(DE/
     -MCS)))* /        )
 1030 FORMAT (60H
     1                                 )
 1040 FORMAT (2F10.0,I5,3F5.0,3I5,F5.0)
 1050 FORMAT(1H 2X *SURFACE LATITUDE (THO) =* F8.2,4X *PLASMA PARTICLE (
     -POPF) =* F5.0, 10X *INTEGRATION STEPS* 5X *PITCH ANGLE (NALPHA), =*
     --I5/ * EQUATORIAL DENSITY (XNO) =* F6.2,4X *DENSITY MODEL (NTYPEQ)
     -=* I5,39X *LATITUDE (NX) =* I5 / 10X * PROPAGATION FREQ./EQUATORIAL
     - CYCLOTRON FREQ. (DELY) =* F5.3,21X *PERPENDICULAR VELOCITY (NBETA
     -P) =* I5 / 10X *BAND LIMITS* 2X *(YS) =* F8.3,4X *(YE) =* F8.3)
 1060 FORMAT(1H0 *PROPAG. FREQ./EQTRL CYCLOTRON FREQ.* 5X *NET AMPLIFICA
     -TION (DECIBELS)* )
 1070 FORMAT( 15X F8.3, 25X E14.6  )
 1100 FORMAT(1H0 * LOCAL B/EQTRL B* 2X *REFRACTIVE* 8X *LOCAL AMPLITUDE
     --EXPONENT* 11X *SINE*/ 19X 8HINDEX**2 5X *STREAMING* 4X *QUIESCENT*
     - 8X *NET* 5X *(LATITUDE)*/ 8X *(B)* 8X *(XN2)*11X *(XJS)* 8X *(XJQ
     -)* 7X *(XNIXY)* 6X *(X)* )
 1110 FORMAT(1H0 *PROPAG. FREQ./EQTRL. CYCLOTRON FREQ.  (LOCAL) =* F7.4)
 1121 FORMAT(1H0 * PLASMA DENSITY* 7X *PITCH ANGLE* 7X *PLASMA DENSITY*
     - 7X *PITCH ANGLE* / *  QUIESCENT/COLD* 5X *QUIESCENT NORM.* 5X *ST
     -REAMING/COLD* 5X *STREAMING NORM.* // E15.4,3E20.4)
 2000 FORMAT (3I2)
      END
```

```
      SUBROUTINE SIMPX(A,B,N,FI)
C
C     INTEGRATION OF AMPLITUDE EXPONENT ALONG FIELD LINE
C
      IF(A.GE.1.E-5) GO TO 3
      AUSF = 1.E-5
      GO TO 4
    3 AUSF = A
    4 IF (N) 10,10,20
   10 FI=0
      RETURN
   20 FN=N
      DX = (B-AUSE)/FN
      TDX=2.*DX
      HT = XNIXY(AUSE)
      AI=0.
      BI=0.
      X = AUSE-DX
      XA=AUSE
      NN=N/2
      DO 30 J=1,NN
      X=X+TDX
      XA=XA+TDX
      AI=AI+XNIXY(X)
      IF(J.EQ.NN) GO TO 30
      BI=BI+XNIXY(XA)
   30 CONTINUE
      FI = XNIXY(B) + HI
      FI=DX*(FI+4.*AI+2.*BI)/3.
      RETURN
      END
```

```
      FUNCTION XNIXY(X)
      REAL LAMBDA
      DIMENSION           HQ(50),HS(50),XNQ(50),XNS(50),ALPHAQ(50),
     1ALPHAS(50),EMCQ(50),EMCS(50),SPLCNS(50),SPLCHQ(4,50),SPLCHS(4,50),
     2SPLCNQ(4,50)
      COMMON HQ,HS,XNQ,XNS,ALPHAQ,ALPHAS,EMCQ,EMCS,SPLCHQ,SPLCHS,SPLCNQ,
     1   SPLCNS,RAD,PI,THQ,XNO,CQ,CS,WPO,THOR,COSTH,SINTH,WCO,Y,Y2,WCO2,
     2   B2,XN2,B,XN,DEG,BETAS1,BETAS2,PORE,NUMHQ,NUMHS,NUMNQ,NUMNS,
     3   NTYPEQ,NTYPE,NBETAP,NPAGE,MONTH,NDAY,NYR
C
C  AMPLITUDE EXPONENT
C
C  EVALUATE LOCAL FIELD LINE PARAMETERS
C
      X2=X*X
      B= SQRT(1.+3.*X2)/((1.-X2)**3)
      B2=3*B
      IF(NTYPEQ.NE.6) GO TO 600
      LAMBDA=ASIN(X)
      COSL4=COS(LAMBDA)**4
C     30 DEG = .5236 RADIANS
      XA=SIN(LAMBDA-.5236)**2
  600 WP2=WPO*WPO*G(X2,XA,COSTH,COSL4,NTYPEQ)
      IF (PORE-10.)1,2,2
    1 Z=Y
      GO TO 3
    2 Z=B
    3 XN2=1.+WP2/(WCO2+Z*(B-Y))*PORE
```

```
C     LITHIUM SHAPED CHARGE INJECTION
C        CASE 5
      IF(X2.GT.0.008) GO TO 5
      IF(Y.LT.B/7.) GO TO 4
      XNIXY=0.
      RETURN
    4 XN2=XN2+(((1.06*(EXP(-(X2/(.16*COSTH**4))))))*(WPO/WCO)**2)*(7.*PORE
     - )/(7.*Y*(B-7.*Y)))
```

For lithium injection only
at $\sqrt{Dt}$ = 0.5 R_e (t = 50 minutes)
Delete for other models.

```
    5 XN= SQRT(XN2)
C  INTEGRATE BETA PERPENDICULAR OVER DISTRIBUTIONS
      BETAPM= SQRT(1.-Y2/B2+Y2/(B2*(1.+B2/(XN2*Y2))))
      NTYPE=3
      IF(PORE.GT.10.) GO TO 8
      CALL SIMP(0.,BETAPM,NBETAP,XJQ )
      GO TO 9
    8 CALL SIMP(0.,.01,NBETAP,XJQ1)
      CALL SIMP(.01,BETAPM,NBETAP,XJQ2)
      XJQ=XJQ1+XJQ2
    9 IF(NUMNS.GT.0) GO TO 20
   10 XJS=0.
```

```
      GO TO 30
  20  BETAP1=BETAN(BETAS1,B,Y,XN2)
      BETAP2=BETAN(BETAS2,B,Y,XN2)
      IF(BETAP1.EQ.-1..OR.BETAP2.EQ.-1.) GO TO 10
      NTYPE=4
      CALL SIMP(BETAP1,BETAP2,NBETAP,XJS)
  30  ZNIXY=4.934*WP2/(XN2*Y2*WC02)*(XJS+XJQ)

      XNIXY=ZNIXY
      WRITE(3,1000) B,XN2,XJS,XJQ,ZNIXY,X
1000  FORMAT(E13.4,E16.4,3E13.4,F10.4)
      RETURN
      END
```

```
      SUBROUTINE SIMP(A,B,N,FI)
C
C     INTEGRATION OVER BETA PERPENDICULAR FOR AMPLITUDE EXPONENT
C
      IF(A.GE.1.E-7) GO TO 3
      AUSE = 1.E-5
      GO TO 4
    3 AUSE = A
    4 IF (N) 10,10,20
   10 FI=0
      RETURN
   20 IF (ABS(A) + ABS(B)) 30,10,30
   30 FN=N
      DX = (B-AUSE)/FN
      TDX=2.*DX
      FI = GRANF(AUSE)+GRANF(B)
      AI=0.
      BI=0.
      X = AUSE-DX
      NN=N/2
      DO 40 J=1,NN
      X=X+TDX
   40 AI=AI+GRANF(X)
      X = AUSE
      NM=NN-1
      DO 50 J=1,NM
      X=X+TDX
   50 BI=BI+GRANF(X)
      FI=DX*(FI+4.*AI+2.*BI)/3.
      RETURN
      END
```

```
      FUNCTION GRANF(X)
      DIMENSION          HQ(50),HS(50),XNQ(50),XNS(50),ALPHAQ(50),
     1ALPHAS(50),EMCQ(50),EMCS(50),SPLCNS(50),SPLCHQ(4,50),SPLCHS(4,50),
     2SPLCNQ(4,50)
      COMMON HQ,HS,XNQ,XNS,ALPHAQ,ALPHAS,EMCQ,EMCS,SPLCHQ,SPLCHS,SPLCNQ,
     1  SPLCNS,RAD,PI,THO,XNO,CQ,CS,WPO,THOR,COSTH,SINTH,WCO,Y,Y2,WCO2,
     2  B2,XN2,B,XN,DEG,BETAS1,BETAS2,PORE,NUMHQ,NUMHS,NUMNQ,NUMNS,
     3  NTYPEQ,NTYPE,NBETAP,NPAGE,MONTH,NDAY,NYR
C
C
C     EVALUATION OF VARIOUS INTEGRANDS
C
      GO TO (10,20,40,40,180,190),NTYPE
C
C NTYPE 1 OR 2      PITCH ANGLE DISTRIB INTEGRAND
   10 CALL SPLINE(ALPHAQ,HQ,NUMHQ,SPLCHQ,X*DEG,YY,DX)
      GO TO 30
   20 CALL SPLINE(ALPHAS,HS,NUMHS,SPLCHS,X*DEG,YY,DX)
   30 GRANF=YY* SIN(X)
      RETURN
C
C NTYPE 3 OR 4      AMPLITUDE EXPONENT INTEGRAND
   40 N=NTYPE-2
      X2 = X*X
      C1=1 -(1.+B2/(XN2*Y2))*(1.-(1.-X2)/(Y2/B2))
      IF(C1.LT.0.) C1=0.
      BETAR=(1.- SQRT(C1))/(XN*(1.+B2/(XN2*Y2)))
      BETA= SQRT(X2+BETAR**2)
      C1=1.-BETA**2
      IF (C1)90,100,100
   90 WRITE (3,1010)X,C1,BETA,BETAR,B2,XN2
      C1=-C1
  100 GAMMA=1./ SQRT(C1)
      ALPHA= ATAN(-X/BETAR)
      ALPHA = ABS(ALPHA)
      XX=(GAMMA-1.)*PORE
      IF(X.GT.0.) GO TO 120
      WRITE (3,1020)X,C1,GAMMA,XX
      GRANF=0.0
      RETURN
  120 XX = ALOG10(XX)
      BSQR=1./ SQRT(B)
      U=BSQR* SIN(ALPHA)
      C1= ASIN(U)
      GO TO (130,140),N
  130 CALL SPLINE (EMCQ,XNQ,NUMNQ,SPLCNQ,XX,YY,ZZ)
      IF(YY.GT.-10.) GO TO 133
      GRANF= 0.0
      RETURN
  133 CALL SPLINE(ALPHAQ,HQ,NUMHQ,SPLCHQ,C1*DEG,H,DH)
  134 C=CQ
      GO TO 150
  140 CALL SPLINE (EMCS,XNS,NUMNS,SPLCNS,XX,YY,ZZ)
      CALL SPLINE(ALPHAS,HS,NUMHS,SPLCHS,C1*DEG,H,DH)
      C=CS
```

```
  150 G=(10.**YY)/(XN0*GAMMA**2*BETA)* PORE
      IF (C1*DEG-10.)160,170,170
  160 H=0.
      DH=C
  170 F=G*C*H
      DF=G*C*DH*DEG
      GAMMA4=GAMMA**4
      GRANF = GAMMA4*(2.*X-X2*X)*F-GAMMA4*(1.-B/(GAMMA*Y))*X2/BETAR*DF
      RETURN
C
C
C  NTYPE 5 OR 6      ENERGY DISTRIB INTEGRAND
  180 GAMMA=1./ SQRT(1.-X*X)
      XX = ALOG10((GAMMA-1.)*PORE)
      CALL SPLINE(EMCQ,XNQ,NUMNQ,SPLCNQ,XX,YY,DH)
      GO TO 200
  190 GAMMA = 1./ SQRT(1.-X*X)
      XX = ALOG10((GAMMA-1.)*PORE)
      CALL SPLINE(EMCS,XNS,NUMNS,SPLCNS,XX,YY,DH)
  200 GRANF= 10.**YY * GAMMA**3 * X / XN0* PORE
      RETURN
 1000 FORMAT (2H015E15.6)
 1010 FORMAT (2H026E15.6)
 1020 FORMAT (2H034E15.6)
      END
```

```
      SUBROUTINE SPLICN(X,Y,M,C)
      DIMENSION          X(50),Y(50),D(50),P(50),E(50),B(50),Z(50),
     - C(4,50),A(50,3)
C
C
C   CURVE FIT COEFFICIENT ROUTINE
C

      MM=M-1
      DO 10 K=1,MM
      D(K)=X(K+1)-X(K)
      P(K)=D(K)/6.
 10   E(K)=(Y(K+1)-Y(K))/D(K)
      DO 20 K=2,MM
 20   B(K)=E(K)-E(K-1)
      A(1,2)=-1.-D(1)/D(2)
      A(1,3)=D(1)/D(2)
      A(2,3)=P(2)-P(1)*A(1,3)
      A(2,2)=2.*(P(1)+P(2))-P(1)*A(1,2)
      A(2,3)=A(2,3)/A(2,2)
      B(2)=B(2)/A(2,2)
      DO 30 K=3,MM
      A(K,2)=2.*(P(K-1)+P(K))-P(K-1)*A(K-1,3)
      B(K)=B(K)-P(K-1)*B(K-1)
      A(K,3)=P(K)/A(K,2)
      Q=D(M-2)/D(M-1)
 30   B(K)=B(K)/A(K,2)
      A(M,1)=1.+Q+A(M-2,3)
      A(M,2)=-Q-A(M,1)*A(M-1,3)
      B(M)=B(M-2)-A(M,1)*B(M-1)
      Z(M)=B(M)/A(M,2)
      MN=M-2
      DO 40 I=1,MN
      K=M-I
 40   Z(K)=B(K)-A(K,3)*Z(K+1)
      Z(1)=-A(1,2)*Z(2)-A(1,3)*Z(3)
      DO 50 K=1,MM
      Q=1./(6.*D(K))
      C(1,K)=Z(K)*Q
      C(2,K)=Z(K+1)*Q
      C(3,K)=Y(K)/D(K)-Z(K)*P(K)
 50   C(4,K)=Y(K+1)/D(K)-Z(K+1)*P(K)
      RETURN
      END
```

```
      SUBROUTINE SPLINE(X,Y,M,C,XINT,YINT, DT )
      DIMENSION X(50),Y(50),C(4,50)
C
C     CURVE FIT ROUTINE
C
C     THIS SUBROUTINE USES SPLINE COEFFICIENTS FROM SPLICON
C
C     FIND WHAT TWO VALUES OF XINT IS BETWEEN
C
      IF(XINT.GE.X(1)) GO TO 50
      YINT=Y(1)
      DT=0.
      RETURN
   50 IF(XINT.LE.X(M)) GO TO 60
      YINT=Y(M)
      DT=0.
      RETURN
   60 DO 100 J=2,M
      IF(XINT.LE.X(J-1).OR.XINT.GT.X(J)) GO TO 100
      MU=J
      ML=J-1
      GO TO 110
  100 CONTINUE
      WRITE(3,1000)
      STOP
C
C     SOLVE FUNCTION FOR DEPENDENT VARIABLE (YINT)
C     DT IS THE DERIVATIVE OF Y = F(XINT)
C
  110 X1=(X(MU)-XINT)**2
      X2=(XINT-X(ML))**2
      YINT=(X(MU)-XINT)*(C(1,ML)*X1+C(3,ML))
      YINT=YINT+(XINT-X(ML))*(C(2,ML)*X2+C(4,ML))
  120 DT=-3.*C(1,ML)*X1+3.*C(2,ML)*X2-C(3,ML)+C(4,ML)
      RETURN
 1000 FORMAT (13H1OUT OF RANGEE15.6)
      END
```

```
      FUNCTION Q(X2,XA,COSTH,COSL4,NTYPEQ)
C
C  COLD PLASMA DENSITY MODELS
C
      REAL LAMBDA
      GO TO (10,20,30,40,50,60,70,80) ,NTYPEQ
C  B-FIELD MODEL
   10 Q=1./((1.-X2)**3)
      RETURN
C  HYDROSTATIC EQUILIB MODEL
   20 Q=( EXP(X2/(1.-X2)))**(3.*COSTH**2)
      RETURN
C  ECTRL INJECTION MODEL
   30 Q=1./((1.-X2)**3)+68.0*(EXP(-(X2/(.01*COSTH**4))))
      RETURN
   40 Q=1./((1.-X2)**3)+8.55*(EXP(-(X2/(.04*COSTH**4))))
      RETURN
   50 Q=1./((1.-X2)**3)+1.06*(EXP(-(X2/(.16*COSTH**4))))
      RETURN
C     NONEQUATORIAL BURST
   60 Q=1./((1.-X2)**3)+8.55*(EXP(-COSL4*XA/(.04*COSTH**4)))
      RETURN
C     BARIUM SHAPED CHARGE MODEL - FIELD ALIGNED STEP FUNCTION
C     30 DEG - X - 38 DEG        SET XN0=1.
   70 Q=1./((1.-X2)**3)
      IF(X2.GE..25.AND.X2.LE..37904) Q=Q+30.
      RETURN
C     BARIUM SHAPED CHARGE MODEL - FIELD ALIGNED STEP FUNCTION
C     8 DEG - X - 25 DEG                SET XN0=1.
   80 Q=1./((1.-X2)**3)
      IF(X2.GE..01937.AND.X2.LE..17861) Q=Q+5.
      RETURN
      END
```

```
      FUNCTION BETAN(BETA,B,Y,XN2)
C
C  INTEGRATION LIMITS FOR BETA PERPENDICULAR
C
      BSM2=BETA**2
      C1= SQRT(1.-BSM2)
      FACT= BSM2-(1.-C1*B/Y)**2/XN2
      IF(FACT.LT.0..OR.FACT.GE.1.) GO TO 5
      BETAN=SQRT(FACT)
      RETURN
    5 BETAN=-1.
      RETURN
      END
```

```
      SUBROUTINE SPRINT
      DIMENSION          HQ(50),HS(50),XNQ(50),XNS(50),ALPHAQ(50),
     1ALPHAS(50),EMCQ(50),EMCS(50),SPLCNS(50),SPLCHQ(4,50),SPLCHS(4,50),
     2SPLCNQ(4,50)
      COMMON HQ,HS,XNQ,XNS,ALPHAQ,ALPHAS,EMCQ,EMCS,SPLCHQ,SPLCHS,SPLCNQ,
     1  SPLCNS,RAD,PI,TH0,XN0,CQ,CS,WP0,THOR,COSTH,SINTH,WC0,Y,Y2,WC02,
     2  B2,XN2,B,XN,DEG,BETAS1,BETAS2,PORE,NUMHQ,NUMHS,NUMNQ,NUMNS,
     3  NTYPEQ,NTYPE,NBETAP,NPAGE,MONTH,NDAY,NYR
C
C
C
C
C  DATE,MONTH,YEAR AND PAGE NO
C
      WRITE (3,1000)MONTH,NDAY,NYR,NPAGE
      NPAGE=NPAGE+1
      RETURN
 1000 FORMAT (1H1I2,1H/I2,1H/I2,40X8HPAGE NO.I4/)
      END
```